

International Journal of Modern Physics E
© World Scientific Publishing Company

NEUTRINO-LESS DOUBLE BETA DECAY AND PARTICLE PHYSICS

WERNER RODEJOHANN

*Max-Planck-Institut für Kernphysik
Postfach 103980, D-69029 Heidelberg
Germany
werner.rodejohann@mpi-hd.mpg.de*

We review the particle physics aspects of neutrino-less double beta decay. This process can be mediated by light massive Majorana neutrinos (*standard interpretation*) or by something else (*non-standard interpretations*). The physics potential of both interpretations is summarized and the consequences of future measurements or improved limits on the half-life of neutrino-less double beta decay are discussed. We try to cover all proposed alternative realizations of the decay, including light sterile neutrinos, supersymmetric or left-right symmetric theories, Majorons, and other exotic possibilities. Ways to distinguish the mechanisms from one another are discussed. Experimental and nuclear physics aspects are also briefly touched, alternative processes to double beta decay are discussed, and an extensive list of references is provided.

2 *W. Rodejohann***Contents**

1	Introduction: General Aspects of Double Beta Decay and Lepton Number Violation	3
2	Experimental aspects	5
3	Nuclear physics aspects	11
3.1	Standard mechanism	11
3.2	Non-standard mechanisms	16
4	Standard Interpretation	17
4.1	Neutrino physics	18
4.1.1	Neutrino mass and mixing: theoretical origin	18
4.1.2	Neutrino mass and mixing: observational status	21
4.2	Standard three neutrino picture and $0\nu\beta\beta$	29
4.2.1	Normal mass ordering	31
4.2.2	Inverted mass ordering	35
4.2.3	Mass scale	36
4.2.4	Mass ordering: testing the inverted hierarchy	39
4.2.5	Majorana CP phases	40
4.2.6	Vanishing effective mass	43
4.2.7	Renormalization	44
4.2.8	Distinguishing neutrino models	45
4.2.9	Light sterile neutrinos	46
4.2.10	Exotic modifications of the three neutrino picture	49
5	Non-Standard Interpretations	51
5.1	Heavy neutrinos	52
5.2	Higgs triplets	56
5.3	Left-right symmetric theories	57
5.4	Supersymmetric theories	62
5.5	Majorons	68
5.6	Other mechanisms	70
6	Distinguishing mechanisms for neutrino-less double beta decay	72
6.1	Distinguishing via effects in other observables	73
6.2	Distinguishing via decay products	73
6.3	Distinguishing via nuclear physics	74
6.4	Simultaneous presence of several mechanisms	76
7	Alternative Processes to Neutrino-less Double Beta Decay	77
8	Summary	82

1. Introduction: General Aspects of Double Beta Decay and Lepton Number Violation

Neutrino-less double beta decay ($0\nu\beta\beta$) is a process of fundamental importance for particle physics. It is defined as the transition of a nucleus into a nucleus with proton number larger by two units, and the emission of two electrons¹:

$$(A, Z) \rightarrow (A, Z + 2) + 2 e^- \quad (0\nu\beta\beta). \quad (1)$$

There are no leptons in the initial state, but two in the final state. Observation of $0\nu\beta\beta$ would therefore show that lepton number, an accidental and classical symmetry of the Standard Model (SM) of particle physics, is violated by Nature. The process therefore stands on equal footing with baryon number violation, i.e. proton decay. For this reason a huge amount of experimental and theoretical activity is pursued in order to detect and predict the process^{2,3,4,5,6,7,8,9,10,11,12}.

As well known, the main motivation to search for $0\nu\beta\beta$ is the fact that neutrinos are, in contrast to the prediction of the SM, massive particles and that basically all theories beyond the SM predict them to be Majorana¹³ particles. However, as we will discuss in this review, there are many other well-motivated particle physics scenarios and frameworks that allow for $0\nu\beta\beta$. Before discussing these aspects, let us first give some general comments on lepton number violation.

Why should we look for Lepton Number Violation (LNV)? The conservation of lepton (and baryon) number in the SM is an accidental one at the classical level only. In fact, chiral anomalies actually violate this conservation law, and it can be shown that the currents associated with baryon and lepton number have non-vanishing divergences: $\partial^\mu J_\mu^{B,L} = c G_{\mu\nu} \tilde{G}^{\mu\nu} \neq 0$. Here $G_{\mu\nu}$ is the electroweak gauge field strength and $J_\mu^B = \sum \bar{q}_i \gamma_\mu q_i$, $J_\mu^L = \sum \bar{\ell}_i \gamma_\mu \ell_i$. Though this LNV is not the one related to $0\nu\beta\beta$ or Majorana neutrinos, and the rates of processes associated to it are negligible at low temperatures, it shows that lepton number is nothing sacred, not even in the Standard Model. Extending the picture from the SM to Grand Unified Theories (GUTs), quarks and leptons live together in multiplets, and hence both B and L are not expected to be conserved quantities. The combination $B - L$, which is conserved in the SM both at the classical and quantum level, often plays an important role in GUTs, and is broken at some stage. In the spirit of baryogenesis, one needs to require that baryon number is violated, and hence lepton number should be violated too. The search for baryon number violation proceeds in proton decay, or neutron–anti-neutron oscillation experiments. Lepton number violation is investigated in neutrino-less double beta decay experiments, and should be treated on the same level as baryon number violation. An observation of LNV would be far more fundamental than a “simple” measurement of neutrino properties, which is often quoted as the main goal of $0\nu\beta\beta$ -searches. Its implications are far beyond that.

In this review we wish to summarize the particle physics aspects of limits and possible measurements of this process. A large number of theories and mechanisms to violate lepton number exists, and the most often considered light Majorana

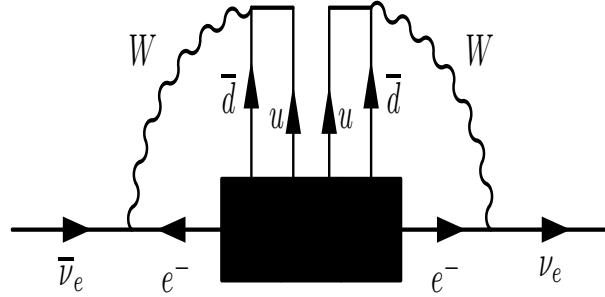


Fig. 1. Black-box illustration of neutrino-less double beta decay.

neutrino exchange (though well-motivated) is only one possibility. We should note that via the black-box, or Schechter-Valle, theorem¹⁴ (see also¹⁵), all realizations of Eq. (1) are connected to a Majorana neutrino mass. Crossing the process on the quark level gives from $dd \rightarrow uu e^- e^-$ the relation $0 \rightarrow u\bar{d}u\bar{d}e^-e^-$, and with the only input of $SU(2)_L$ gauge theory one can couple each $u\bar{d}$ pair via a W to the electrons, as illustrated in Fig. 1. The result is a $\bar{\nu}_e - \nu_e$ transition, which is nothing but a Majorana mass term. Needless to say, this is a tiny mass generated at the 4-loop level, and too small to explain the neutrino mass scale (or its splitting) as observed in oscillation experiments. Naively, one can estimate the contribution to neutrino mass as

$$(m_\nu)_{ee} \lesssim \frac{1}{(16\pi^2)^4} \frac{\text{MeV}^5}{m_W^4} \simeq 10^{-23} \text{ eV}, \quad (2)$$

where we inserted a factor $1/(16\pi^2)$ for each loop, put m_W^{-2} for each of the two W in the loop, and MeV is the typical mass of the involved electron, up- and down-quark. An explicit calculation of the 4-loop diagram with an effective operator as the source of $0\nu\beta\beta$ yields a very similar number¹⁶. Note that this tiny mass is much smaller than the Planck-scale contribution to the Majorana neutrino mass, which is $v^2/M_{\text{Pl}} \simeq 10^{-5} \text{ eV}$. There are now two main possibilities:

- (i) the mechanism leading to $0\nu\beta\beta$ is connected to neutrino oscillation. Here there are again two possibilities:
 - (ia) there is a direct connection to neutrino oscillation. This is the standard mechanism of light neutrino exchange;
 - (ib) there is an indirect connection to neutrino oscillation. Examples would be heavy neutrino exchange, where the heavy neutrinos are responsible for light neutrino masses via the seesaw mechanism. Another case would be R -parity violating SUSY particles generating $0\nu\beta\beta$, where via loops the same particles generate light neutrino masses;

- (ii) the mechanism leading to $0\nu\beta\beta$ is *not* connected to neutrino oscillation. The underlying physics of $0\nu\beta\beta$ could be either:
 - (iia) giving a sub-leading contribution to neutrino mass, maybe R -parity violating SUSY being responsible for only one of the neutrino masses;
 - (iib) giving no contribution to neutrino mass, for instance a right-handed Higgs triplet in the absence of a Dirac mass matrix for neutrinos. Hence only the Schechter-Valle term from Eq. (2) can generate a neutrino mass.

In both cases (iia) and (iib) we would need another source for neutrino mass and oscillation¹⁶.

As already mentioned, the assumption that massive Majorana neutrinos generate $0\nu\beta\beta$ is presumably the best motivated one, though there are many more. We can thus classify the possible interpretations of $0\nu\beta\beta$ as follows:

- (1) *Standard Interpretation:*
neutrino-less double beta decay is mediated by light and massive Majorana neutrinos (the ones which oscillate) and all other mechanisms potentially leading to $0\nu\beta\beta$ give negligible or no contribution;
- (2) *Non-Standard Interpretations:*
neutrino-less double beta decay is mediated by some other lepton number violating physics, and light massive Majorana neutrinos (the ones which oscillate) potentially leading to $0\nu\beta\beta$ give negligible or no contribution.

In this review we will consider both cases and aim to discuss all possible realizations of $0\nu\beta\beta$. In Sections 2 and 3 we will deal with experimental and nuclear physics aspects of $0\nu\beta\beta$, respectively. The standard interpretation of light neutrino exchange is discussed in Section 4, where we summarize in detail our current understanding of neutrino physics and its many aspects which can be tested with $0\nu\beta\beta$. Section 5 is devoted to the various non-standard interpretations, such as left-right symmetric theories, R -parity violating supersymmetry, Majorons, and other proposals. Section 6 deals with possibilities to distinguish the mechanisms from one another, and Section 7 is concerned with alternative processes to $0\nu\beta\beta$. A summary is presented in Section 8. For all aspects we provide an extensive list of references.

2. Experimental aspects

Neutrino-less double beta decay can only be observed if the usual beta decay is energetically forbidden. This is the case for some even-even nuclei (i.e. even proton and neutron numbers), whose ground states are energetically lower than their odd-odd neighbors. If the nucleus with atomic number higher by one unit has a smaller binding energy (preventing beta decay from occurring), and the nucleus with atomic number higher by two units has a larger binding energy, the double beta decay process is allowed. In principle 35 nuclei can undergo $0\nu\beta\beta$, though realistically only

nine emerge as interesting candidates and are under investigation in competitive experiments, namely ^{48}Ca , ^{76}Ge , ^{82}Se , ^{96}Zr , ^{100}Mo , ^{116}Cd , ^{130}Te , ^{136}Xe , ^{150}Nd . There is no “super isotope”, one has to find compromises between the natural abundance, reasonably priced enrichment, the association with a well controlled experimental technique or the Q -value, because the decay rate for $0\nu\beta\beta$ goes with Q^5 (except for Majoron emission, see Section 5.5). Table 1 and Fig. 2 give the relevant parameters of all 11 isotopes with a Q -value above 2 MeV, including the nine most studied isotopes given above. The experimental signal is the sum of energy of the two emitted electrons, which should equal the known Q -value. The neutrino-less mode has to be distinguished from 2 neutrino double beta decay¹⁷

$$(A, Z) \rightarrow (A, Z + 2) + 2e^- + 2\bar{\nu}_e \quad (2\nu\beta\beta), \quad (3)$$

which experimentally can be an irreducible background for the neutrino-less mode. The half-life of $2\nu\beta\beta$ is typically around 10^{19} – 10^{21} yrs (it is important to note that the process is allowed in the SM), and has been observed for a number of isotopes already, see¹¹ for a list of results. Obviously, the countless peaks arising from natural radioactivity, cosmic ray reactions etc. need to be understood and/or the experiments have to be ultrapure and/or heavily shielded. The energy release Q should also be large due to the background of natural radioactivity, which drops significantly beyond 2.614 MeV, which is the highest significant γ -line in the natural decay chains of Uranium and Thorium. In general, the decay rate for $0\nu\beta\beta$ can be factorized as

$$\Gamma^{0\nu} = G_x(Q, Z) |\mathcal{M}_x(A, Z) \eta_x|^2, \quad (4)$$

where η_x is a function of the particle physics parameters responsible for the decay. The nuclear matrix element (NME) $\mathcal{M}_x(A, Z)$ depends on the mechanism and the nucleus. The term $\mathcal{M}_x(A, Z) \eta_x$ can in fact be a sum of several terms, therefore

Table 1. Q -value, natural abundance and phase space factor G (standard mechanism) for all isotopes with $Q \geq 2$ MeV using $r_0 = 1.2$ fm. Values taken from Table 6 of⁶ and scaled to $g_A = 1.25$. Note that there is a misprint in Ref.⁶, which quotes $G^{0\nu}$ for ^{100}Mo as $11.3 \times 10^{-14} \text{ yrs}^{-1}$.

Isotope	$G [10^{-14} \text{ yrs}^{-1}]$	$Q [\text{keV}]$	nat. abund. [%]
^{48}Ca	6.35	4273.7	0.187
^{76}Ge	0.623	2039.1	7.8
^{82}Se	2.70	2995.5	9.2
^{96}Zr	5.63	3347.7	2.8
^{100}Mo	4.36	3035.0	9.6
^{110}Pd	1.40	2004.0	11.8
^{116}Cd	4.62	2809.1	7.6
^{124}Sn	2.55	2287.7	5.6
^{130}Te	4.09	2530.3	34.5
^{136}Xe	4.31	2461.9	8.9
^{150}Nd	19.2	3367.3	5.6

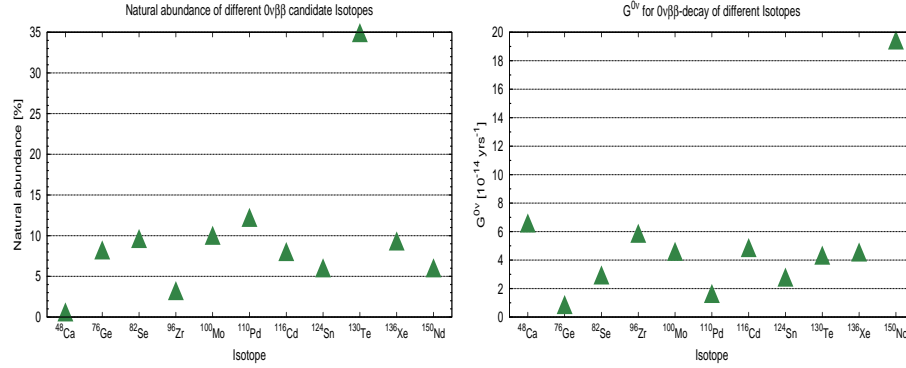


Fig. 2. Natural abundance and phase space factor for all 11 $0\nu\beta\beta$ -isotopes above $Q = 2$ MeV.

including the possibility of destructive or constructive interference, a situation we will deal with in Section 6.4. Finally, $G_x(Q, Z)$ is a phase space factor which can have dependence on the particle physics. For most of the processes in which only two electrons are emitted, the phase space factor can be considered almost independent of the mechanism. The biggest effect for G occurs in double beta decay with Majoron emission, in which the final state contains one or two additional particles, see Section 5.5. Table 2 summarizes the current best limits on the half-life. Neutrino-less double beta decay is definitely a rare process. In Table 2 we already quote the limits on the effective mass (the particle physics parameter in the standard interpretation) from the respective experiments, for which we used a compilation of nuclear matrix elements discussed later.

Table 2. Experimental limits at 90% C.L. on the most interesting isotopes for $0\nu\beta\beta$. Using the nuclear matrix element ranges from Table 5 we also give the maximal and minimal limits on $\langle m_{ee} \rangle$.

Isotope	$T_{1/2}^{0\nu}$ [yrs]	Experiment	$\langle m_{ee} \rangle_{\min}^{\text{lim}}$ [eV]	$\langle m_{ee} \rangle_{\max}^{\text{lim}}$ [eV]
^{48}Ca	5.8×10^{22}	CANDLES ¹⁸	3.55	9.91
^{76}Ge	1.9×10^{25}	HDM ¹⁹	0.21	0.53
	1.6×10^{25}	IGEX ²⁰	0.25	0.63
^{82}Se	3.2×10^{23}	NEMO-3 ²¹	0.85	2.08
^{96}Zr	9.2×10^{21}	NEMO-3 ²²	3.97	14.39
^{100}Mo	1.0×10^{24}	NEMO-3 ²¹	0.31	0.79
^{116}Cd	1.7×10^{23}	SOLOTVINO ²³	1.22	2.30
^{130}Te	2.8×10^{24}	CUORICINO ²⁴	0.27	0.57
^{136}Xe	5.0×10^{23}	DAMA ²⁵	0.83	2.04
^{150}Nd	1.8×10^{22}	NEMO-3 ²⁶	2.35	5.08

Note: The limits on $T_{1/2}^{0\nu}$ from NEMO-3 measurements assume the standard light neutrino mechanism.

In the past the search relied mainly on geo- and radiochemical measurements, which are insensitive to the mode of double beta decay, but led to the first observation that two neutrino double beta decay occurs in nature²⁷. Here the approach is to identify accumulation of the decay isotope (in particular if it is a noble gas, for which mass spectroscopy can be done very precisely) during geological time periods in samples which are rich in a double beta decay isotope. In principle, this method can be used to test the time-dependence of the parameters associated with the mechanism of double beta decay.

Nowadays only direct methods are applied, based mainly on the observation of the two electrons in the form of measuring their total sum energy, which should equal the Q -value of the decay. Some experiments have the possibility of tracking the individual electrons. There are a number of recent reviews on the experimental situation in double beta decay, to which we refer for more details^{8,9,11,12}. The number of expected events in an experiment can be written as

$$N = \ln 2 a M t N_A (T_{1/2}^{0\nu})^{-1}, \quad (5)$$

where a is the abundance of the isotope, M the used mass, t the time of measurement and N_A is Avogadro's number. The half-life sensitivity depends on whether there is background or not²⁸:

$$(T_{1/2}^{0\nu})^{-1} \propto \begin{cases} a M \varepsilon t & \text{without background,} \\ a \varepsilon \sqrt{\frac{M t}{B \Delta E}} & \text{with background.} \end{cases} \quad (6)$$

Here B is the background index with natural units of counts/(keV kg yr) and ΔE the energy resolution at the peak. In Table 3 we follow the classification proposed by A. Guilian¹² and list some properties of the main up-coming experiments. Table 4 lists the most developed experiments according to¹¹. Roughly speaking, at present

Table 3. Planned experiments categorized according to¹² and the isotope(s) under consideration.

Name	Isotope	source = detector; calorimetric with			source \neq detector with
		high energy res.	low energy res.	sensit. to event topology	sensit. to event topology
CANDLES ²⁹	⁴⁸ Ca	—	✓	—	—
COBRA ³⁰	¹¹⁶ Cd (and ¹³⁰ Te)	—	—	✓	—
CUORE ³¹	¹³⁰ Te	✓	—	—	—
DCBA ³²	¹⁵⁰ Nd	—	—	—	✓
EXO ³³	¹³⁶ Xe	—	—	✓	—
GERDA ³⁴	⁷⁶ Ge	✓	—	—	—
KamLAND-Zen ³⁵	¹³⁶ Xe	—	✓	—	—
LUCIFER ³⁶	⁸² Se or ¹⁰⁰ Mo or ¹¹⁶ Cd	✓	—	—	—
MAJORANA ³⁷	⁷⁶ Ge	✓	—	—	—
MOON ³⁸	⁸² Se or ¹⁰⁰ Mo or ¹⁵⁰ Nd	—	—	—	✓
NEXT ³⁹	¹³⁶ Xe	—	—	✓	—
SNO+ ⁴⁰	¹⁵⁰ Nd	—	✓	—	—
SuperNEMO ⁴¹	⁸² Se or ¹⁵⁰ Nd	—	—	—	✓
XMASS ⁴²	¹³⁶ Xe	—	✓	—	—

Table 4. Sensitivity at 90% C.L. of the seven most developed projects for about three (phase II of GERDA and MAJORANA, KamLAND, SNO+) five (EXO, SuperNEMO and CUORE) and ten (full-scale GERDA plus MAJORANA) years of measurements. Taken from¹¹.

Experiment	Isotope	Mass of Isotope [kg]	Sensitivity $T_{1/2}^{0\nu}$ [yrs]	Status	Start of data-taking
GERDA	^{76}Ge	18	3×10^{25}	running	~ 2011
		40	2×10^{26}	in progress	~ 2012
		1000	6×10^{27}	R&D	~ 2015
CUORE	^{130}Te	200	$6.5 \times 10^{26*}$	in progress	~ 2013
			$2.1 \times 10^{26**}$		
MAJORANA	^{76}Ge	30-60	$(1-2) \times 10^{26}$	in progress	~ 2013
		1000	6×10^{27}	R&D	~ 2015
EXO	^{136}Xe	200	6.4×10^{25}	in progress	~ 2011
		1000	8×10^{26}	R&D	~ 2015
SuperNEMO	^{82}Se	100-200	$(1-2) \times 10^{26}$	R&D	$\sim 2013-2015$
KamLAND-Zen	^{136}Xe	400	4×10^{26}	in progress	~ 2011
		1000	10^{27}	R&D	$\sim 2013-2015$
SNO+	^{150}Nd	56	4.5×10^{24}	in progress	~ 2012
		500	3×10^{25}	R&D	~ 2015

Note: * For a background of $10^{-3}/\text{keV}/\text{kg}/\text{yr}$; ** for a background of $10^{-2}/\text{keV}/\text{kg}/\text{yr}$.

the transition from 10 kg yrs to 100 kg yrs experiments is being made, background levels below 10^{-2} counts/(keV kg yr) are planned, and half-life sensitivities above 10^{26} yrs are foreseen.

The current best values come from the Heidelberg-Moscow¹⁹ experiment, using ^{76}Ge enriched Germanium calorimetric detectors. As is well known, part of the collaboration claims observation of the process⁴³, at the level of about 2×10^{25} yrs, with a 99.73% C.L. range of $(0.7 - 4.2) \times 10^{25}$ yrs. This has been criticized by a large part of the community⁴⁴, but eventually needs to be tested experimentally. In the later part of this review we will discuss limits on lepton number violating parameters from $0\nu\beta\beta$. As the limit on the half-life of ^{76}Ge corresponds roughly to the claimed signal, one could easily translate the limits of the lepton number violating parameters into their values, in case the claim is actually valid.

A bolometric experiment, also run in Gran Sasso, was CUORICINO²⁴, using ^{130}Te in the form of TeO_2 crystals. Similar limits to Heidelberg-Moscow could be reached. An experiment with source \neq detector was NEMO-3²¹, using foils of several potential $0\nu\beta\beta$ -emitters in a magnetized tracking volume. Here the main point is measuring the energy of the individual energies and their angular distribution. This approach is of interest in testing different mechanisms for $0\nu\beta\beta$, as we will discuss later. Again, limits of the order of Heidelberg-Moscow were obtained.

We shortly discuss presently running and upcoming experiments. Basically all of them will use enriched material, and all are located in underground laboratories. GERDA³⁴ and MAJORANA³⁷ will use ^{76}Ge , in the case of GERDA operated in

liquid Argon. Phase I consists of 18 kg previously used by IGEX and Heidelberg-Moscow and will test in the very near future (till 2013) the Heidelberg-Moscow claim, which unambiguously will only be possible with the same isotope. Phase II will work with 40 kg and depending on the outcome, a phase III, probably joined with MAJORANA (2×60 kg), is possible. Inauguration of GERDA was in November 2010. CUORE³¹ extends CUORICINO to several towers of material, aiming at 200 kg ^{130}Te and a start of data taking in 2013. EXO³³, whose prototype with 200 kg of liquid Xenon enriched to 80% is in commissioning, will apply liquid or gaseous Xenon; by using a time-projection chamber there is sensitivity to event topology. It will be attempted in a later phase to laser-tag the $^{136}\text{Ba}^{++}$ ion, which is the decay product of the isotope under investigation, ^{136}Xe . SuperNEMO⁴¹ uses the NEMO-3 approach and will work with about 100 kg of ^{82}Se or ^{150}Nd . SNO+⁴⁰ wishes to fill the large SNO detector with a total of 44 kg of ^{150}Nd . KamLAND-Zen³⁵ pursues a similar approach with the KamLAND experiment, using ^{136}Xe . CANDLES²⁹ will investigate CaF_2 scintillators, and is currently analyzing enrichment options for later phases. COBRA³⁰ will be an array of CdZnTe room temperature semiconductors, mainly sensitive to $0\nu\beta\beta$ of ^{116}Cd , but to other decay modes as well. LUCIFER³⁶ proposes to use scintillating bolometers at low temperature. MOON³⁸ wants to use scintillators in between source foils, DCBA³² aims at putting source foils with ^{150}Nd in a magnetized drift chamber. XMASS⁴² proposes liquid scintillating Xenon, NEXT³⁹ a gaseous Xenon TPC. Some of the experiments can also be used as solar neutrino or dark matter experiments, such as XMASS, NEXT or MOON. More details on the experiments can be found in the respective publications and the reviews^{8,9,11,12}.

It is encouraging that different experimental techniques will be pursued, and that different isotopes are under study. Eventually, a multi-isotope determination of $0\nu\beta\beta$ would be preferable, to make it more unlikely that a peak coming from an unidentified background process mimics the signal. This is the **first reason for multi-isotope determination**.

We will focus in this review on neutrino-less double beta decay. However, there are similar processes called neutrino-less double beta⁺ decay ($0\nu\beta^+\beta^+$), or beta⁺-decay electron capture ($0\nu\beta^+\text{EC}$), or double electron capture ($0\nu\text{ECEC}$) of bound state electrons e_b^- , which can also be searched for:

$$(A, Z) \rightarrow (A, Z - 2) + 2e^+ \quad (0\nu\beta^+\beta^+), \quad (7)$$

$$e_b^- + (A, Z) \rightarrow (A, Z - 2) + e^+ \quad (0\nu\beta^+\text{EC}), \quad (8)$$

$$2e_b^- + (A, Z) \rightarrow (A, Z - 2)^* \quad (0\nu\text{ECEC}). \quad (9)$$

Observation of one of those processes would also imply the non-conservation of lepton number. The rates depend on the particle physics parameters in the same way as $0\nu\beta\beta$ does. The creation of two positrons reduces the phase space and renders rates for $0\nu\beta^+\beta^+$ very low. Somewhat less suppressed are ($0\nu\beta^+\text{EC}$) processes. In

$0\nu\text{E}^2\text{EC}$ the final atom (and sometimes the nucleus) are in excited states and generate photons (and γ rays). The rate is low, unless a resonance can be met. This occurs⁴⁵ for certain $0\nu\text{E}^2\text{EC}$ modes, if the initial and final states of the system are degenerate in energy. Here the $^{152}\text{Gd}-^{152}\text{Sm}$ transition has, via Penning-trap mass-ratio measurements, recently been identified as an interesting candidate for neutrino-less double electron capture⁴⁶, though it is currently unclear if an experiment competitive to $0\nu\beta\beta$ -searches can be realized. The current limits of the reactions (7,8,9) are summarized in¹¹. The main focus of future experiments is on the standard process $0\nu\beta\beta$ in Eq. (1). The other reactions could however be used to distinguish different $0\nu\beta\beta$ -mechanisms from each other, see Section 6.

3. Nuclear physics aspects

Nuclear physics is (unfortunately) an almost irreducible difficulty in making interpretations of neutrino-less double beta decay. Observation of the process means of course the proof of lepton number violation, but more precise particle physics interpretations suffer from any nuclear physics uncertainty. The calculation of the Nuclear Matrix Element (NME) \mathcal{M} is a complicated many body nuclear physics problem as old as $0\nu\beta\beta$. It basically describes the overlap of the nuclear wave functions of the initial and final states. A nuclear model typically has a set of single-particle states with a number of possible wave function configurations, and diagonalizes a Hamiltonian in a mean background field. A general property of solving Hamiltonians is that the energy levels are rather stable in what regards small modifications. Wave functions, and hence overlap, are however very sensitive to small modifications of the Hamiltonian, and this is the origin of the uncertainty in the values of NMEs.

3.1. Standard mechanism

Most theoretical work has been invested into the study of the standard mechanism of light neutrino exchange, on which we will focus in the following discussion. The process is evaluated as two pointlike Fermi vertices and the exchange of a light neutrino with momentum of about $q \simeq 0.1$ GeV, corresponding to the average distance $r \simeq 1/q \simeq 1$ fm between the two decaying nuclei. Since the neutrino is very light with respect to the energy scale one denotes the situation as a “long-range process”.

The expression for the decay rate is

$$\Gamma^{0\nu} = G^{0\nu}(Q, Z) |\mathcal{M}^{0\nu}|^2 \frac{\langle m_{ee} \rangle^2}{m_e^2}, \quad (10)$$

with the phase space factor $G^{0\nu}(Q, Z)$, $\langle m_{ee} \rangle$ the particle physics parameter^a in case of light neutrino exchange (to be defined in Section 4), and $\mathcal{M}^{0\nu}$ the NME.

^aSometimes one includes the electron mass m_e^2 in the phase space factor.

The quantity $\langle m_{ee} \rangle$ is usually called the “effective mass”, or the “effective electron neutrino mass”. The 5 main approaches to tackle the problem are the Quasi-particle Random Phase Approximation (QRPA, including its many variants and evolution steps)^{47,48}, the Nuclear Shell Model (NSM)⁴⁹, the Interacting Boson Model (IBM)⁵⁰, the Generating Coordinate Method (GCM)⁵¹, and the projected Hartree-Fock-Bogoliubov model (pHFB)⁵². We will not go into comparing in detail the different procedures, and refer the reader to the cited papers and the reviews^{2,3,4,5,6,7,8,9,10}. One example on how the approaches differ is to note that QRPA calculations can take into account a huge number of single particle states but only a limited set of configurations, whereas in the NSM the situation is essentially the opposite. The issue of which method should be used is far from settled. Another point are short-range correlations (SRC), since the main contribution to NMEs comes from internucleon distances $r \lesssim (2-3) \text{ fm}$ ⁵³, and the nucleons tend to overlap. SRC take the hard core repulsion into account. There are different proposals on how to treat SRC, namely via a Jastrow-like function, Unitary Correlation Operator Method (UCOM), or Coupled Cluster Method (CCM). The Jastrow method leads typically to a reduction of NMEs by about 20% while UCOM and CCM both reduce NME by about 5% as compared to calculations without SRC^{53,47}.

In contrast to $2\nu\beta\beta$, which involves only Gamov-Teller transitions through intermediate 1^+ states (because of low momentum transfer), $0\nu\beta\beta$ involves all multipolarities in the intermediate odd-odd $(A, Z+1)$ nucleus, and contains a Fermi and a Gamov-Teller part (plus a negligible tensor contribution from higher order currents):

$$\mathcal{M}^{0\nu} = \left(\frac{g_A}{1.25} \right)^2 \left(\mathcal{M}_{\text{GT}}^{0\nu} - \frac{g_V^2}{g_A^2} \mathcal{M}_{\text{F}}^{0\nu} \right). \quad (11)$$

The matrix elements for the final and initial states $|f\rangle$ and $|i\rangle$ can be written as

$$\begin{aligned} \mathcal{M}_{\text{GT}}^{0\nu} &= \langle f | \sum_{lk} \sigma_l \sigma_k \tau_l^- \tau_k^- H_{\text{GT}}(r_{lk}, E_a) | i \rangle, \\ \mathcal{M}_{\text{F}}^{0\nu} &= \langle f | \sum_{lk} \tau_l^- \tau_k^- H_{\text{F}}(r_{lk}, E_a) | i \rangle, \end{aligned} \quad (12)$$

where $r_{lk} \simeq 1/q \simeq 1/(0.1 \text{ GeV})$ is the distance between the two decaying neutrons and E_a is an average energy (closure approximation due to the large momentum of the virtual neutrino). The “neutrino potential”

$$H(x, y) \propto \frac{1}{x} \int_0^\infty dq \frac{\sin qx}{x + y - (E_i + E_f)/2} \quad (13)$$

integrates over the virtual neutrino momenta. The two emitted electrons are usually described in s -wave form because one focusses on $0_{\text{g.s.}}^+ \rightarrow 0_{\text{g.s.}}^+$ transitions. p -wave emission, which would lead to transitions to excited states, is suppressed in the standard neutrino exchange mechanism³, see Section 6.2. The $2\nu\beta\beta$ matrix elements can be written as (note the different energy dependence in comparison with the

Table 5. Dimensionless NMEs calculated in different frameworks, normalized to $r_0 = 1.2$ fm and $g_A = 1.25$. The method used to take into account short range correlations is indicated in brackets. There is also a pseudo- $SU(3)$ model⁵⁸ for the highly deformed nucleus ^{150}Nd , with a matrix element 1.00. Taken from⁵⁵.

Isotope	NSM (UCOM) ⁴⁹	Tübingen (CCM) ⁴⁷	Jyväskylä (UCOM) ⁴⁸	IBM (Jastrow) ⁵⁰	GCM (UCOM) ⁵¹	pHFB (mixed) ⁵²
^{48}Ca	0.85	-	-	-	2.37	-
^{76}Ge	2.81	4.44 - 7.24	4.195 - 5.355	4.636 - 5.465	4.6	-
^{82}Se	2.64	3.85 - 6.46	2.942 - 3.722	3.805 - 4.412	4.22	-
^{96}Zr	-	1.56 - 2.31	2.764 - 3.117	-	5.65	2.24 - 3.46
^{100}Mo	-	3.17 - 6.07	3.103 - 3.931	3.732 - 4.217	5.08	4.71 - 7.77
^{110}Pd	-	-	-	-	-	5.33 - 8.91
^{116}Cd	-	2.51 - 4.52	2.996 - 3.935	-	4.72	-
^{124}Sn	2.62	-	-	-	4.81	-
^{130}Te	2.65	3.19 - 5.50	3.483 - 4.221	3.372 - 4.059	5.13	2.99 - 5.12
^{136}Xe	2.19	1.71 - 3.53	2.38 - 2.802	-	4.2	-
^{150}Nd	-	3.45	-	2.321 - 2.888	1.71	1.98 - 3.7

NMEs for $0\nu\beta\beta$)

$$\mathcal{M}_{\text{GT}}^{2\nu} = \sum_n \frac{\langle f | \sum_a \sigma_a \tau_a^- | n \rangle \langle n | \sum_b \sigma_b \tau_b^- | i \rangle}{E_n - (M_i - M_f)/2}, \quad (14)$$

$$\mathcal{M}_{\text{F}}^{2\nu} = \sum_n \frac{\langle f | \sum_a \tau_a^- | n \rangle \langle n | \sum_b \tau_b^- | i \rangle}{E_n - (M_i - M_f)/2},$$

where the sum over n includes only 1^+ states. This is the reason why $2\nu\beta\beta$ gives only indirect information on $0\nu\beta\beta$.

We would like to stress here that care has to be taken when different calculations are compared^{54,55}: for instance, NMEs are made dimensionless by putting a factor $1/R_A^2 = 1/(r_0 A^{\frac{1}{3}})^2$ in the phase space factor (in the convention of Eq. (11) the phase space becomes independent of g_A), where in the nuclear radius R_A the parameter r_0 is sometimes chosen as 1.1 fm or 1.2 fm. The axial-vector coupling g_A is often chosen to be 1.25 or 1.0. In addition, it is often overlooked (see the discussion in^{54,56}) that the phase space factors $G^{0\nu}(Q, Z)$ can differ by up to order 10%, for instance when one compares the results from⁶ or⁵⁷. The results from⁶ are given in Table 1. In Table 5 and Fig. 3 we give a compilation⁵⁵ of NME values from different calculations (see Refs.^{59,60,61} for similar recent compilations). For definiteness, we will often apply the values of this table in what follows. Main features of the current status are that NMEs using QRPA seem to agree with each other and also with IBM calculations. NSM evaluations are consistently smaller and show little dependence on Z . However, it is encouraging that conceptually different approaches give results in the same ballpark. All in all, there has been some improvement in recent years, in particular the number of groups and approaches, as well as experimental support, has increased. However, full understanding and/or consensus has not been reached yet. Currently, one has to take the uncertainty at face value and keep it in

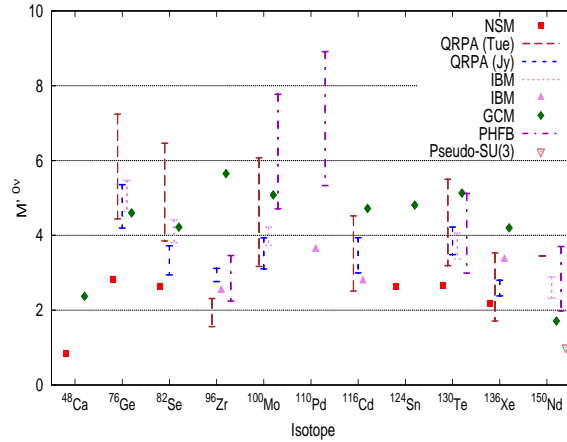


Fig. 3. Nuclear Matrix Elements for $0\nu\beta\beta$, different isotopes and calculational approaches. 'Tue' and 'Jy' are both QRPA results.

mind when interpreting the results of $0\nu\beta\beta$ experiments. Table 2 gives the current limits on the effective mass $\langle m_{ee} \rangle$ obtained with the NME compilation from Table 5 and the phase space factors from Table 1. The best limit on $\langle m_{ee} \rangle$ is provided by ^{76}Ge , but, as we will see, for some other mechanisms stronger limits stem from other isotopes, in particular ^{130}Te .

If available, we include uncertainties of the NMEs in Table 5 and Fig. 3. However, not all authors provide errors in their calculations. Those theoretical uncertainties can arise from varying g_A , g_{pp} (the particle-particle strength parameter in QRPA models), or other model details. One can distinguish here between correlated (e.g. the use of SRC or the value of g_A or g_{pp}) and uncorrelated errors (e.g. the model space of the single particle base)⁶². Eventually, a multi-isotope determination of $0\nu\beta\beta$ would be preferable, to disentangle the different types of errors. This is the **second reason for multi-isotope determination**. Ideally, if there was one adjustable parameter x in the calculations, then two measurements would suffice to fix $\langle m_{ee} \rangle$ and x (up to degeneracies). A third result would overconstrain the system⁶³ and allow for cross checks. This requires analyses of degeneracies and realistic estimates of theoretical errors, an effort which has recently started⁶². With the factorization in Eq. (4) it is clear that the ratios of two measured half-lives are

$$\frac{T_{1/2}^{0\nu}(A_1, Z_1)}{T_{1/2}^{0\nu}(A_2, Z_2)} = \frac{G(Q_2, Z_2) |\mathcal{M}(A_2, Z_2)|^2}{G(Q_1, Z_1) |\mathcal{M}(A_1, Z_1)|^2}, \quad (15)$$

i.e. the particle physics parameter drops out. The ratio is sensitive to the NME calculation⁶³, and systematic errors are expected to cancel. Fig. 4, taken from⁶², shows the error ellipses of matrix elements within a QRPA analysis.

Free parameters of an Ansatz can in principle also be fixed or tested by other means, for instance the particle-particle strength parameter g_{pp} in QRPA models can be adjusted to reproduce the $2\nu\beta\beta$ ⁶⁴, single beta decay⁶⁵ or electron capture rates. Overconstraining the parameters is possible if data on all these processes is available⁶⁶.

In recent years the uncertainty of the individual approaches to NMEs, which was somewhat overestimated in the past⁶⁷, has been reduced. An experimental program to support the calculations with as much information as possible was launched⁶⁸, including charge exchange reactions⁶⁹ to determine Gamov-Teller transition strengths. The latter are directly related to $2\nu\beta\beta$ matrix elements; applying the results to $0\nu\beta\beta$ requires theoretical input, see e.g.⁷⁰. Occupation numbers of neutron valence orbits in the initial and final nuclei are not known very well, and measurements⁷¹ via nucleon transfer reactions are helpful for all NME approaches. Muon capture rates can also be useful⁷², because the momentum transfer is of order $m_\mu \simeq 100$ MeV, i.e. of the same order as for $0\nu\beta\beta$. Determinations of Q -values⁷³ with precision spectroscopy⁷⁴ are also ongoing. This is particularly helpful for experiments in which the energy resolution is comparable to the current uncertainty of the Q -value. Another motivation for precise Q -value determinations is the identification of candidates for $0\nu\text{ECEC}$ which show resonance behavior, as mentioned

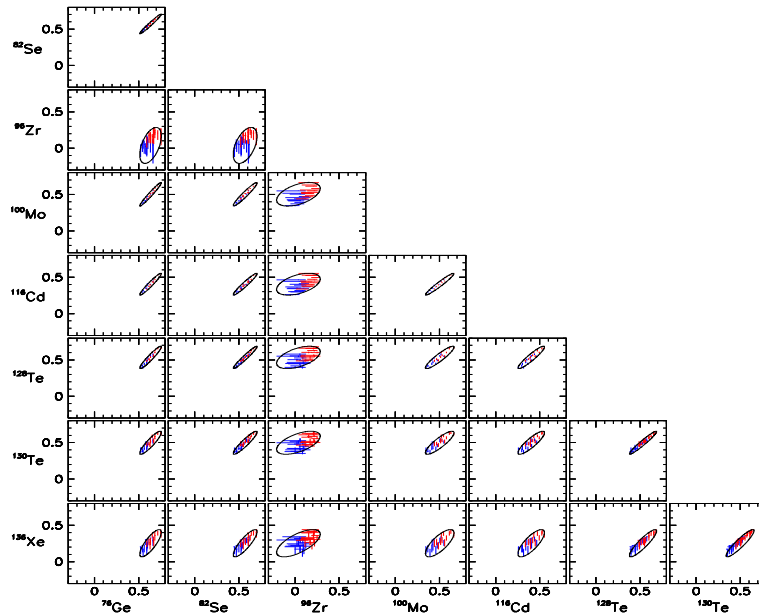


Fig. 4. 1σ error ellipses (logarithms of the NMEs) within QRPA calculations. The major axis corresponds to variation of the short-range correlation model (blue is Jastrow, red is UCOM) and g_A , while the minor axis corresponds to variations of g_{pp} . Taken from⁶².

above.

The QRPA particle-particle strength parameter g_{pp} can be fixed by the measured $2\nu\beta\beta$ rates and used as input for $0\nu\beta\beta$ predictions. However, using this g_{pp} value for calculating the rates of beta-decay or electron capture of the intermediate double beta decay isotope sometimes fails. One particular observational approach to these issues is the TITAN-EC experiment⁷⁵, which aims at testing with ion traps the badly known electron capture rates of the intermediate odd-odd state of double beta decay via observing the de-excitation X -rays.

It is expected that the future the uncertainty in the NMEs will further decrease, though (owing to the enormous complexity of the problem) the precision by the end of the decade will probably not be better than 20%.

3.2. *Non-standard mechanisms*

The evaluation of NMEs in non-standard mechanisms is a less well developed field, with less calculations available, and often only within one particular nuclear physics approach. In general the NMEs can obtain now contributions from Fermi, Gamov-Teller, pseudo-scalar, tensor, etc. contributions, and the realization of $0\nu\beta\beta$ can differ from the standard mechanism in

- (i) the Lorentz structure of the currents (e.g. right-handed currents);
- (ii) the mass scale of the exchanged particle (e.g. exchange of heavy SUSY particles);
- (iii) the number of particles in the final states (e.g. modes with additional Majoron emission);

A frequent feature here is that the scale of lepton number violating physics is larger than the momentum transfer or nuclear energies, in which case one speaks of a “short-range process”. Non-standard physics including light neutrino exchange, hence long-range, is however also possible. Within QRPA, a general Lorentz-invariant parametrization of the $0\nu\beta\beta$ decay rate has been developed for long-⁷⁶ and short-range⁷⁷ processes (these papers are in fact the only entries on SPIRES with the word “superformula” in the title). In those works the most general Lagrangian for $0\nu\beta\beta$ was written down and each term includes an individual prefactor ϵ_i . These ϵ_i can in principle via Fierz-transformations be translated (see also⁷⁸) into the particle physics parameters of the alternative realizations of $0\nu\beta\beta$ which we will discuss in Section 5.

It is possible that the different Lorentz structure leads to additional contributions to the NMEs, which are not present in other realizations. Different Lorentz structure implies also that the energies of the individual electrons, and their angular distribution, may differ from the standard mechanism^{3,79,80}. Further potential differences are modified relations between the rate of $0\nu\beta\beta$ and $0\nu\beta\beta^+EC$ ⁸¹, or with the decay rate to excited states^{82,83,84,85}. Some details will be discussed in Section

6.2. Short distance physics implies that the heavy particles with mass M_X can be integrated out and the pure particle physics amplitude is inversely proportional to M_X or M_X^2 , depending on whether it is a fermion or boson. A nuclear aspect of short distance physics is that the inner structure of the nucleons becomes relevant, which is taken into account by multiplying the weak nucleon vertices with (dipole) form factors⁸⁶

$$g_A(q^2) = \frac{g_A}{(1 - q^2/M_A^2)^2}, \quad (16)$$

with a mass parameter $M_A^2 \simeq (0.9 \text{ GeV})^2$. This introduces e.g. for heavy neutrino exchange a dependence proportional to M_A^2 , after an integration over the neutrino momenta has been performed in the potential Eq. (13). Here the form factor avoids the otherwise exponential suppression of the amplitude due to the repulsion of the nuclei. Finally, if additional particles are emitted in addition to the two electrons, such as in Majoron modes (Section 5.5), significant phase space effects can be expected.

Another aspect of heavy particle exchange is that pion exchange can dominate^{87,88}. This means that the pions which are present in the nuclear medium undergo transitions like $\pi^- \rightarrow \pi^+ e^- e^-$, i.e. the hadronization procedure of the quark level diagram differs from the 2 nucleon mode discussed so far. Though the probability of finding pions in the nuclear soup is less than 1, this can be compensated by the fact that the suppression due to the short-range nature of the usual 2 nucleon mode is absent, because low mass pions can mediate between more distant nucleons. One or both of the two initial quarks can be placed into a pion. In fact, R -parity violating SUSY contributions (Section 5.4), turn out to be dominated by pion NMEs.

We will discuss aspects relevant to particular non-standard mechanisms and means to distinguish them, from one another and from the standard one, in the later sections which deal with the respective mechanisms. Different realizations of the decay influence the NMEs in a way which depends on the isotope and on particle physics. Therefore, eventually a multi-isotope determination of $0\nu\beta\beta$ would be preferable, in order to disentangle the different mechanisms^{89,90,91,92,93}, see Section 6. This is the **third reason for multi-isotope determination**.

4. Standard Interpretation

In this Section we will discuss the standard mechanism of neutrino-less double beta decay, let us repeat for convenience the definition:

Neutrino-less double beta decay is mediated by light and massive Majorana neutrinos (the ones which oscillate) and all other mechanisms potentially leading to $0\nu\beta\beta$ give negligible or no contribution.

We will first summarize the current status of our understanding of lepton mixing and neutrino mass, before discussing the amount of information encoded in $0\nu\beta\beta$ combined with the standard interpretation. Readers who are very familiar

with neutrino physics can go directly to Section 4.2 and skip the summary of neutrino physics in Section 4.1.

4.1. *Neutrino physics*

Most part of the review will deal with the standard, and presumably best motivated, interpretation of $0\nu\beta\beta$, light massive Majorana neutrino exchange. We will first review the current theoretical and phenomenological status of neutrino physics.

4.1.1. *Neutrino mass and mixing: theoretical origin*

The theory behind neutrino mass and lepton mixing has been reviewed in several places^{94,95,96,97}. Lepton mixing is rather different from quark mixing. In addition, the mass of the two lepton partners in an $SU(2)_L$ doublet (e.g. ν_e and e) is extremely hierarchical, in sharp contrast to the partners in quark doublets (e.g. u and d , with $m_u = \mathcal{O}(m_d)$). It is natural to believe that these discrepancies are related to special properties of the neutrinos. Indeed, most, if not all, theorists believe that neutrinos are Majorana particles. This is the case in basically all Grand Unified Theories (GUTs), and also from an effective theory point of view, in which non-renormalizable higher dimensional operators invariant under the SM gauge group are constructed. The lowest dimensional (Weinberg) operator is unique, and reads⁹⁸

$$\mathcal{L}_{\text{eff}} = \frac{1}{2} \frac{h_{\alpha\beta}}{\Lambda} \overline{L_\alpha^c} \tilde{\Phi} \tilde{\Phi}^T L_\beta \xrightarrow{\text{EWSB}} \frac{1}{2} (m_\nu)_{\alpha\beta} \overline{\nu_\alpha^c} \nu_\beta, \quad (17)$$

Here the superscript ‘ c ’ denotes the charge-conjugated spinor, $L_\alpha = (\nu_\alpha, \alpha)^T$ are the lepton doublets of flavor $\alpha = e, \mu, \tau$ and Φ is the Higgs doublet with vacuum expectation value $v = 174$ GeV. A Majorana neutrino mass matrix is induced by this operator, given by $m_\nu = h v^2 / \Lambda$. With the typical mass scale of $m_\nu \simeq 0.05$ eV, it follows that $\Lambda \simeq 10^{15}$ GeV, tantalizingly close to the GUT scale. This is one of the main reasons why neutrino physics is popular: large scales are probed by small neutrino masses. It has been shown that within the minimal standard electroweak gauge model, there are only three tree-level realizations⁹⁹ of the Weinberg operator. One is the canonical type I seesaw mechanism¹⁰⁰ with right-handed neutrinos. Another approach is introducing a scalar Higgs triplet (type II, or triplet seesaw¹⁰¹), and the third one involves hypercharge-less fermion triplets (type III seesaw¹⁰²). In Table 6 we summarize the main approaches for generating small neutrino mass.

Taking first the standard type I seesaw as an example, one introduces 3 (actually 2 would suffice) Majorana neutrinos $N_{R,i}$, which have a Majorana mass matrix M_R . After electroweak symmetry breaking a Dirac mass term with the SM neutrinos is present and the full Lagrangian for neutrino masses is

$$\mathcal{L} = -\frac{1}{2} M_R \overline{N_R} N_R^c - m_D \overline{N_R} \nu_L = -\frac{1}{2} (\overline{\nu_L^c}, \overline{N_R}) \begin{pmatrix} 0 & m_D^T \\ m_D & M_R \end{pmatrix} \begin{pmatrix} \nu_L \\ N_R^c \end{pmatrix}, \quad (18)$$

with $N_R = (N_{R1}, N_{R2}, N_{R3})$ and $\nu_L = (\nu_e, \nu_\mu, \nu_\tau)_L$. We see that the combination of a Dirac and a Majorana mass term is a Majorana mass term, no matter how

Table 6. Tree-level approaches to small neutrino mass classified according to the ingredient which has to be added to the SM, and the electroweak quantum numbers of the new particles. LNV denotes Lepton Number Violation.

approach	ingredient	$SU(2)_L \times U(1)_Y$ quantum number of messenger	\mathcal{L}	m_ν	scale
“SM” (Dirac mass)	RH ν	$N_R \sim (1, 0)$	$h \overline{N_R} \Phi L$	$h v$	$h = \mathcal{O}(10^{-12})$
“effective” (dim 5 operator)	new scale + LNV	–	$h \overline{L^c} \Phi \Phi L$	$\frac{h v^2}{\Lambda}$	$\Lambda = \frac{1}{h} \left(\frac{0.1 \text{ eV}}{m_\nu} \right) 10^{14} \text{ GeV}$
“direct” (type II seesaw)	Higgs triplet + LNV	$\Delta \sim (3, 2)$	$h \overline{L^c} \Delta L + \mu \Phi \Phi \Delta$	$h v_T$	$\Lambda = \frac{1}{h \mu} M_\Delta^2$
“indirect 1” (type I seesaw)	RH ν + LNV	$N_R \sim (1, 0)$	$h \overline{N_R} \Phi L + \overline{N_R} M_R N_R^c$	$\frac{(h v)^2}{M_R}$	$\Lambda = \frac{1}{h} M_R$
“indirect 2” (type III seesaw)	fermion triplets + LNV	$\Sigma \sim (3, 0)$	$h \overline{\Sigma} L \Phi + \text{Tr} \overline{\Sigma} M_\Sigma \Sigma$	$\frac{(h v)^2}{M_\Sigma}$	$\Lambda = \frac{1}{h} M_\Sigma$

small the Majorana mass is. Being SM singlets, the scale of M_R is not connected to the only energy scale of the SM (the Higgs vacuum expectation value), and hence can be arbitrarily high. Integrating out the heavy states, or block-diagonalizing^b the mass matrix in Eq. (18) gives a Majorana mass term for the light neutrinos,

$$m_\nu = -m_D^T M_R^{-1} m_D, \quad (19)$$

plus terms of order m_D^4/M_R^3 . The states for which this mass matrix is valid are the initial ν_L plus a contribution of N_R^c , which is however suppressed by m_D/M_R . We see that the Weinberg operator is realized with $\Lambda \simeq M_R$.

Often one considers a triplet term for neutrino masses, generated by an $SU(2)_L$ triplet scalar with non-zero vev v_L of its neutral component. The coupling of the triplet to two lepton doublets with the Yukawa coupling matrix h gives a neutrino mass $m_\nu = M_L$, i.e. a direct contribution (see Section 5.2). Of course, both the type I and the type II term could be present. In this case the zero in the upper left entry of Eq. (18) is filled with a term M_L . The neutrino mass matrix in this case reads

$$m_\nu = M_L - m_D^T M_R^{-1} m_D. \quad (20)$$

Finally, type III seesaw introduces 3 hypercharge-less fermion triplets (one for each massive light neutrino), whose neutral components play the role of the N_{Ri} of type I seesaw.

What about production of low scale seesaw messengers at colliders? A recent review on the situation can be found in¹⁰³. While Majorana neutrino production proves difficult because of the constraint of its small mixing with SM particles, Higgs and fermion triplets have gauge quantum numbers and can be observed up to TeV masses. Note that in left-right symmetric models, or models with gauged

^bThe condition for this is that the eigenvalues of M_R are much heavier than the entries of m_D .

$B - L$, the right-handed neutrinos can have gauge interactions and can be produced more easily at colliders. The lepton number violation associated with the seesaw messengers can lead to their identification and spectacular *like-sign lepton events*. For this to be realized one needs to bring the seesaw scale down to TeV, see¹⁰⁴ for a recent review on how to achieve this.

It is clear that, either way, neutrinos are Majorana particles, i.e.

$$\nu_i^c = C \bar{\nu}_i^T = \nu_i. \quad (21)$$

Here we have chosen a convention in which there is no phase in the above relation.

In general the mass matrices for neutrinos (m_ν) and for charged leptons (m_ℓ) are non-trivial. Diagonalizing those matrices with unitary^c U_ν and U_ℓ , respectively, results in the charged current term in the appearance of the Pontecorvo-Maki-Nakagawa-Sakata (PMNS) matrix $U = U_\ell^\dagger U_\nu$:

$$\mathcal{L}_{CC} = -\frac{g}{\sqrt{2}} \bar{\ell}_\alpha \gamma^\mu U_{\alpha i} \nu_i W_\mu^- . \quad (22)$$

In the basis in which the charged leptons are real and diagonal, the neutrino mass matrix is diagonalized by U . It is useful for our purposes to stay in this basis, in which the mass matrix for Majorana neutrinos can be written as

$$m_\nu = U^* m_\nu^{\text{diag}} U^\dagger, \text{ where } m_\nu^{\text{diag}} = \text{diag}(m_1, m_2, m_3). \quad (23)$$

The mass matrix is complex and symmetric; after rephasing of three phases there are 9 physical parameters. Because the mass term goes as $\bar{\nu}^c \nu \propto \nu^T \nu$, the Lagrangian is not invariant under a global transformation $\nu \rightarrow e^{i\phi} \nu$. The charge associated with this transformation, lepton number, is therefore not a conserved quantity and L is violated by two units^d. This is exactly what is required for the presence of neutrino-less double beta decay.

Another appealing prediction of seesaw is the possible generation of the baryon asymmetry of the Universe via leptogenesis¹⁰⁷. Here the heavy seesaw messengers decay out of equilibrium (Sakharov condition I) in the early Universe and, due to CP violating phases (condition II), create a lepton asymmetry which subsequently is transferred into a baryon asymmetry via $B + L$ violating (condition III) non-perturbative SM processes. In this context, proving the Majorana nature of neutrinos and the presence of CP violation in the lepton sector would strengthen our belief in this already very appealing mechanism. This remains true even though a model-independent connection between the low energy CP phases and the necessary CP violation for leptogenesis cannot be established¹⁰⁷. In general, taking the

^cStrictly speaking the matrix U_ν is not unitary in type I seesaw, due to mixing of the leptons with the heavy neutrinos. This is however usually a very small effect $|U_\nu U_\nu^\dagger - \mathbb{1}| \sim (m_D/M_R)^2$ and phenomenologically constrained to be less than a permille effect¹⁰⁵.

^dIt should be noted that there are alternatives to the seesaw mechanism, see¹⁰⁶ for a discussion. Examples are radiative mechanisms, supersymmetric scenarios, or extra-dimensional approaches. It can happen that lepton number is conserved in such frameworks and $0\nu\beta\beta$ cannot take place, but this is clearly a rare exception rather than the rule.

standard type I seesaw as an example, there are in total six CP phases, three of which get lost when the heavy Majorana neutrino mass matrix is integrated out to obtain m_ν (see Eq. (19)). In principle, one could construct models in which the “low energy phases” take CP conserving values, while the remaining three phases are responsible for leptogenesis^e. Leaving this seemingly unnatural possibility aside, one expects that CP violation in the lepton sector at low energy is present if there is “high energy” CP violation responsible for leptogenesis. One should however not expect that the Majorana phases are “more connected” to leptogenesis than the Dirac phase. At the fundamental (seesaw) scale, there are six CP phases and the three low energy phases will be some complicated function of these phases and the other seesaw parameters. From this point of view, the low energy Dirac and Majorana phases are not different from each other.

A final remark necessary here is that a link between $0\nu\beta\beta$ and the baryon asymmetry is *not guaranteed*. The often-made and popular statement that $0\nu\beta\beta$ -experiments probe the origin of matter in the Universe is not true. For instance, if neutrino mass is simply generated by a Higgs triplet, then this triplet alone cannot generate a baryon asymmetry, but $0\nu\beta\beta$ is very well possible.

4.1.2. Neutrino mass and mixing: observational status

Neutrino oscillations have been observed with solar, atmospheric and man-made (reactor, accelerator) neutrinos, see^{108,109} for extensive reviews on the status of neutrino physics. This implies that in the charged current term of electroweak interactions the neutrino flavor states ν_e, ν_μ and ν_τ are superpositions of neutrino mass states:

$$\nu_\alpha = U_{\alpha i}^* \nu_i, \quad (24)$$

where $\alpha = e, \mu, \tau$ and $i = 1, 2, 3$. The PMNS mixing matrix U is unitary and can be written in its standard parametrization as

$$U = \begin{pmatrix} c_{12}c_{13} & s_{12}c_{13} & s_{13}e^{-i\delta} \\ -s_{12}c_{23} - c_{12}s_{23}s_{13}e^{i\delta} & c_{12}c_{23} - s_{12}s_{23}s_{13}e^{i\delta} & s_{23}c_{13} \\ s_{12}s_{23} - c_{12}c_{23}s_{13}e^{i\delta} & -c_{12}s_{23} - s_{12}c_{23}s_{13}e^{i\delta} & c_{23}c_{13} \end{pmatrix} P, \quad (25)$$

where $s_{ij} = \sin \theta_{ij}$, $c_{ij} = \cos \theta_{ij}$ and δ is the “Dirac phase” responsible for CP violation in neutrino oscillation experiments. This phase is expressible in a parametrization independent form as a Jarlskog invariant:

$$J_{\text{CP}} = \text{Im} \{ U_{e1}^* U_{\mu 3}^* U_{e3} U_{\mu 1} \} = \frac{1}{8} \sin 2\theta_{12} \sin 2\theta_{23} \sin 2\theta_{13} \cos \theta_{13} \sin \delta, \quad (26)$$

where we have given it in its explicit form for the standard parameterization. In Eq. (25) we have included a diagonal phase matrix P , containing the two “Majorana

^eNote that the opposite case is also possible.

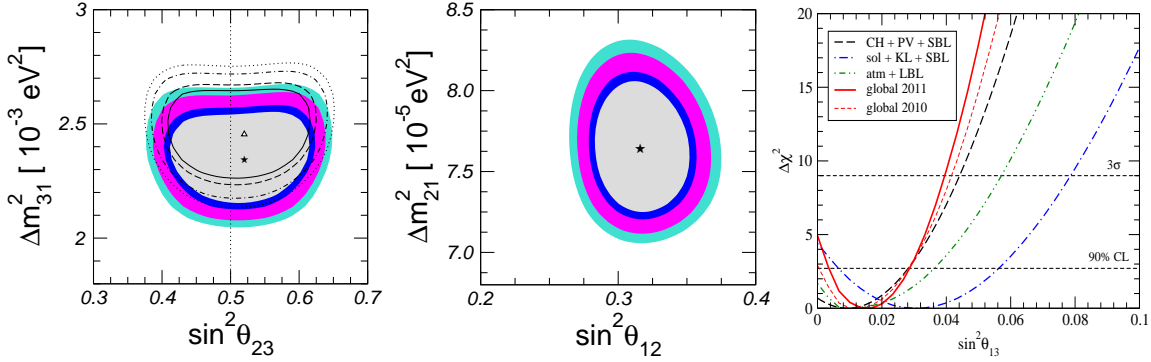


Fig. 5. Left plot: allowed ranges (lines are for NH, colored regions for IH) of $|\Delta m_{31}^2|$ and $\sin^2 \theta_{23}$ at 90%, 95%, 99% and 99.73%. Middle plot: allowed ranges Δm_{21}^2 and $\sin^2 \theta_{12}$. Right plot: constraints on $\sin^2 \theta_{13}$ from various experiments. Taken from¹¹³.

phases" α and β :

$$P = \text{diag}(1, e^{i\alpha}, e^{i(\beta+\delta)}). \quad (27)$$

These phases are physical¹¹⁰ if neutrinos are Majorana particles. Note that we have included δ in P , in which case the first row of the PMNS matrix is independent of δ . For three neutrinos we have therefore 9 physical parameters, three masses $m_{1,2,3}$, three mixing angles $\theta_{12}, \theta_{13}, \theta_{23}$ and three phases δ, α, β .

One can also define invariants for the Majorana phases¹¹¹, for instance $S_1 = \text{Im}\{U_{e1}U_{e2}^*\} = -c_{12}s_{12}c_{13}^2\sin\alpha$ and $S_2 = \text{Im}\{U_{e2}U_{e3}^*\} = s_{12}c_{13}s_{13}\sin(\delta-\beta)$. Note that CP violation due to the Majorana phases is present only if, in addition to $S_1 = \text{Im}\{U_{e1}U_{e2}^*\} \neq 0$, $\text{Re}\{U_{e1}U_{e2}^*\} \neq 0$ also holds. The reason for this is that the cases $\alpha, \beta = \pi/2$ correspond to the CP parities of the Majorana fields¹¹², which can be either positive or negative. Majorana phases are present because the mass term in the Lagrangian is proportional to $(m_\nu)_{\alpha\beta}\nu_\alpha^T\nu_\beta$ and a rephasing of the spinors ν_α can eliminate fewer phases than in the Dirac case, where the mass term is $(m_\nu)_{\alpha\beta}\bar{\nu}_\alpha\nu_\beta$. For N Majorana neutrinos, there are $N-1$ Majorana phases in addition to $\frac{1}{2}(N-2)(N-1)$ Dirac phases and $\frac{1}{2}N(N-1)$ mixing angles^f.

For three fermion families, neutrino oscillation experiments are sensitive to the three mixing angles, the two independent mass-squared differences (including their

^fThis counting is valid for active neutrinos only. For N massive families including $0 \neq N_s = N-3$ massive sterile neutrinos, one has $N-1 = N_s+2$ Majorana phases, $3(N-2) = 3(N_s+1)$ mixing angles and $2N-5 = 2N_s+1$ Dirac phases. The number of angles and Dirac phases is less because the $\frac{1}{2}N_s(N_s-1)$ rotations between sterile states are unphysical.

Table 7. Current values from global fits to the world's neutrino oscillation experiments. Taken from¹¹³. The values in brackets are for the inverted ordering.

parameter	best-fit $^{+1\sigma}_{-1\sigma}$	2σ	3σ
Δm_{21}^2 [10^{-5} eV ²]	$7.64^{+0.19}_{-0.18}$	$7.27 - 8.03$	$7.12 - 8.23$
$ \Delta m_{31}^2 $ [10^{-3} eV ²]	$2.45^{+0.09}_{-0.09}$ $(2.34^{+0.10}_{-0.09})$	$2.28 - 2.64$ $(2.17 - 2.54)$	$2.18 - 2.73$ $(2.08 - 2.64)$
$\sin^2 \theta_{12}$	$0.316^{+0.016}_{-0.016}$	$0.29 - 0.35$	$0.27 - 0.37$
$\sin^2 \theta_{23}$	$0.51^{+0.06}_{-0.06}$ $(0.52^{+0.06}_{-0.06})$	$0.41 - 0.61$ $(0.42 - 0.61)$	$0.39 - 0.64$ $(0.39 - 0.64)$
$\sin^2 \theta_{13}$	$0.017^{+0.007}_{-0.009}$ $(0.020^{+0.008}_{-0.009})$	≤ 0.031 (≤ 0.036)	≤ 0.040 (≤ 0.044)

sign), and the Dirac phase δ . The general formula for oscillation probabilities is

$$\begin{aligned}
 P(\nu_\alpha \rightarrow \nu_\beta) = & \delta_{\alpha\beta} - 4 \sum_{i>j} \text{Re} \left\{ U_{\alpha i}^* U_{\beta j}^* U_{\beta i} U_{\alpha j} \right\} \sin^2 \frac{\Delta m_{ij}^2 L}{4E} \\
 & + 2 \sum_{i>j} \text{Im} \left\{ U_{\alpha i}^* U_{\beta j}^* U_{\beta i} U_{\alpha j} \right\} \sin \frac{\Delta m_{ij}^2 L}{2E},
 \end{aligned} \tag{28}$$

with E the neutrino energy and L the baseline. To leading order, using the hierarchy of $\Delta m_\odot^2 \equiv \Delta m_{21}^2 \ll |\Delta m_{31}^2| \simeq |\Delta m_{32}^2| \equiv \Delta m_\text{A}^2$, this formula usually breaks down to two neutrino oscillation formulas. The angle θ_{12} and $\Delta m_{21}^2 \equiv \Delta m_\odot^2$ are responsible for solar neutrino (suitably modified with matter effects) and long-baseline reactor neutrino oscillations. Atmospheric neutrinos are governed by θ_{23} and Δm_{32}^2 , the same parameters which long-baseline accelerator neutrinos are sensitive to. Finally, θ_{13} (if non-zero) and Δm_{31}^2 are responsible for short-baseline reactor neutrino and long-baseline $\nu_\mu \rightarrow \nu_e$ oscillations. Non-zero θ_{13} also provides a link between the solar and atmospheric sector and is intensively searched for, as leptonic CP violation in oscillations would be absent if it was zero. Our current knowledge of the oscillation quantities is summarized in Fig. 5 and Table 7, taken from¹¹³. It is noteworthy that the sign of the (atmospheric) mass-squared difference is unknown, as are the three CP phases, thus including the Majorana phases. The hint¹¹⁴ towards non-zero θ_{13} recently exceeded the 3σ level¹¹⁵, after the T2K long-baseline experiment provided evidence for electron neutrino appearance¹¹⁶.

A recent review on the details of current and future determinations of the parameters can be found in Ref.¹⁰⁸. An extensive program to improve the precision on θ_{13} , θ_{23} and Δm_{31}^2 (including its sign) has been launched, while improvement in the precision of θ_{12} and Δm_{21}^2 is not on top of the neutrino community's agenda, mostly because they are currently the best-known parameters. As we will see below, precision determination of the solar parameters may be required if the inverted mass ordering is to be tested with $0\nu\beta\beta$. The unknown sign of the atmospheric mass-squared difference defines the mass ordering (see Fig. 6): normal for $\Delta m_\text{A}^2 > 0$,

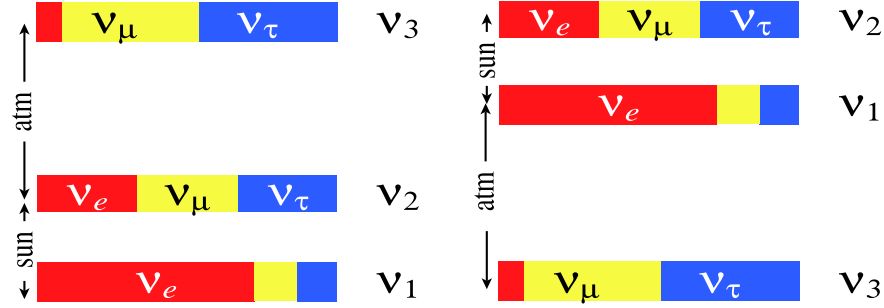


Fig. 6. Normal (left) vs. inverted (right) mass ordering. The red area denotes the electron content $|U_{ei}|^2$ in the mass state ν_i . Accordingly, the yellow and blue areas denote the muon and tau contents. Taken from¹⁰⁹.

inverted for $\Delta m_A^2 < 0$. The two larger masses for each ordering are given in terms of the smallest mass and the mass squared differences as

$$\begin{aligned} \text{normal:} \quad m_2 &= \sqrt{m_1^2 + \Delta m_\odot^2}, \quad m_3 = \sqrt{m_1^2 + \Delta m_A^2}, \\ \text{inverted:} \quad m_2 &= \sqrt{m_3^2 + \Delta m_\odot^2 + \Delta m_A^2}; \quad m_1 = \sqrt{m_3^2 + \Delta m_A^2}. \end{aligned} \quad (29)$$

Note that the oscillation data and the possible mass spectra and orderings are independent on whether neutrinos are Dirac or Majorana particles. The two possible mass orderings are shown in Fig. 6. Of special interest are the following three extreme cases:

$$\begin{aligned} \text{normal hierarchy (NH):} \quad m_3 &\simeq \sqrt{\Delta m_A^2} \gg m_2 \simeq \sqrt{\Delta m_\odot^2} \gg m_1, \\ \text{inverted hierarchy (IH):} \quad m_2 &\simeq m_1 \simeq \sqrt{\Delta m_A^2} \gg m_3, \\ \text{quasi-degeneracy (QD):} \quad m_0^2 &\equiv m_1^2 \simeq m_2^2 \simeq m_3^2 \gg \Delta m_A^2. \end{aligned} \quad (30)$$

As can be seen from Fig. 5 and Table 7, the current data is well described by so-called tri-bimaximal mixing¹¹⁷, corresponding to $\sin^2 \theta_{13} = 0 \times \cos^2 \theta_{13}$, $\sin^2 \theta_{12} = \frac{1}{2} \times \cos^2 \theta_{12}$ and $\sin^2 \theta_{23} = 1 \times \cos^2 \theta_{23}$:

$$U = \begin{pmatrix} \sqrt{\frac{2}{3}} & \sqrt{\frac{1}{3}} & 0 \\ -\sqrt{\frac{1}{6}} & \sqrt{\frac{1}{3}} & \sqrt{\frac{1}{2}} \\ \sqrt{\frac{1}{6}} & -\sqrt{\frac{1}{3}} & \sqrt{\frac{1}{2}} \end{pmatrix}. \quad (31)$$

The application of flavor symmetries to the fermion sector, in order to obtain this and other possible mixing schemes is a very active field of research. For references and an overview of flavor symmetry models, see¹¹⁸.

A longstanding issue in oscillation physics is the indication of the presence of sterile neutrinos. The LSND experiment¹¹⁹ found evidence for $\bar{\nu}_\mu \rightarrow \bar{\nu}_e$ transitions

which, when interpreted in terms of oscillations, are described by a $\Delta m^2 \sim \text{eV}^2$ and small mixing $\lesssim 0.1$. These values survive even when combined^{120,121,122} with the negative results from the KARMEN experiment¹²³. This mass scale cannot be compatible with solar and atmospheric oscillation and hence a fourth, sterile neutrino needs to be introduced. So-called 1+3 (3+1) scenarios would then be realized, in which one sterile neutrino is heavier (lighter) than the three active ones, separated by a mass gap of order eV. The MiniBooNE experiment was designed to test the LSND scale with different L and E , but very similar L/E . The results¹²⁴ could not rule out the LSND parameters, and are also compatible with the presence of 2 sterile neutrinos¹²⁵. In fact, the difference between MiniBooNE's neutrino and anti-neutrino results can be explained by two additional eV-like Δm^2 plus CP violation. Here one could envisage 2+3 or 3+2 scenarios, in which 2 sterile neutrinos lie above or below the three active ones, or 1+3+1 scenarios¹²⁶, in which one sterile neutrino is heavier than the three active ones and the other sterile neutrino is lighter. Recently, reactor neutrino fluxes have been re-evaluated and an underestimation of 3% with respect to previous results has been found¹²⁷. The null results of previous very short-baseline reactor experiments can now be interpreted as in fact being a deficit of neutrinos, which again is compatible with oscillations corresponding to $\Delta m^2 \sim \text{eV}^2$ and small mixing $\lesssim 0.1$. A recent analysis of short-baseline neutrino oscillation data in a framework with one or two sterile neutrinos can be found in Ref.¹²⁸. The global fit improves considerably when the existence of two sterile neutrinos is assumed.

We will discuss the situation on neutrino mass from now on. Neutrino mass can be measured in three and complementary different ways^g:

1) Kurie-plot experiments,

in which the non-zero neutrino mass influences the energy distribution of electrons in beta decays close to the kinematical endpoint of the spectrum. As long as the energy resolution is larger than the mass splitting, the spectrum is described by a function

$$(E_e - Q) \sqrt{(E_e - Q)^2 - m_\beta^2}, \quad (32)$$

where the observable neutrino mass parameter is

$$m_\beta \equiv \sqrt{\sum |U_{ei}|^2 m_i^2}. \quad (33)$$

The current limit to this quantity from spectrometer approaches is 2.3 eV at 95% C.L., obtained from the Mainz¹³⁰ and Troitsk¹³¹ collaborations. The KATRIN experiment^{132,133} has a design sensitivity of $m_\beta = 0.2$ eV at (90% C.L.) and a discovery potential of $m_\beta = 0.35$ eV with 5σ significance. It represents the ultimate

^gAlternatives such as time-of-flight measurements of supernova neutrinos cannot give comparable limits. Other ideas¹²⁹ are presumably not realizable.

spectrometer experiment for neutrino mass, in which an external source of beta emitters (tritium) is used. Further improvement of the limits must e.g. come from calorimeter approaches, where the source is identical to the detector. The MARE¹³⁴ proposal will use ¹⁸⁷Re modular crystal bolometers. A history of neutrino mass limits from beta decays and reviews of upcoming experiments can be found in¹³⁵. A different Ansatz called Project 8 aims to detect the coherent cyclotron radiation emitted by mildly relativistic electrons (like those in tritium decay) in a magnetic field. The relativistic shift of the cyclotron frequency allows to extract the electron energy from the emitted radiation¹³⁶. In principle, MARE and Project 8 can reach limits of 0.1 eV. Investigation of beta spectra is usually considered to be the least model-dependent Ansatz to probe neutrino mass. For instance, Refs.¹³⁷ have shown that admixture of right-handed currents can be not more than a 10% effect in KATRIN's determination of m_β ;

2) Cosmological and astrophysical observations

are sensitive to neutrino mass, see¹³⁸ for a review. In particular, effects of neutrinos in cosmic structure formation are used to extract limits on neutrino masses. The quantity which is constrained by such efforts is

$$\Sigma = \sum m_i, \quad (34)$$

familiar from the contribution of neutrinos to hot dark matter^h, $\Omega_\nu h^2 = \Sigma/(94.57 \text{ eV})$. Finite neutrino masses suppress the matter power spectrum on scales smaller than the free-streaming scale $k_{\text{FS}} \simeq 0.8 h m_i / \text{eV Mpc}^{-1}$. However, neutrino mass is highly degenerate with other cosmological parameters, for instance¹⁴⁰ with the dark energy equation of state parameter ω , so that one needs to break the degeneracies with different and complementary data sets. Besides cosmic microwave background (CMB) experiments, one can use the Hubble constant (H0) measurements, high-redshift Type-I supernovae (SN) results, information from large scale structure (LSS) surveys, the LSS matter power spectrum (LSSPS) and baryon acoustic oscillations (BAO). The impact on the neutrino mass limit is shown in Table 8, taken from¹⁴¹, in which a fit to a cosmological model allowing for neutrino mass, non-vanishing curvature, dark energy with equation of state $\omega \neq -1$, and the presence of new particle physics whose effect on the present cosmological observations can be parameterized in terms of additional relativistic degrees of freedom ΔN_{rel} , has been performed. As can be seen, depending on the data sets, the limit on Σ varies by a factor of 3. Future cosmological probes will add additional information, a summary of expectations for this is shown in Table 9.

At the present stage it is worth noting that precision cosmology and Big Bang nucleosynthesis mildly favor extra radiation in the Universe beyond photons and ordinary neutrinos. While this could be any relativistic degree of freedom, the in-

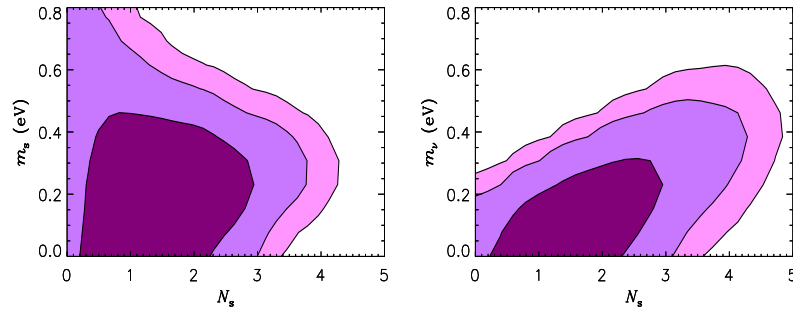
^hWhile one usually considers light neutrinos as a sub-leading part of dark matter, arguments in favor of neutrino hot dark matter are given in¹³⁹.

Table 8. 95% C.L. upper bound on the sum of the neutrino masses from different cosmological analyses. Taken from¹⁴¹.

Model	Observables	$\sum m_i$ [eV]
$\omega\text{CDM} + \Delta N_{\text{rel}} + m_\nu$	CMB+H0+SN+BAO	≤ 1.5
$\omega\text{CDM} + \Delta N_{\text{rel}} + m_\nu$	CMB+H0+SN+LSSPS	≤ 0.76
$\Lambda\text{CDM} + m_\nu$	CMB+H0+SN+BAO	≤ 0.61
$\Lambda\text{CDM} + m_\nu$	CMB+H0+SN+LSSPS	≤ 0.36
$\Lambda\text{CDM} + m_\nu$	CMB (+SN)	≤ 1.2
$\Lambda\text{CDM} + m_\nu$	CMB+BAO	≤ 0.75
$\Lambda\text{CDM} + m_\nu$	CMB+LSSPS	≤ 0.55
$\Lambda\text{CDM} + m_\nu$	CMB+H0	≤ 0.45

Table 9. Future probes of neutrino mass, with their projected sensitivity. Sensitivity in the short term means within the next few years, while long term means by the end of the decade. Taken from¹³⁸.

Probe	Potential sensitivity [eV] (short term)	Potential sensitivity [eV] (long term)
CMB	0.4–0.6	0.4
CMB with lensing	0.1–0.15	0.04
CMB + Galaxy Distribution	0.2	0.05–0.1
CMB + Lensing of Galaxies	0.1	0.03–0.04
CMB + Lyman- α	0.1–0.2	Unknown
CMB + Galaxy Clusters	–	0.05
CMB + 21 cm	–	0.0003–0.1

Fig. 7. 68%, 95% and 99% C.L. regions for the neutrino mass and thermally excited number of degrees of freedom N_s . The left plot is the $N_s + 3$ scheme, in which ordinary neutrinos have $m_\nu = 0$, while sterile states have a common mass scale m_s , hence $\Sigma \simeq N_s m_s$. The right plot is for the $3 + N_s$ scheme, where the sterile states are taken to be massless $m_s = 0$, and 3.046 species of ordinary neutrinos have a common mass m_ν , hence $\Sigma \simeq 3 m_\nu$. Taken from¹⁴⁵.

terpretation in terms of additional sterile neutrino species is straightforward (recall the discussion on sterile neutrinos from above). Fit results very well compatible with more radiation than the SM value have been found e.g. by the WMAP collaboration¹⁴² or in¹⁴³. This is supported by the recently reported higher ^4He

abundance¹⁴⁴, which in the framework of Big Bang Nucleosynthesis can be accommodated by additional relativistic degrees of freedom, as this leads to earlier freeze-out of the weak reactions, resulting in a higher neutron-to-proton ratio. In Fig. 7 the result of a recent fit¹⁴⁵ to cosmological data is shown, in which two situations are analyzed: massless active neutrinos plus N_s massive sterile states ($N_s + 3$ scheme); and N_s massless sterile states plus 3 massive active states ($3 + N_s$). The Planck satellite, with a projected sensitivity of ± 0.2 to the number of extra degrees of freedom, will be decisive in order to test this presence of additional radiation. It is rather interesting that hints for the presence of sterile neutrinos are given by fundamentally different probes: neutrino oscillations, Big Bang Nucleosynthesis and CMB + LSS.

Cosmological mass limits can be considered robust with respect to reasonable modifications of the Λ CDM model¹⁴⁶, in particular if different and complementary data sets are applied. However, several non-standard cosmologies exist for which no detailed study on the effect on the Σ bound has been performed yet, for instance coupled dark energy scenarios. Nevertheless, it is fair to say that neutrino masses heavier than $\Sigma \simeq 2$ eV or so would be rather surprising, and correspond to very unusual scenarios. Note however that any information about the neutrino mass can be obtained only by way of statistical inference from the observational data after a parametric model has been chosen as the basis for the analysis¹⁴⁶. This is a difference to the investigation of energy spectra in single or double beta decay experiments;

3) Neutrino-less Double Beta Decay

This possibility to test neutrino mass will be dealt with in Section 4.2.3 in some detail. In the ideal case, results from two or all three approaches to neutrino mass are present, and we will discuss this interesting case too. Neutrino mass limits from neutrino-less double beta decay need to assume that neutrinos are Majorana particles, and that no mechanism other than light neutrino exchange is responsible for the process. Let us note here that from $0\nu\beta\beta$ limits one can extract two different “masses”. First, we can extract the physical masses, i.e. the eigenvalues of the mass matrix. These quantities are the ones tested in the other approaches. Second, $0\nu\beta\beta$ tests directly the quantity $(m_\nu)_{ee}$, i.e. the ee element of the neutrino mass matrix in the charged lepton basis:

$$\sqrt{\frac{1}{T_{1/2}^{0\nu}}} \propto |(m_\nu)_{ee}| \quad \text{with} \quad (m_\nu)_{ee} = \frac{h_{ee} v^2}{\Lambda} \quad \text{in} \quad \mathcal{L}_{\text{eff}} = \frac{1}{2} \frac{h_{\alpha\beta}}{\Lambda} \bar{L}_\alpha^c \tilde{\Phi} \tilde{\Phi}^T L_\beta. \quad (35)$$

Thus, the decay width is directly proportional to the fundamental quantity which originates at the fundamental large (seesaw) scale, without any diagonalization procedure dependent on known and unknown parameters. Note that in order to extract neutrino mass limits from $0\nu\beta\beta$ one needs to assume the neutrinos are Majorana particles, and that no other mechanism contributes. We will comment later on the complementarity of the three neutrino mass observables.

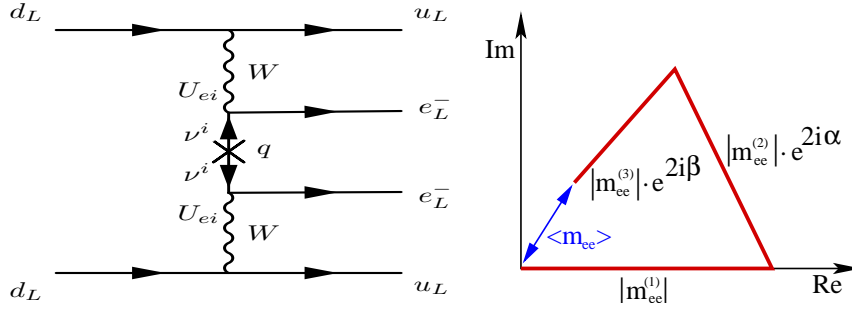


Fig. 8. Left: quark level Feynman diagram for the standard interpretation of neutrino-less double beta decay. Right: geometrical visualization of the effective mass.

4.2. Standard three neutrino picture and $0\nu\beta\beta$

In this Section we will summarize the standard analysis of neutrino-less double beta decay with the standard three neutrino framework. Several works have been devoted in the literature to this^{147,148,149,150,151,152,153,61}, an earlier review can be found in¹⁵⁴.

The Feynman diagram for $0\nu\beta\beta$ on the quark level in this interpretation is shown in Fig. 8. Due to the typical structure of the process it is sometimes called “lobster diagram”. The amplitude of the process is for the $V - A$ interaction of the SM proportional to

$$\begin{aligned} \sum G_F^2 U_{ei}^2 \gamma_\mu \gamma_+ \frac{\not{q} + m_i}{q^2 - m_i^2} \gamma_\nu \gamma_- &= \sum G_F^2 U_{ei}^2 \frac{m_i}{q^2 - m_i^2} \gamma_\mu \gamma_+ \gamma_\nu \\ &\simeq \sum G_F^2 U_{ei}^2 \frac{m_i}{q^2} \gamma_\mu \gamma_+ \gamma_\nu, \end{aligned} \quad (36)$$

where $\gamma_\pm = \frac{1}{2}(1 \pm \gamma_5)$, m_i is the neutrino mass, $q \simeq 100$ MeV is the typical neutrino momentum, and U_{ei} an element of the first row of the PMNS matrix. The linear dependence on the neutrino mass is expected from the requirement of a spin-flip, as the neutrino can be thought of being emitted as a right-handed state and absorbed as a left-handed state. In case the interactions are not left-handed at one of the vertices, the linear dependence on m_i will be absent; we will consider these cases later in Section 5.3. If both interactions are right-handed, the same linear dependence on m_i appears. Note that the amplitude is proportional to a coherent sum, which implies the possibility of cancellations. The decay width is proportional to the square of the so-called effective mass

$$\langle m_{ee} \rangle = \left| \sum U_{ei}^2 m_i \right| = \left| |m_{ee}^{(1)}| + |m_{ee}^{(2)}| e^{2i\alpha} + |m_{ee}^{(3)}| e^{2i\beta} \right|, \quad (37)$$

which is visualized in Fig. 8 as the sum of three complex vectors $m_{ee}^{(1,2,3)}$. If one cannot form a triangle with the $m_{ee}^{(1,2,3)}$, then the effective mass is non-zero. The Majorana phases 2α and 2β correspond to the relative orientation of the three

vectors. The standard analysis of the effective mass is the geometry of the three vectors expressed in terms of neutrino parameters. In the standard parametrization of the PMNS matrix we have

$$\begin{aligned} |m_{ee}^{(1)}| &= m_1 |U_{e1}|^2 = m_1 c_{12}^2 c_{13}^2, \\ |m_{ee}^{(2)}| &= m_2 |U_{e2}|^2 = m_2 s_{12}^2 c_{13}^2, \\ |m_{ee}^{(3)}| &= m_3 |U_{e3}|^2 = m_3 s_{13}^2. \end{aligned} \quad (38)$$

The individual masses can, using Eq. (29), be expressed in terms of the smallest mass and the mass-squared differences, whose currently allowed ranges, as well as those of the mixing angles, are given in Table 7. From Table 2 we can read off the current limit on the effective mass:

$$\langle m_{ee} \rangle \lesssim 0.5 \text{ eV}. \quad (39)$$

For later use we define the standard amplitude for light Majorana neutrino exchange:

$$\mathcal{A}_l \propto G_F^2 \frac{\langle m_{ee} \rangle}{q^2} \simeq 7 \times 10^{-18} \left(\frac{\langle m_{ee} \rangle}{0.5 \text{ eV}} \right) \text{ GeV}^{-5}. \quad (40)$$

Fig. 9 shows the future limits on the effective mass for different isotopes and half-life limits (see also^{59,61}). We have again used the NME compilation from Table 5.

The effective mass depends on 7 out of the 9 physical parameters of low energy neutrino physics (only θ_{23} and δ do not appear), hence contains an enormous amount of information. It is the only realistic observable in which the two Majorana phases appear. For the other five quantities there will be complementary information from oscillation experiments or other experiments probing neutrino mass. It is also noteworthy that $\langle m_{ee} \rangle$ is the ee element of the neutrino mass matrix m_ν , see Eq. (23), which is a fundamental object in the low energy Lagrangian. In terms of the origin of neutrino mass, $\langle m_{ee} \rangle$ is $h_{ee} v^2/\Lambda$, see Eq. (17) and the realizations of Λ in terms of fundamental mass scales in Table 6.

A typical analysis of the effective mass would plot it against the smallest neutrino mass, while varying the Majorana phases and/or the oscillation parameters. This results in Fig. 10, for which the best-fit values and 3σ ranges of the oscillation parameters have been used. The blue shaded area is of interest because it can only be covered if the CP phases are non-trivial, i.e. if $\alpha, \beta \neq 0, \pi/2$. The values $\alpha, \beta = 0, \pi/2$ correspond to CP conserving situations, associated with positive or negative signs of the neutrino masses, and the resulting span of $\langle m_{ee} \rangle$ is also indicated in the figure. For comparison, the other mass-related observables Σ and m_β are shown as a function of the smallest neutrino mass in Fig. 11. Actually, the smallest neutrino mass is not really an observable, so it is interesting to plot the effective mass against Σ and m_β , which is shown in Fig. 12. The analytical expressions for the effective mass in certain extreme cases are given in Fig. 13.

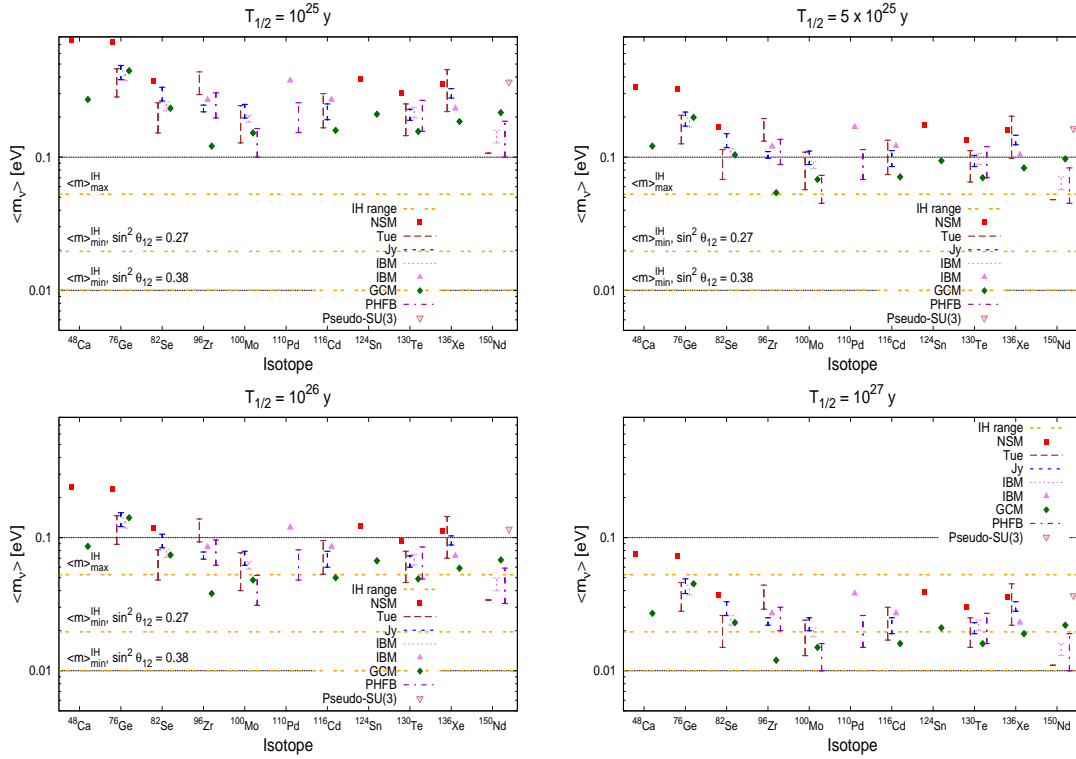


Fig. 9. Limits on the effective mass for different half-life limits. The horizontal lines are the maximal and minimal values of $\langle m_{ee} \rangle$ in the inverted mass ordering.

4.2.1. Normal mass ordering

Let us begin with the normal mass ordering. The effective mass is

$$\langle m_{ee} \rangle^{\text{nor}} = \left| m_1 c_{12}^2 c_{13}^2 + \sqrt{m_1^2 + \Delta m_{\odot}^2} s_{12}^2 c_{13}^2 e^{2i\alpha} + \sqrt{m_1^2 + \Delta m_{\text{A}}^2} s_{13}^2 e^{2i\beta} \right|. \quad (41)$$

The maximum of the effective mass is obtained when the Majorana phases are given by $\alpha = \beta = 0$. The case of small m_1 , which corresponds to a normal hierarchy (NH) defines the “hierarchical regime” in Fig. 13. Neglecting m_1 gives

$$\langle m_{ee} \rangle^{\text{NH}} = \left| \sqrt{\Delta m_{\odot}^2} s_{12}^2 c_{13}^2 + \sqrt{\Delta m_{\text{A}}^2} s_{13}^2 e^{2i(\alpha-\beta)} \right|, \quad (42)$$

where both terms can be of comparable magnitude. If $\theta_{13} = 0$ one has

$$\langle m_{ee} \rangle = \left| m_1 c_{12}^2 e^{2i\alpha} + \sqrt{\Delta m_{\odot}^2 + m_1^2} s_{12}^2 \right|, \quad (43)$$

where both terms can again be comparable. Note that in the last two expressions, as well as for other situations with small m_1 , the effective mass can vanish, a special

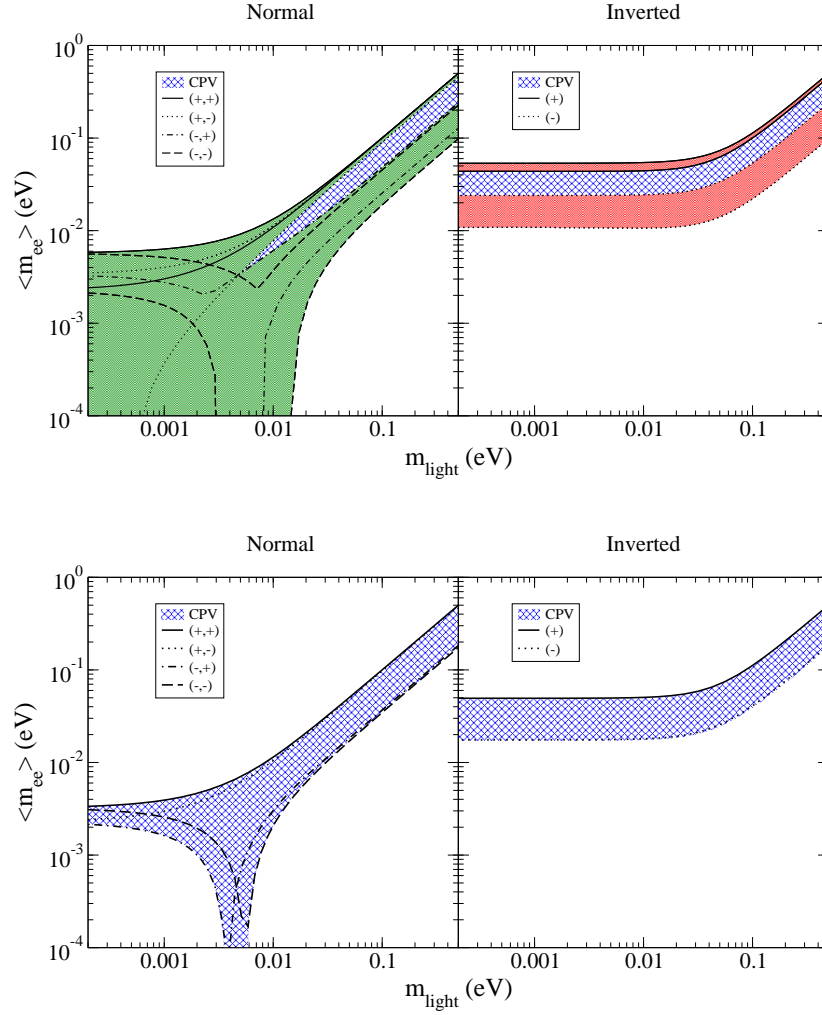
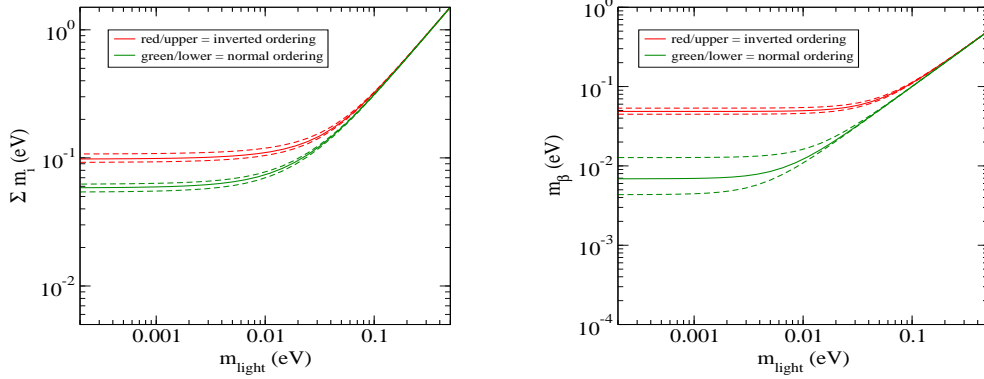
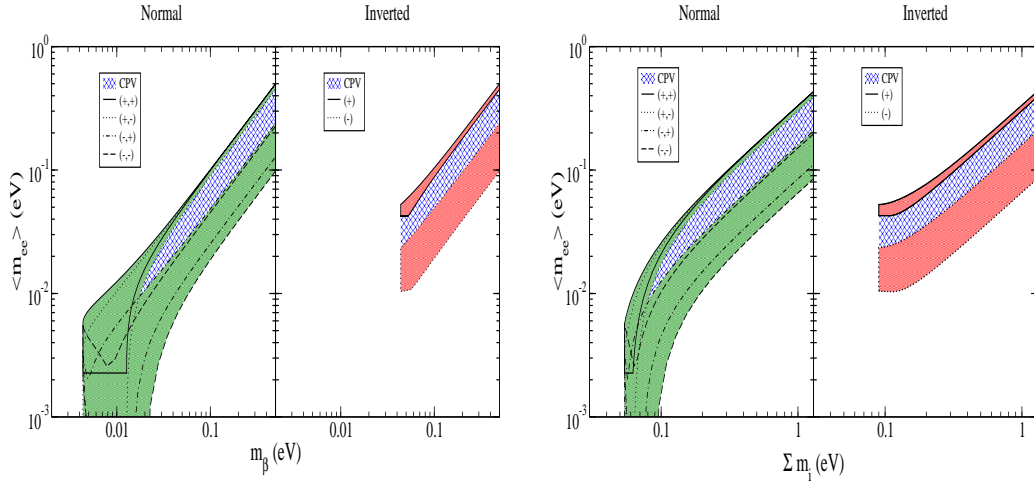


Fig. 10. Effective mass against the smallest neutrino mass for the 3σ ranges (top) and best-fit values (bottom) of the oscillation parameters. CP conserving and violating areas are indicated.

case we will deal with in Section 4.2.6. If the smallest mass m_1 is much larger than the mass-squared differences, the effective mass for quasi-degenerate neutrinos is obtained:

$$\langle m_{ee} \rangle^{\text{QD}} = m_0 \left| c_{12}^2 c_{13}^2 + s_{12}^2 c_{13}^2 e^{2i\alpha} + s_{13}^2 e^{2i\beta} \right|. \quad (44)$$

Recall that m_0 denotes the common neutrino mass for QD neutrinos. The third term is now much smaller than the minimal combination of the first two terms, $m_0(c_{12}^2 - s_{12}^2)$, because θ_{12} lies below $\pi/4$. Therefore, the effective mass cannot


 Fig. 11. Sum of masses Σ and kinematic neutrino mass m_β against the smallest neutrino mass.

 Fig. 12. Effective mass against sum of masses Σ and kinematic neutrino mass m_β for the 3σ ranges of the oscillation parameters. CP conserving and violating areas are indicated.

vanish for quasi-degenerate neutrinos. The estimate for the effective mass in case of quasi-degenerate neutrinos is

$$\cos 2\theta_{12} m_0 \lesssim \langle m_{ee} \rangle^{\text{QD}} \lesssim m_0. \quad (45)$$

This corresponds, for $\langle m_{ee} \rangle^{\text{QD}} \simeq 0.1$ eV, to half-lives in the regime of 10^{25} to 10^{26} yrs. Current experiments are testing this regime, thus $\lesssim 100$ kg yrs facilities with 10^{-2} or less background counts are sufficient for the QD regime.

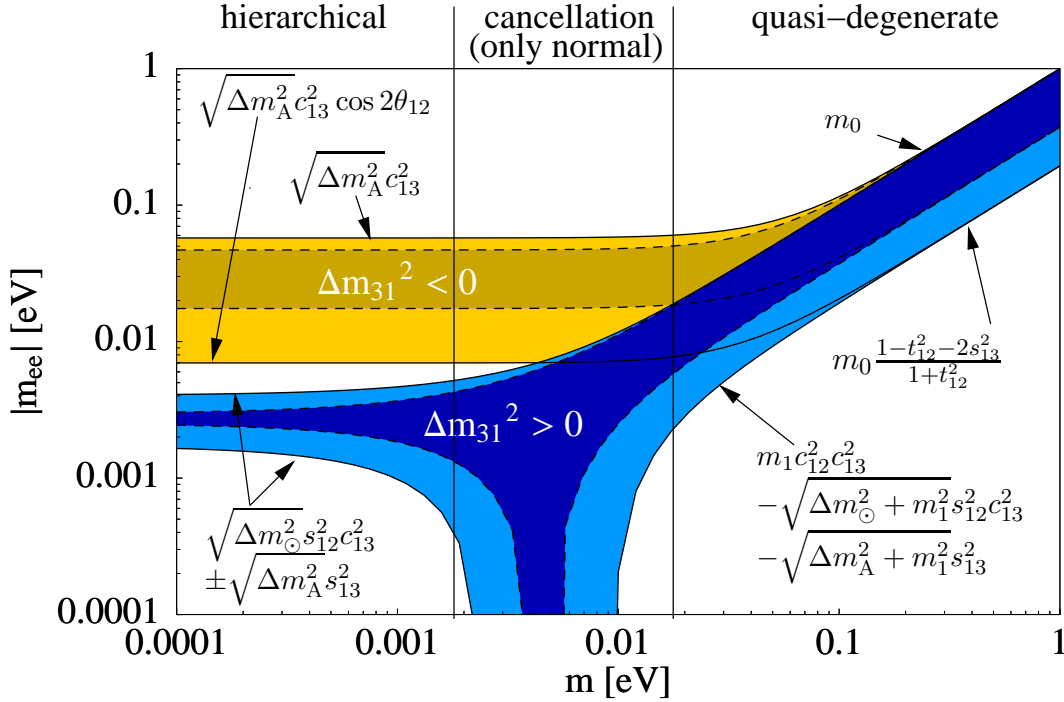


Fig. 13. The main properties of the effective mass as function of the smallest neutrino mass. We indicate the relevant formulae and the three important regimes: hierarchical, cancellation (only possible for normal mass ordering) and quasi-degeneracy. $c_{ij} = \cos \theta_{ij}$, $s_{ij} = \sin \theta_{ij}$ and $t_{ij} = \tan \theta_{ij}$. Taken from¹⁵³.

A rough estimate for the effective mass in terms of a normal hierarchy is

$$\langle m_{ee} \rangle^{\text{NH}} \sim \begin{cases} \sqrt{\Delta m_{\odot}^2} \sin^2 \theta_{12} & \simeq 0.003 \text{ eV}, \\ \left(\text{or } \sqrt{\Delta m_{\text{A}}^2} \sin^2 \theta_{13} \lesssim 0.003 \text{ eV} \right). \end{cases} \quad (46)$$

The meV scale of the effective mass should be the final goal of experiments, but the possibility of strong or even complete cancellation has to be kept in mind. The half-lives corresponding to meV effective masses are 10^{28} to 10^{29} yrs. Multi-ton scale experiments are necessary for such extremely low numbers, with background levels below 10^{-4} . It has been argued that if single electron events cannot be distinguished from double electron events, the elastic $\nu_e e$ scattering of solar neutrinos represents an irreducible background for $0\nu\beta\beta$ -experiments probing the NH regime¹⁵⁵.

In Figs. 11 and 12 we see that in case of NH m_{β} lies below KATRIN's sensitivity of about 0.2 eV for the normal hierarchy regime. With $\Sigma \simeq \sqrt{\Delta m_{\text{A}}^2} \simeq 0.05$ eV, only very optimistic or far future cosmological observations can test this value. If

the quasi-degenerate scenario is realized we find $\Sigma \simeq 3 m_\beta \simeq 3 \langle m_{ee} \rangle^{\max} \simeq 3 m_0$. Table 10 shows the mass observables for the NH and QD schemes. The interplay of the mass observables assumes unitarity of the PMNS matrix; corrections due to possible non-unitarity have been discussed in Ref.¹⁵⁶ and found to be negligible.

4.2.2. Inverted mass ordering

For the inverted mass ordering, the smallest neutrino mass is denoted m_3 and the mass matrix element is given by

$$\langle m_{ee} \rangle^{\text{inv}} = \left| \sqrt{m_3^2 + \Delta m_A^2} c_{12}^2 c_{13}^2 + \sqrt{m_3^2 + \Delta m_\odot^2 + \Delta m_A^2} s_{12}^2 c_{13}^2 e^{2i\alpha} + m_3 s_{13}^2 e^{2i\beta} \right|. \quad (47)$$

The maximal effective mass is – as for the normal mass ordering – obtained when $\alpha = \beta = 0$. The minimal value is

$$\langle m_{ee} \rangle_{\min}^{\text{inv}} = \sqrt{m_3^2 + \Delta m_A^2} c_{12}^2 c_{13}^2 - \sqrt{m_3^2 + \Delta m_\odot^2 + \Delta m_A^2} s_{12}^2 c_{13}^2 - m_3 s_{13}^2. \quad (48)$$

The third term of $\langle m_{ee} \rangle$ is usually negligible because θ_{13} is small and m_3 is the smallest mass. In this case:

$$\begin{aligned} \langle m_{ee} \rangle^{\text{IH}} &\simeq \sqrt{\Delta m_A^2} c_{13}^2 |c_{12}^2 + s_{12}^2 e^{2i\alpha}| \\ \text{and } \langle m_{ee} \rangle_{\max}^{\text{IH}} &\equiv \sqrt{\Delta m_A^2} c_{13}^2 \leq \langle m_{ee} \rangle^{\text{IH}} \leq \sqrt{\Delta m_A^2} c_{13}^2 \cos 2\theta_{12} \equiv \langle m_{ee} \rangle_{\min}^{\text{inv}}. \end{aligned} \quad (49)$$

It is important to note that owing to the non-maximal value of θ_{12} the minimal value of the effective mass is non-vanishing¹⁵⁰. Therefore, if limits below the minimal value

$$\langle m_{ee} \rangle_{\min}^{\text{inv}} = \langle m_{ee} \rangle_{\min}^{\text{IH}} = (1 - |U_{e3}|^2) \sqrt{\Delta m_A^2} (1 - 2 \sin^2 \theta_{12}), \quad (50)$$

are reached by an experiment, the inverted mass ordering is ruled out if neutrinos are Majorana particles. If we knew by independent evidence that the mass ordering is inverted (by a long-baseline oscillation experiment or a galactic supernova observation) then we would rule out the Majorana nature of neutrinos. Of course, one has to assume here that no other lepton number violating mechanism interferes. The two scales of $\langle m_{ee} \rangle$ corresponding to the minimal and maximal value of $\langle m_{ee} \rangle$ in case of the inverted hierarchy, given in Eq. (49), should be the intermediate or long-term goal of future experiments.

The typical effective mass values of order $\simeq 0.03$ eV are one order of magnitude larger than for the normal hierarchy and roughly one order of magnitude smaller than for quasi-degenerate neutrinos. They implies half-lives of order 10^{26} to 10^{27} yrs. A few 100 kg yrs of data taking with background levels below 10^{-2} counts will be necessary. Upcoming next generation experiments will test the inverted ordering, but cannot completely rule it out.

A more detailed analysis, focussing on the important dependence on θ_{12} , will be summarized in Section 4.2.4.

Table 10. Approximate analytical expressions for the neutrino mass observables for the extreme cases of the mass ordering. For $0\nu\beta\beta$ the typical (isotope-dependent) half-lives are also given.

	Σ	m_β	$\langle m_{ee} \rangle$
NH	$\sqrt{\Delta m_A^2}$ $\simeq 0.05$ eV	$\sqrt{\sin^2 \theta_{12} \Delta m_\odot^2 + U_{e3} ^2 \Delta m_A^2}$ $\simeq 0.01$ eV	$ \sin^2 \theta_{12} \sqrt{\Delta m_\odot^2} + U_{e3} ^2 \sqrt{\Delta m_A^2} e^{2i(\alpha-\beta)} $ ~ 0.003 eV $\Rightarrow T_{1/2}^{0\nu} \gtrsim 10^{28-29}$ yrs
IH	$2\sqrt{\Delta m_A^2}$ $\simeq 0.1$ eV	$\sqrt{\Delta m_A^2}$ $\simeq 0.05$ eV	$\sqrt{\Delta m_A^2} \sqrt{1 - \sin^2 2\theta_{12} \sin^2 \alpha}$ ~ 0.03 eV $\Rightarrow T_{1/2}^{0\nu} \gtrsim 10^{26-27}$ yrs
QD	$3m_0$	m_0	$m_0 \sqrt{1 - \sin^2 2\theta_{12} \sin^2 \alpha}$ $\gtrsim 0.1$ eV $\Rightarrow T_{1/2}^{0\nu} \gtrsim 10^{25-26}$ yrs

 Table 11. “Neutrino mass matrix” for the present decade. It is assumed that KATRIN will reach its sensitivity limit of $m_\beta = 0.2$ eV, that $0\nu\beta\beta$ -experiments can obtain values down to $\langle m_{ee} \rangle = 0.02$ eV, and that cosmology can probe the sum of masses down to $\Sigma = 0.1$ eV. N-SI denotes non-standard interpretation of $0\nu\beta\beta$, N-SC is non-standard cosmology.

	KATRIN		$0\nu\beta\beta$		cosmology	
	yes	no	yes	no	yes	no
KATRIN	yes	—	QD + Majorana	QD + Dirac	QD	N-SC
	no	—	N-SI	low IH or NH or Dirac	$m_\nu \lesssim 0.1$ eV or N-SC	NH
$0\nu\beta\beta$	yes	•	—	—	(IH or QD) + Majorana	N-SC or N-SI
	no	•	—	—	low IH or (QD + Dirac)	NH
cosmology	yes	•	•	•	—	—
	no	•	•	•	—	—

The transition to the quasi-degenerate regime takes place when $m_3 \gtrsim 0.03$ eV. If the smallest mass assumes such values, the normal and inverted mass ordering generate identical predictions for the effective mass. The results in this case are therefore identical to the ones for the normal mass ordering treated above in Section 4.2.1.

For the inverted hierarchy case m_β is again below KATRIN’s sensitivity, and $\Sigma \simeq 2\sqrt{\Delta m_A^2} \simeq 0.1$ eV is in the range of future limits. Table 10 shows the mass observables for the IH scheme. The values of the effective mass for the various special cases are displayed in Fig. 13. In Table 11 it is attempted to illustrate the complementarity of neutrino mass observables. Prospective sensitivity values of $m_\beta = 0.2$ eV, $\langle m_{ee} \rangle = 0.02$ eV, and $\Sigma = 0.1$ eV are assumed and the interpretation of positive and/or negative results in all 3 approaches is given.

4.2.3. Mass scale

As mentioned above, from the fundamental quantity $\langle m_{ee} \rangle$ one can also extract information on the masses of the individual neutrinos. We focus here on the quasi-degenerate regime, which is the easiest, though still non-trivial, case. The smallest effective mass can be written as

$$\langle m_{ee} \rangle_{\min}^{\text{QD}} = m_0 (|U_{e1}|^2 - |U_{e2}|^2 - |U_{e3}|^2) = m_0 \frac{1 - \tan^2 \theta_{12} - 2|U_{e3}|^2}{1 + \tan^2 \theta_{12}}. \quad (51)$$

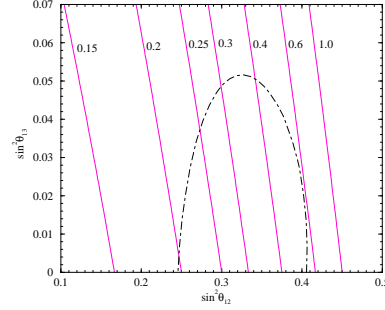


Fig. 14. Lines of constant m_0 in the $\sin^2 \theta_{12} - \sin^2 \theta_{13}$ plane, predicted for a QD mass spectrum with $\langle m_{ee} \rangle = 0.1$ eV. Also shown is an allowed 3σ region in $\sin^2 \theta_{12}$ and $\sin^2 \theta_{13}$.

We show in Fig. 14 iso-contours¹⁵² of m_0 in the plane spanned by $\sin^2 \theta_{12}$ and $|U_{e3}|^2$. With a limit $\langle m_{ee} \rangle_{\min}^{\text{exp}}$ on the effective mass at hand, one can translate this into a limit on the neutrino mass, which reads

$$m_0 \leq \langle m_{ee} \rangle_{\min}^{\text{exp}} \frac{1 + \tan^2 \theta_{12}}{1 - \tan^2 \theta_{12} - 2|U_{e3}|^2} \equiv \langle m_{ee} \rangle_{\min}^{\text{exp}} f(\theta_{12}, \theta_{13}). \quad (52)$$

This function $f(\theta_{12}, \theta_{13})$ varies from 2.57 to 3.29 at 1σ and from 2.17 to 4.77 at 3σ . The limit on the effective mass is about 0.5 eV (see Table 2), and hence $m_0 \leq 1.6$ eV and 2.4 eV, respectively. Therefore, the current limit on m_0 from $0\nu\beta\beta$ is very similar to the one from the Mainz experiment.

Perhaps more interesting is the determination of the neutrino mass scale in future experiments if information from complementary neutrino mass observables is combined. For instance¹⁵⁷, consider the scenario defined by

m_3 [eV]	$\langle m_{ee} \rangle$ [eV]	m_β [eV]	Σ [eV]
0.3	0.11 – 0.30	0.30	0.91

The prospective errors one can use are $\sigma(m_\beta^2) = 0.025 \text{ eV}^2$ and $\sigma(\Sigma) = 0.05 \text{ eV}$, and an “experimental error” $\sigma(\langle m_{ee} \rangle_{\text{exp}}) = \frac{1}{2} \langle m_{ee} \rangle_{\text{exp}} \sigma(\Gamma_{\text{obs}})/\Gamma_{\text{obs}}$, where $\sigma(\Gamma_{\text{obs}})/\Gamma_{\text{obs}}$ is motivated by the GERDA proposal³⁴ to be $\simeq 23\%$. The “theoretical error” from the NME uncertainty was defined as $\sigma(\langle m_{ee} \rangle) = (1 + \zeta) \left(\langle m_{ee} \rangle + \sigma(\langle m_{ee} \rangle_{\text{exp}}) \right) - \langle m_{ee} \rangle$. Depending on the measured effective mass $\langle m_{ee} \rangle_{\text{exp}}$ one can now obtain the values of m_0 which can be reconstructed. Fig. 15 shows the results of the analysis. If $\zeta = 0$ one finds $\sigma(m_3) \simeq 15\%$ at 3σ , while for $\zeta = 0.25$ it holds that $\sigma(m_3) \simeq 25\%$. If one includes a wrong cosmological input the reconstruction of m_3 can be wrong by up to one order of magnitude. Leaving Σ out of the analysis yields $\sigma(m_3) \simeq 50\%$, showing that the precision is largely determined by cosmology.

A detailed analysis was performed in Ref.¹⁵¹, from where we have taken Fig. 16. As was noted in that paper, the uncertainty of the oscillation parameters is of little importance in determining m_0 . To take into account the NME uncertainty

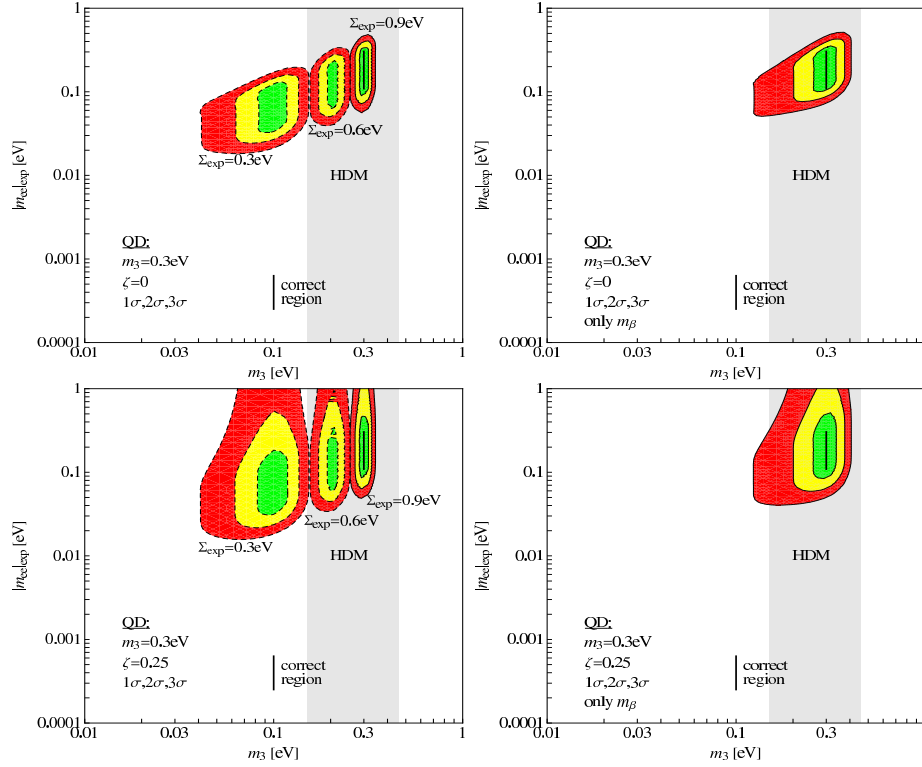


Fig. 15. 1σ , 2σ and 3σ regions in the m_3 - $\langle m_{ee} \rangle_{\text{exp}}$ plane for a quasi-degenerate neutrino mass scenario. The upper plots are for no NME uncertainty, the lower plots assume 25% uncertainty. The left plots show the correct (solid line) as well as two possible incorrect cosmological measurements (dashed lines). The right plots leave Σ out of the fit. The area denoted HDM is the range of $\langle m_{ee} \rangle$ from the claim of part of the Heidelberg-Moscow collaboration. Taken from¹⁵⁷.

the following procedure was proposed: \mathcal{M} is the unknown true NME and \mathcal{M}_0 is the NME used to obtain $\langle m_{ee} \rangle_{\text{exp}}$, which denotes the effective mass extracted from an experiment. The parameter F is connected to the ratio $\xi = \mathcal{M}/\mathcal{M}_0$ in the sense that ξ ranges from $1/\sqrt{F}$ to F . If the experimental error on $\langle m_{ee} \rangle_{\text{exp}}$ is sufficiently small ($\lesssim 0.06$ eV for NME uncertainty $F \lesssim 3$), the neutrino mass spectrum will be shown to be QD, and m_0 will be constrained to lie in a rather narrow interval of values limited from below by $m_0 \gtrsim 0.1$ eV. The uncertainty in the NME directly translates into an uncertainty in m_0 , in analogy to Eq. (52). In the case of an intermediate value of $\langle m_{ee} \rangle_{\text{exp}} = 0.04$ eV, shown in the middle column of Fig. 16, an allowed range of $0.01 \text{ eV} \lesssim m_0 \lesssim 0.1 \text{ eV}$ could be established for precise measurements. In the case of an inverted ordering only an upper bound $m_0 \lesssim 0.1$ eV will be obtained. This result can be easily understood from the usual $\langle m_{ee} \rangle$ vs. smallest mass plots, which are basically flat for the inverted ordering and $m_3 \lesssim 0.1$ eV.

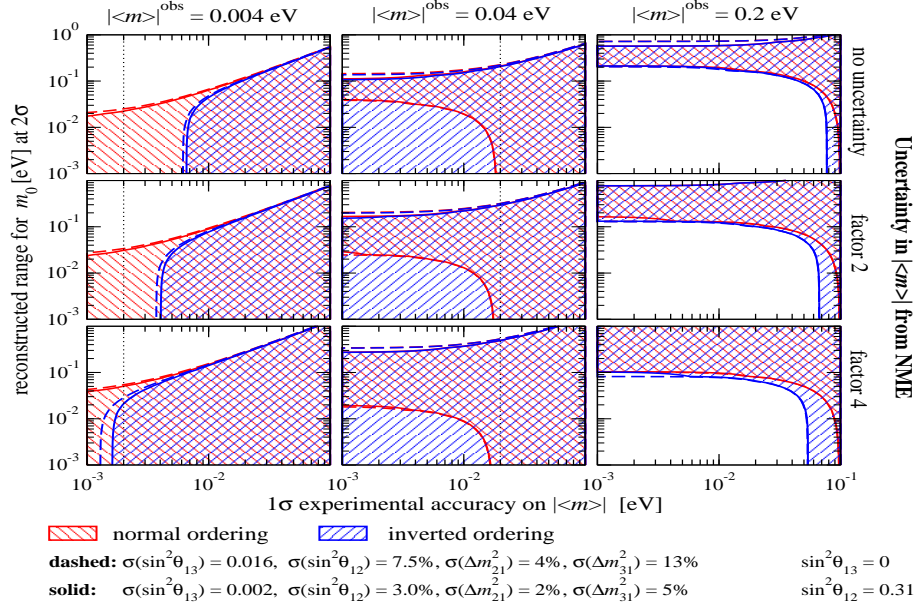


Fig. 16. The reconstructed range for the lightest neutrino mass at 2σ C.L. for normal and inverted mass ordering as a function of the 1σ experimental error on $\langle m_{ee} \rangle_{\text{exp}}$ (here called $|\langle m \rangle|^{\text{obs}}$). The results are shown for three representative values $\langle m_{ee} \rangle^{\text{obs}} = 0.004, 0.04, 0.2$ eV, and for fixed NME (first row), and an uncertainty of a factor of $F = 2$ and $F = 4$ in the NME (second and third rows). The dashed (solid) lines correspond to the present uncertainties in the oscillation parameters. To the left of the dotted lines, a positive signal is obtained at 2σ , whereas to the right only an upper bound can be set. Taken from¹⁵¹.

Other analyses on neutrino mass extraction from different neutrino mass experiments including $0\nu\beta\beta$ can be found in Refs.^{158,62,159}.

4.2.4. Mass ordering: testing the inverted hierarchy

From Fig. 10 the interesting possibility of ruling out the inverted mass ordering becomes obvious. The minimal value of the effective mass, repeated here for convenience, is non-zero and given by

$$\langle m_{ee} \rangle_{\text{min}}^{\text{inv}} = (1 - |U_{e3}|^2) \sqrt{\Delta m_A^2} (1 - 2 \sin^2 \theta_{12}). \quad (53)$$

If a limit on the effective mass below this value is obtained, the inverted ordering is ruled out if neutrinos are Majorana particles. In case the mass ordering is known to be inverted (e.g. by a long-baseline experiment or by observation of a galactic supernova) then the Majorana nature of neutrinos would be ruled out.

As a rough requirement for experiments we calculate the difference between the minimal effective mass for the inverted ordering and the maximal effective mass for the normal ordering multiplied with the nuclear matrix element uncertainty factor

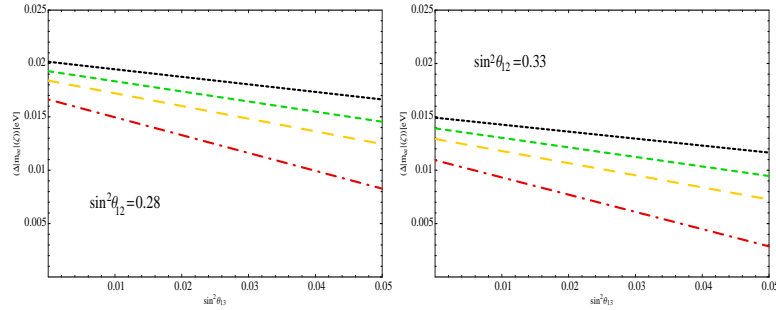


Fig. 17. The difference $\Delta\langle m_{ee} \rangle$ of $\langle m_{ee} \rangle_{\min}^{\text{inv}}$ and $\zeta \langle m_{ee} \rangle_{\max}^{\text{nor}}$ as a function of $\sin^2 \theta_{13}$ for different nuclear matrix element uncertainty factors $\zeta = 1, 1.5, 2$ and 3 (from top to bottom). We have chosen an illustrative value of the smallest mass of 0.005 eV and $\sin^2 \theta_{12} = 0.28$ (left) and $\sin^2 \theta_{12} = 0.33$ (right).

$\zeta^{160,152,153}$

$$\Delta\langle m_{ee} \rangle \equiv \langle m_{ee} \rangle_{\min}^{\text{inv}} - \zeta \langle m_{ee} \rangle_{\max}^{\text{nor}}. \quad (54)$$

We plot this difference as a function of $\sin^2 \theta_{13}$ in Fig. 17. Obviously, the largest dependence stems from θ_{12} , and the smaller θ_{12} is, the better. This is clear from the previous discussion and Fig. 13, because the smaller θ_{12} is, the larger is $\langle m_{ee} \rangle_{\min}^{\text{inv}}$. The effect¹⁵³ of non-zero θ_{13} is to slightly decrease $\langle m_{ee} \rangle_{\min}^{\text{inv}}$ and to slightly increase $\langle m_{ee} \rangle_{\max}^{\text{nor}}$.

One can translate the effective mass necessary to rule out (or touch) the inverted hierarchy into half-lives. The very important dependence on θ_{12} has recently been discussed in Ref.⁵⁵. The plots in Fig. 18 are generated using the compilation of NMEs from Table 5. The current 3σ range corresponds to an uncertainty of a factor 2 in the minimal value of the effective mass, which is of the same order as the current uncertainty in the NMEs. The factor 2 due to θ_{12} corresponds to a factor of $2^2 = 4$ in half-life. In experiments with background, see Eq. (6), this means a rather non-trivial combined factor of $2^4 = 16$ in the product of measuring time, energy resolution, background index and detector mass. Therefore, a precision determination of the solar neutrino mixing angle would be very desirable to evaluate the requirements and physics potential of upcoming $0\nu\beta\beta$ -experiments in order to test the inverted ordering⁵⁵.

4.2.5. Majorana CP phases

Apart from measuring the effective mass in case of a normal hierarchy, determination of a Majorana CP phase from neutrino-less double beta decay is probably the

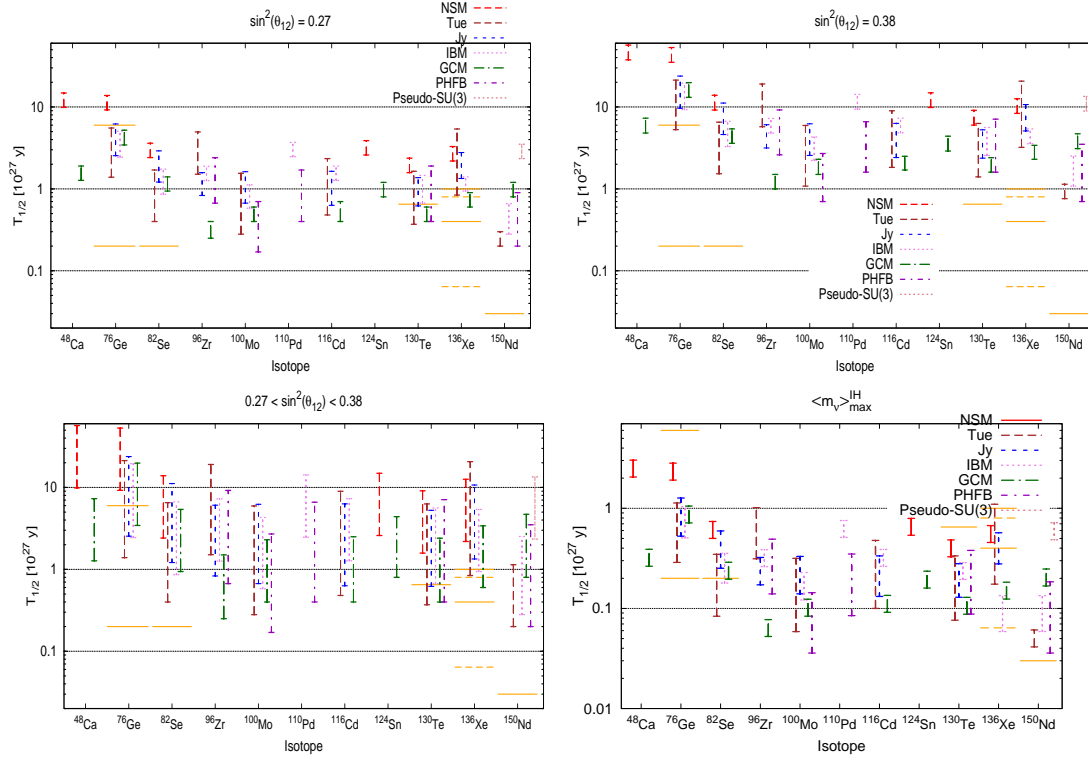


Fig. 18. Required half-life sensitivities to exclude and touch the inverted hierarchy for different values of θ_{12} . The upper plots show the necessary half-lives for $\sin^2 \theta_{12} = 0.27$ (upper left) and $\sin^2 \theta_{12} = 0.38$ (upper right). The lower left plot includes the current 3σ uncertainty for θ_{12} . The lower right plot shows the necessary half-lives in order to touch the inverted ordering, which is independent on θ_{12} . The small horizontal lines show expected half-life sensitivities at 90% C.L. of running and planned $0\nu\beta\beta$ -experiments. When two sensitivity expectations are given for one experiment they correspond to near and far time goals, see Table 4. Taken from⁵⁵.

most difficult physics goal related to this processⁱ. One general point to be made here is that there is only one observable, $\langle m_{ee} \rangle$, and thus only one of the two Majorana phases (or a combination of the two phases) can be extracted. In addition, complementary information on the neutrino mass scale has to be put in for such a measurement. A final remark is that the process is not CP violating, i.e. the rate of the $0\nu\beta^+\beta^+$ process depends on the same quantity as the $0\nu\beta\beta$ process^j.

The prospects of measuring the CP phase in neutrino-less double beta decay have been discussed in several papers¹⁶³. A somewhat pessimistic conclusion

ⁱThough $|U_{e3}|$ has some influence on $0\nu\beta\beta$ ¹⁵³, extracting it from a measurement is also impractical¹⁶¹.

^jManifest CP violation from Majorana phases is discussed e.g. in¹⁶².

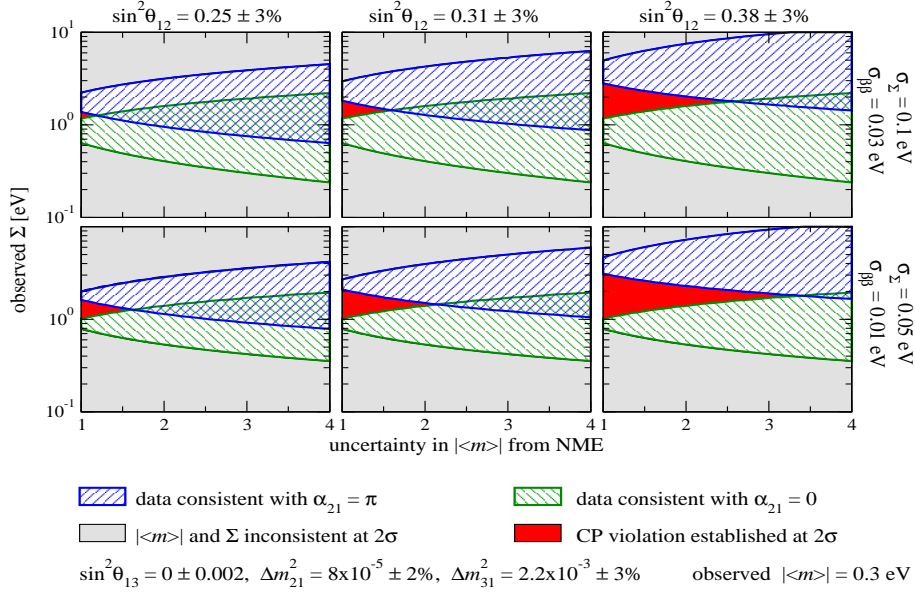


Fig. 19. Constraints on the Majorana phase 2α (here called α_{21}) at 95% C.L. from an observed $\langle m_{ee} \rangle_{\text{exp}} = 0.3 \text{ eV}$ and prospective data on Σ , as a function of the NME uncertainty factor F . Shown are the regions in which the data are consistent with one of the CP-conserving values (hatched), observed Σ is inconsistent with $\langle m_{ee} \rangle_{\text{exp}}$ (light-shaded), and Majorana CP-violation is established (red/dark-shaded). Taken from¹⁵¹.

has been drawn in Ref.¹⁶⁴, whereas the requirements for such a measurement have been discussed in¹⁶⁵, and found to be not too unrealistic.

The requirement for determining the phases is clear from Figs. 10 and 12. Experimentally one should find results lying in the areas indicated with “CPV”, which are however smeared by experimental and theoretical uncertainties. This is realistic only for the inverted ordering or the quasi-degenerate scheme. Neglecting θ_{13} , the effective mass is in these cases is proportional to

$$\langle m_{ee} \rangle \propto |\cos^2 \theta_{12} + e^{2i\alpha} \sin^2 \theta_{12}| = \sqrt{1 - \sin^2 2\theta_{12} \sin^2 \alpha}. \quad (55)$$

Therefore, the larger θ_{12} is, the more promising it is to extract α from measurements. Recall that ruling out the inverted mass ordering is easier if θ_{12} is small.

A detailed statistical analysis has been performed in¹⁵¹, from which we present Fig. 19. One can see that, as expected, for larger values of θ_{12} the areas in parameter space become larger. For instance, if $\sin^2 \theta_{12} \gtrsim 0.3$ and $\simeq 10\%$ errors in the measured $\langle m_{ee} \rangle_{\text{exp}}$ and Σ are present, the NME has to be known to better than within a factor of 1.5. For smaller values of the errors, $\sigma_{\beta\beta} \simeq 0.01 \text{ eV}$ and $\sigma_\Sigma \simeq 0.05 \text{ eV}$, Majorana CP-violation could be established even for $F \simeq 2$ (See Section 4.2.3 for the definition of F). Finally, the Majorana phase 2α has to have

a value approximately in the interval $\sim (\pi/4 - 3\pi/4)$. In the inverted hierarchy the required errors have to be smaller, and the determination of the phase is more challenging.

4.2.6. Vanishing effective mass

Unfortunately, the normal mass hierarchy can allow for complete cancellation of the effective mass (see e.g.¹⁶⁶). In terms of Fig. 8, this “cancellation regime” means that a triangle can be formed. If $|U_{e3}| = 0$ then the requirement is

$$\frac{m_1}{m_2} = \tan^2 \theta_{12} \simeq \frac{1}{2}, \quad (56)$$

while for $m_1 = 0$ one needs

$$\frac{m_2}{m_3} = \frac{\tan^2 \theta_{13}}{\sin^2 \theta_{12}} \simeq 3 \tan^2 \theta_{13}. \quad (57)$$

In both cases the Majorana phases need to be such that the two surviving terms have opposite sign. For the case of arbitrary θ_{13} one finds¹⁶⁷

$$\begin{aligned} \cos 2\alpha &= \frac{m_3^2 s_{13}^4 - c_{13}^4 (m_1^2 c_{12}^4 + m_2^2 s_{12}^4)}{2 m_1 m_2 s_{12}^2 c_{12}^2 c_{13}^4}, \\ \cos 2\beta &= -\frac{m_3^2 s_{13}^4 + c_{13}^4 (m_2^2 s_{12}^4 - m_1^2 c_{12}^4)}{2 m_2 m_3 s_{12}^2 s_{13}^2 c_{13}^2}. \end{aligned} \quad (58)$$

It may seem unnatural that the 7 parameters on which $\langle m_{ee} \rangle$ depends conspire in such a way that the effective mass vanishes. However, recall that the effective mass is the ee element of the Majorana neutrino mass matrix^k. This matrix is generated by the underlying theory of mass generation, and texture zeros occur frequently in such (flavor) models, see Ref.¹⁷⁰ for a general analysis and¹⁷¹ for symmetries leading to $\langle m_{ee} \rangle = 0$.

One may ask whether the effective mass remains zero, or whether corrections lead to small but non-zero $\langle m_{ee} \rangle$. In fact, there are several possibilities for non-zero $0\nu\beta\beta$ -rates, even if $\langle m_{ee} \rangle = 0$:

- the first point to make here is that the dependence of the amplitude on the neutrino parameters goes as (see Eq. (40))

$$U_{ei}^2 \frac{m_i}{q^2 - m_i^2} \simeq U_{ei}^2 m_i \left(1 + \frac{m_i^2}{q^2} \right) = \langle m_{ee} \rangle + U_{ei}^2 m_i^3 \frac{1}{q^2}.$$

While the second term is very much suppressed by $m_i^2/q^2 \lesssim 10^{-12}$ with respect to the usual effective mass term, it is in general non-zero, even when $\langle m_{ee} \rangle$ is zero;

- another source of correction arises from radiative corrections. While in the effective theory the renormalization of the mass matrix is multiplicative (see

^kZeros of the remaining elements of m_ν have been studied in¹⁶⁸, the presence of two zeros in¹⁶⁹.

Section 4.2.7), this may no longer be true in the theory beyond the effective one. For instance, if m_ν is generated via the type I seesaw mechanism, then threshold corrections from integrating out the heavy neutrinos one by one will in general lead to non-zero $\langle m_{ee} \rangle$, even if the ee entry of $m_D^T M_R^{-1} m_D$ is zero;

- in the type I seesaw mechanism, m_D^2/M_R is actually only the leading order term. “Next-to-leading order” corrections m_D^4/M_R^3 are present and in general induce non-zero terms in the ee entry, even if $(m_D^T M_R^{-1} m_D)_{ee}$ is zero¹⁷²;
- if another source of lepton number violation is present, then a non-zero ee entry of the neutrino mass matrix will be induced via the Schechter-Valle diagrams from Fig. 1, even if $\langle m_{ee} \rangle = 0$;
- finally, it is plausible that a flavor-blind Planck scale term is present, which induces an effective mass of order $v^2/M_{\text{Pl}} \simeq 10^{-5}$ eV. This term arises from the Weinberg operator Eq. (17) with the Planck scale inserted as Λ .

All these sources give of course very small but in general non-zero contributions to the effective mass. One might ask whether one can determine experimentally by other means if the effective mass vanishes. While this is not possible, one can show however that the effective mass cannot vanish: from Fig. 12 note that $\langle m_{ee} \rangle \simeq 0$ corresponds to $m_\beta \lesssim 0.02$ eV and $\Sigma \lesssim 0.1$ eV. Thus, finding these quantities above such values immediately rules out the possibility of vanishing $\langle m_{ee} \rangle$. Of course, determining experimentally that the inverted mass ordering is realized also implies that $\langle m_{ee} \rangle \neq 0$.

4.2.7. Renormalization

The renormalization group (RG) evolution of neutrino parameters has recently been reviewed in¹⁷³. If some unknown high energy theory at a scale Λ leads to a mass matrix m_ν^0 , then in the effective theory one has the following mass matrix at low scale λ , where measurements take place:

$$m_\nu = I_{\alpha_\nu} \begin{pmatrix} (m_\nu^0)_{ee} I_e^2 & (m_\nu^0)_{e\mu} I_e I_\mu & (m_\nu^0)_{e\tau} I_e I_\tau \\ \cdot & (m_\nu^0)_{\mu\mu} I_\mu^2 & (m_\nu^0)_{\mu\tau} I_\mu I_\tau \\ \cdot & \cdot & (m_\nu^0)_{\tau\tau} I_\tau^2 \end{pmatrix}, \quad (59)$$

where

$$I_\alpha \simeq 1 + \frac{C}{16\pi^2} y_\alpha^2 \ln \frac{\lambda}{\Lambda} \text{ and } I_{\alpha_\nu} \simeq 1 + \frac{1}{16\pi^2} \alpha_\nu \ln \frac{\lambda}{\Lambda}, \quad (60)$$

with $\alpha, \beta \in \{e, \mu, \tau\}$, $C = 1$ in the MSSM and $C = -\frac{3}{2}$ in the SM. One can safely drop y_e and y_μ from the above expression and describe the RG evolution with I_τ and I_{α_ν} only. We furthermore have

$$\begin{aligned} \alpha_\nu^{\text{SM}} &= -3g_2^2 + 2(y_\tau^2 + y_\mu^2 + y_e^2) + 6(y_t^2 + y_b^2 + y_c^2 + y_s^2 + y_d^2 + y_u^2) + \lambda_H, \\ \alpha_\nu^{\text{MSSM}} &= -\frac{6}{5}g_1^2 - 6g_2^2 + 6(y_t^2 + y_c^2 + y_u^2). \end{aligned} \quad (61)$$

Here $g_{1,2}$ are the electroweak gauge couplings, y_x the Yukawa coupling of fermion x , and λ_H the Higgs self-coupling. The RG evolution of $\langle m_{ee} \rangle$ is therefore basically a

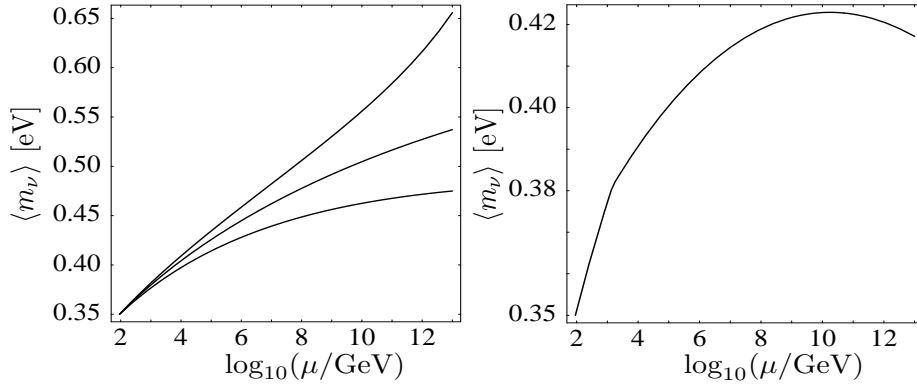


Fig. 20. Extrapolation of the effective mass from 0.35 eV at low scale to higher energies. The SM curves in the left plot correspond to Higgs masses of 114 GeV, 165 GeV and 190 GeV (from bottom to top). In the MSSM plot on the right, the Higgs mass is 120 GeV, $\tan\beta = 50$, $M_{\text{SUSY}} = 1.5$ TeV. Taken from¹⁷⁴.

rescaling of the effective mass with $I_{\alpha\nu}$. In contrast to the running of the individual parameters of $\langle m_{ee} \rangle$ (θ_{12} , θ_{13} , m_1 , m_2 , m_3 , α and β), which can be very dramatic, the RG evolution of $\langle m_{ee} \rangle$ is modest. Its running does basically not depend on the mass ordering or any of the other neutrino mass and mixing parameters. It is an interesting exercise to consider the β functions of the 7 parameters of $\langle m_{ee} \rangle$ and to show that at the end all dependence on θ_{12} , θ_{13} , m_1 , m_2 , m_3 , α and β drops out. The effective mass typically increases from low to high scale, Fig. 20 shows an example for its running¹⁷⁴.

4.2.8. Distinguishing neutrino models

We have mentioned in Section 4.1.2 that the peculiar and unexpected form of lepton mixing (see Eq. (31)) is assumed to have its origin in the presence of flavor symmetries¹¹⁸. There is a large abundance of such models, many leading to the same neutrino mixing scheme, for instance tri-bimaximal mixing (TBM). The question arises how to distinguish them from one another. It turns out that neutrino mass observables can help in disentangling the vast amount of flavor symmetry models. One example is that the flavor symmetry leads to correlations of the mass matrix elements, which imply correlations of observables. For instance, the effective mass could be correlated with the atmospheric neutrino parameter $\sin^2\theta_{23}$, which was obtained in a model in Ref.¹⁷⁵, see Fig. 21. Recall that in general θ_{23} has no influence on $\langle m_{ee} \rangle$.

Another point are “sum-rules”: the most general neutrino mass matrix giving

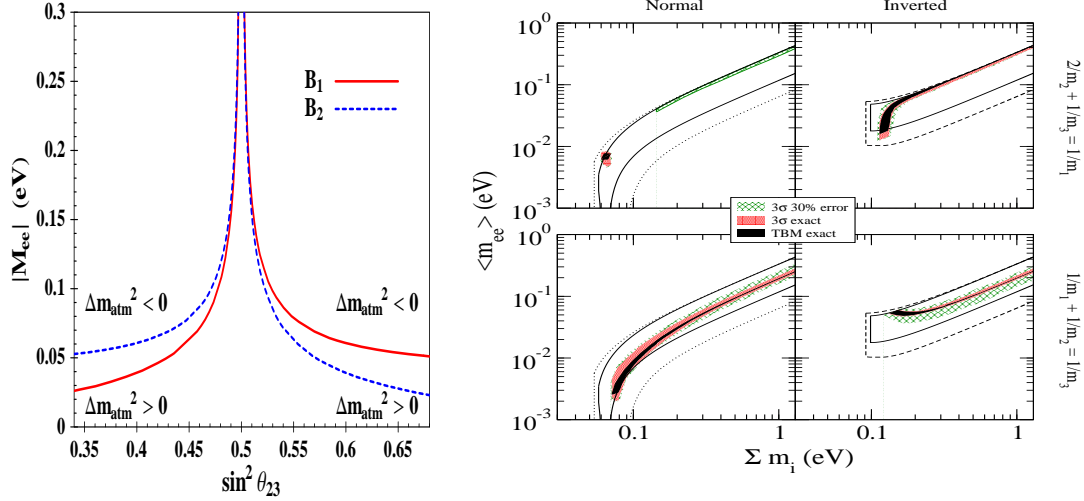


Fig. 21. Left: correlation between the effective mass and the atmospheric neutrino mixing angle in a specific flavor symmetry model. Taken from¹⁷⁵. Right: allowed regions in $\langle m_{ee} \rangle - \Sigma$ parameter space for the sum-rules $\frac{2}{m_2} + \frac{1}{m_3} = \frac{1}{m_1}$ (top) and $\frac{1}{m_1} + \frac{1}{m_2} = \frac{1}{m_3}$ (bottom), for both the TBM (black) and 3σ values (light red) of the oscillation data, as well as for the sum-rules violated by 30% (green hatches). Taken from¹⁷⁶.

rise to TBM is

$$m_\nu = \begin{pmatrix} A & B & B \\ \cdot & \frac{1}{2}(A+B+D) & \frac{1}{2}(A+B-D) \\ \cdot & \cdot & \frac{1}{2}(A+B+D) \end{pmatrix}. \quad (62)$$

As such, the (complex) eigenvalues $A - B$, $A + 2B$ and D are independent of the mixing angles: no matter what A, B, D are, the PMNS mixing is given as Eq. (31). However, very often the structure of the mass matrix is simpler than in Eq. (62), and “sum-rules” between the neutrino masses arise. Examples are¹⁷⁷ $2/m_2 + 1/m_3 = 1/m_1$ or $1/m_2 + 1/m_3 = 1/m_1$, and detailed studies of the predictions can be found in Ref.¹⁷⁶, from which we took the right plot in Fig. 21. Other discussions on mass-related phenomenology of flavor symmetry models can be found in¹⁷⁸.

4.2.9. Light sterile neutrinos

The easiest way to depart from the standard 3 neutrino picture discussed so far is to add light sterile neutrinos. In fact, we have mentioned in Section 4.1 several hints which point to the existence of additional radiation in the Universe, as well as for one or two additional mass-squared differences in the eV regime. With one or two light sterile neutrinos the PMNS matrix becomes a unitary 4×4 or 5×5 matrix.

Short-baseline oscillations depend on U_{e4} (and U_{e5}) as well as $U_{\mu 4}$ (and $U_{\mu 5}$). Only eV-like mass-squared differences play a role for such experiments, and only if two sterile states are added does the possibility of CP violation arise. This can explain the different neutrino and anti-neutrino results from MiniBooNE and MiniBooNE plus LSND, respectively.

Table 12 shows the results¹²⁸ from a global fit to the world's short-baseline data, taking into account the recent re-evaluation of reactor fluxes¹²⁷. The data are not sensitive to whether the two sterile neutrinos are above or below the three active ones (2+3 or 3+2 scenarios), but are sensitive to whether the active neutrinos are sandwiched between two sterile ones (1+3+1). Note that the fit to 1+3+1 scenarios is slightly better than for 3+2/2+3 scenarios. Fitting only the reactor experiments is possible in a 3+1 or 1+3 scenario, and gives¹²⁸ $|U_{e4}| = 0.151$ and $\Delta m_{41}^2 = 1.78$ eV².

If there are two sterile neutrinos, the nomenclature for the 8 possible mass orderings is as follows:

- (i) SSX, where $X = N$ for a normal and $X = I$ for an inverted ordering of the mostly active neutrinos. In these schemes the two predominantly sterile neutrinos are heavier than the three predominantly active neutrinos (2+3 scenarios);
- (ii) XSS ($X = N$ or I as before), where the two predominantly sterile neutrinos are lighter than the three predominantly active neutrinos (3+2 scenarios);
- (iii) SXS with $X = N$ or I , where the three active neutrinos are sandwiched between the sterile ones (1+3+1 scenarios). In this class there can be four possible scenarios, which we denote as SXSa and SXSb. The scheme SXSa corresponds to the state ν_5 higher than the three active states and SXSb corresponds to the state ν_5 lower than the three active states.

The individual masses, expressed in terms of smallest mass and the four mass-squared differences, can be found in Ref.¹²⁶. The new sterile neutrinos will contribute to the sum of masses in cosmology, to the kinematic mass in KATRIN, and, if they are Majorana particles, to $0\nu\beta\beta$. The effects of sterile neutrinos on neutrinoless double beta decay have been studied by various authors^{179,148,149,126,180}. One simply extends the sums in the definitions of Σ , m_β and $\langle m_{ee} \rangle$ from $i = 3$ to $i = 5$. The interpretation of reactor experiments actually observing oscillations, which is possible after the new reactor fluxes¹²⁷ are taken into account, makes the application of the results to $0\nu\beta\beta$ easier. If only LSND and MiniBooNE supply oscillation data, the $\nu_\mu^{(-)} \rightarrow \nu_e^{(-)}$ transitions depend on U_{ei} and $U_{\mu i}$ ($i = 4, 5$). For m_β and $\langle m_{ee} \rangle$ only U_{ei} is required, and one needs to assume something about $U_{\mu i}$ to extract U_{ei} from the fit results. However, reactor oscillation survival probabilities depend only on U_{ei} . There are two more Majorana phases which show up in the modified effective mass, which is the sum of the contribution considered so far ($\langle m_{ee} \rangle^{\text{act}}$) plus

Table 12. Parameter values and χ^2 at the global best-fit points for 3+2 and 1+3+1 oscillations. Taken from¹²⁸.

	$\Delta m_{41}^2 [\text{eV}^2]$	$ U_{e4} $	$ U_{\mu 4} $	$\Delta m_{51}^2 [\text{eV}^2]$	$ U_{e5} $	$ U_{\mu 5} $	χ^2/dof
3+2/2+3	0.47	0.128	0.165	0.87	0.138	0.148	110.1/130
1+3+1	0.47	0.129	0.154	0.87	0.142	0.163	106.1/130

new terms from the sterile states ($\langle m_{ee} \rangle^{\text{st}}$):

$$\langle m_{ee} \rangle' = \underbrace{|U_{e1}|^2 m_1 + |U_{e2}|^2 m_2 e^{2i\alpha} + |U_{e3}|^2 m_3 e^{2i\beta}}_{\langle m_{ee} \rangle^{\text{act}}} + \underbrace{|U_{e4}|^2 m_4 e^{2i\Phi_1} + |U_{e5}|^2 m_5 e^{2i\Phi_2}}_{\langle m_{ee} \rangle^{\text{st}}}.$$

The usual phase space factors and matrix elements as in the standard interpretation apply (nuclear physics is the same as for the standard case, as long as the masses do not exceed $q \simeq 100$ MeV). The additional contribution $\langle m_{ee} \rangle^{\text{st}}$ from the sterile neutrinos could be leading, sub-leading, or of the same order of magnitude as the active neutrino part $\langle m_{ee} \rangle^{\text{act}}$.

Neglecting the smallest neutrino mass and using the best-fit values from Table 12 gives the following predictions for the mass observables¹⁸⁰:

- SSN: the active neutrinos give the same contribution as in the standard case for NH. The contribution to the sum of masses from the sterile states dominates and is given by $\Sigma = \sqrt{\Delta m_{41}^2} + \sqrt{\Delta m_{51}^2} \simeq 1.62$ eV. The contribution to m_β is $\sqrt{\Delta m_{41}^2 |U_{e4}|^2 + \Delta m_{51}^2 |U_{e5}|^2} \simeq 0.16$ eV. The contribution to the effective mass is $|U_{e4}|^2 \sqrt{\Delta m_{41}^2} + e^{2i(\Phi_1 - \Phi_2)} |U_{e5}|^2 \sqrt{\Delta m_{51}^2}$, which is between 0.007 and 0.029 eV, and hence larger than the typical value for NH. Thus, the effective mass cannot vanish (for the best-fit point), in contrast to the standard case.
- SSI: the active neutrinos give the same contribution as in the standard case for IH, and the sterile states give the same predictions for the mass observables as in SSN. The effective mass can therefore vanish, in contrast to the standard three neutrino case.
- NSS: the active neutrinos are QD (normal ordering) with a mass scale $\sqrt{\Delta m_{51}^2} \simeq 0.93$ eV, and this governs the predictions for $\langle m_{ee} \rangle$ and m_β . For cosmology, $\Sigma = 3 \sqrt{\Delta m_{51}^2} + \sqrt{\Delta m_{51}^2 - \Delta m_{41}^2} \simeq 3.4$ eV.
- ISS: same as NSS, except for inversely ordered active neutrinos.
- SNSa: the active neutrinos are QD (normal ordering) with a mass scale $\sqrt{\Delta m_{41}^2} \simeq 0.69$ eV, and this defines the predictions for $\langle m_{ee} \rangle$ and m_β . The sum of masses is $\Sigma = 3 \sqrt{\Delta m_{41}^2} + \sqrt{\Delta m_{41}^2 + \Delta m_{51}^2} \simeq 3.2$ eV.
- SNSb: the active neutrinos are QD (normal ordering) with a mass scale $\sqrt{\Delta m_{51}^2} \simeq 0.93$ eV, and this defines the predictions for $\langle m_{ee} \rangle$ and m_β , up to a small correction of order $|U_{e4}|^2 \sqrt{\Delta m_{51}^2 + \Delta m_{41}^2} \simeq 0.03$ eV e.g. for $\langle m_{ee} \rangle$. The sum of masses is $\Sigma = 3 \sqrt{\Delta m_{51}^2} + \sqrt{\Delta m_{41}^2 + \Delta m_{51}^2} \simeq 4.0$ eV.
- SISa: same as SNSa, except for inversely ordered active neutrinos.
- SISb: same as SNSb, except for inversely ordered active neutrinos.

Note that these are all lower limits, because we have put the smallest neutrino mass to zero. In case of SSI the effective mass can vanish when the 3 active neutrinos are inversely ordered, in contrast to the three neutrino case in Section 4.2.2. If future $0\nu\beta\beta$ -experiments measure a tiny effective mass, or obtain a limit below $\langle m_{ee} \rangle_{\min}^{\text{IH}}$ given in Eq. (50), and the neutrino mass ordering is confirmed to be inverted from long-baseline neutrino oscillations, the sterile neutrino hypothesis would be an attractive explanation for this inconsistency. This is the first example in which a deviation from the standard picture of 3 active neutrinos shows up and influences the interpretation of $0\nu\beta\beta$. We show in Fig. 22 the effective mass against the smallest mass for the 1+3 and 2+3 cases.

Obviously all schemes have difficulties with cosmology, the contribution to the sum of masses exceeds 1.5 eV in all cases. KATRIN and next generation $0\nu\beta\beta$ -experiments will see a signal in all cases except for SSI and SSN, unless the masses and mixings take values at the very high end of their currently allowed ranges. An analysis of KATRIN's potential to separate one or more sterile neutrino component from the active neutrino component has been performed in¹⁸¹. It was shown that KATRIN will definitely be able to separate one or more sterile neutrino components from the active neutrino ones, if they do in fact have mass and mixing in the range considered here. With a limit on the effective mass being around 0.5 eV (see Table 2), the schemes with QD neutrinos with mass scale $\sqrt{\Delta m_{41}^2}$ or $\sqrt{\Delta m_{51}^2}$ are in fact already tested, giving constraints on the Majorana phases α already at the current stage¹²⁶.

If the “reactor only” results of $|U_{e4}| = 0.151$ and $\Delta m_{41}^2 = 1.78 \text{ eV}^2$ are used, then $\Sigma \gtrsim \sqrt{\Delta m_{41}^2} \simeq 1.3 \text{ eV}$ or $\Sigma \gtrsim 3 \sqrt{\Delta m_{41}^2} \simeq 4.0 \text{ eV}$, depending on whether a 1 + 3 or 3 + 1 scheme is realized. The contribution to KATRIN is either 0.52 or 1.3 eV, and the effective mass either receives a contribution of 0.03 eV, or corresponds to QD neutrinos with a mass scale $\sqrt{\Delta m_{41}^2}$. For the 1+3 case, again, the effective mass can vanish if the active neutrinos are inversely ordered.

The existence of sterile neutrinos can also be tested in upcoming oscillation experiments and via cosmological observations, as discussed in Section 4.1.2.

4.2.10. Exotic modifications of the three neutrino picture

Exotic modifications of the 3-neutrino framework are possible and may spoil the discussion presented so far in this Section.

The most obvious modification is that neutrinos are **Dirac particles**, in which case there is no neutrino-less double beta decay and writing this review was all in vain. A useful way to show this in the effective mass is to note that one Dirac neutrino can be written as two maximally mixed Majorana neutrinos with common mass m_i and opposite CP parity. The effective mass is then

$$\sum_i \sqrt{\frac{1}{2}} |U_{ei}|^2 (m_i + m_i e^{i\pi}) = 0. \quad (63)$$

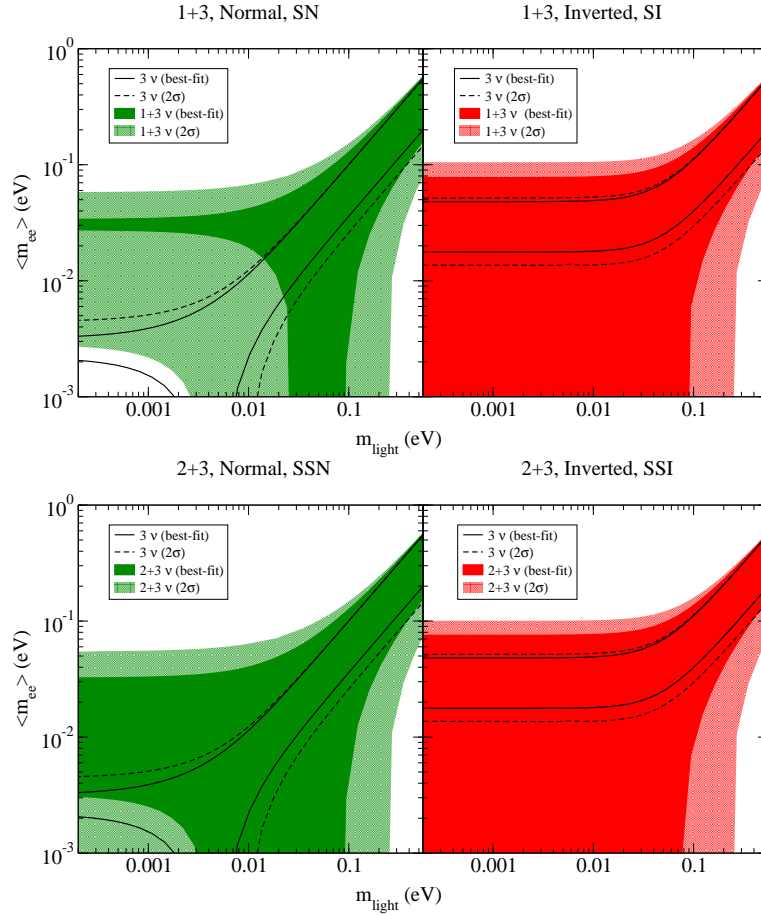


Fig. 22. Top: Effective mass against the smallest mass for the 1+3 scheme, with $\Delta m_{41}^2 = 1.78 \text{ eV}^2$, $|U_{e4}|^2 = 0.023$ (dark) and the 2σ range $\Delta m_{41}^2 = (1.61 - 2.01) \text{ eV}^2$, $|U_{e4}|^2 = 0.006 - 0.040$ (light). Bottom: same as above for 2+3 scheme, with $\Delta m_{41}^2 = 0.47 \text{ eV}^2$, $\Delta m_{51}^2 = 0.87 \text{ eV}^2$, $|U_{e4}|^2 = 0.016$, $|U_{e5}|^2 = 0.019$ (dark) and $\Delta m_{41}^2 = (0.42 - 0.52) \text{ eV}^2$, $\Delta m_{51}^2 = (0.77 - 0.97) \text{ eV}^2$, $|U_{e4}|^2 = 0.004 - 0.029$, $|U_{e5}|^2 = 0.005 - 0.033$ (light). The black solid and dashed lines correspond to the standard 3 neutrino best-fit and 2σ cases.

A small splitting of the degeneracy can be described with the mass matrix

$$m_i \begin{pmatrix} \epsilon & 1 \\ 1 & 0 \end{pmatrix} \rightarrow U = \sqrt{\frac{1}{2}} \begin{pmatrix} 1 + \frac{\epsilon}{4} & -1 + \frac{\epsilon}{4} \\ 1 - \frac{\epsilon}{4} & 1 + \frac{\epsilon}{4} \end{pmatrix} \text{ and } m_i^\pm = m_i \left(\pm 1 + \frac{\epsilon}{2} \right), \quad (64)$$

with the indicated new eigenstates and mixing matrix. These **Pseudo-Dirac neutrinos** lead to a contribution to the effective mass of about $\epsilon m_i = \frac{1}{2} \delta m^2 / m_i$, with $\delta m^2 = (m_i^+)^2 - (m_i^-)^2$. Regarding limits on such splitting, roughly speaking, values larger than $\delta m^2 \simeq 10^{-11} \text{ eV}^2$ for m_1 and m_2 are forbidden by solar neutrino data, and $\delta m^2 \gtrsim 10^{-3} \text{ eV}^2$ for m_3 by atmospheric data¹⁸². If all three states are Pseudo-

Dirac the effective mass is basically zero¹⁸³, while if one or two are Pseudo-Dirac interesting predictions for the effective mass arise. This can happen in “bimodal” or “**schizophrenic**” scenarios¹⁸⁴, in which at leading order one or two mass states are Dirac particles while the other one is Majorana. Because lepton number is not conserved, loop corrections imply small Pseudo-Dirac terms for the Dirac states. For instance, if ν_2 is a Dirac particle then the effective mass in the inverted hierarchy is¹⁸⁴ $\langle m_{ee} \rangle \simeq \sqrt{\Delta m_A^2} c_{12}^2 c_{13}^2$, roughly a factor of two larger than the minimal value in the standard case, see Eq. (49). A generalization to all possibilities can be found in¹⁸⁵.

A possible modification of the three neutrino picture mentioned before is the possible **non-unitarity of the PMNS matrix**, which has however negligible effect on the effective mass¹⁵⁶.

Another exotic property is **CPT violation**. Interesting consequences for $0\nu\beta\beta$ have been considered in¹⁸⁶, where a simple one family example is discussed. In the $(\nu, \bar{\nu})$ basis, where CPT transforms ν into $\bar{\nu}$ up to a phase, the mass matrix can be written as

$$M = \begin{pmatrix} \mu + \Delta & y^* \\ y & \mu - \Delta \end{pmatrix}. \quad (65)$$

Here y mixes ν and $\bar{\nu}$, while Δ leads to different masses for ν and $\bar{\nu}$. The eigenstates ν_{\pm} with masses $m_{\pm} = \mu \pm \sqrt{|y|^2 + \Delta^2}$ can be shown to be Majorana neutrinos (i.e. CPT transforms ν_{\pm} into ν_{\pm} up to a phase) only if $\Delta = 0$. This in turn would imply however that CPT is conserved. CPT is violated for $\Delta \neq 0$, in which case neutrinos cannot be Majorana particles. The amplitude for $0\nu\beta\beta$ sums over m_+ and m_- and is non-zero¹⁸⁶. Therefore, neutrino-less double beta decay takes place even if neutrinos are strictly speaking not Majorana particles. The neutrino-less double positron decay proceeds with the same “effective mass”.

In principle $0\nu\beta\beta$ can also provide limits on parameters associated with violation of **Lorentz invariance** or the **equivalence principle**. The constraints¹⁸⁷ on the difference of maximal velocities of mass states or on non-universal couplings of neutrinos to the gravitational potential are in general weaker than the ones from neutrino oscillations¹⁸⁸.

It should be mentioned here that $2\nu\beta\beta$ constrains violation of the **spin-statistics theorem** for neutrinos. With two identical particles in the final state there are two diagrams with exchanged momenta $p_1 \leftrightarrow p_2$. Their relative sign depends on whether Fermi-Dirac or Bose-Einstein statistics applies. By writing the amplitude \mathcal{A} as $\cos^2 \phi \mathcal{A}_{\text{fermionic}} + \sin^2 \phi \mathcal{A}_{\text{bosonic}}$, conservative limits of $\sin^2 \phi \lesssim 0.5$ can be set¹⁸⁹.

5. Non-Standard Interpretations

After discussing in some detail the standard interpretation of neutrino-less double beta decay, we turn to non-standard interpretations, repeated here for convenience:

Neutrino-less double beta decay is mediated by some other lepton number violating physics, and light massive Majorana neutrinos (the ones which oscillate) potentially leading to $0\nu\beta\beta$ give negligible or no contribution.

It is convenient to express the decay width of neutrino-less double beta decay in the following form (see Eq. (4))

$$\Gamma^{0\nu} = \sum_x G_x(Q, Z) |\mathcal{M}_x \eta_x|^2. \quad (66)$$

Here we sum over all possible mechanisms which are denoted by a subscript x , with matrix element \mathcal{M}_x and a dimensionless particle physics parameter η_x . For the standard interpretation of light neutrino exchange,

$$\eta_1 = \langle m_{ee} \rangle / m_e \lesssim 9.9 \times 10^{-7}. \quad (67)$$

Note that different mechanisms can interfere coherently, a case we will discuss in Section 6.4. Most of the times the alternative mechanism is connected to a high energy scale. The corresponding particle physics amplitude, which has to be compared with the standard one $G_F^2 \langle m_{ee} \rangle / q^2$ from Eq. (40), could be written as

$$\mathcal{A}_{\text{heavy}} \simeq \frac{c}{\Lambda^5}. \quad (68)$$

Here c contains new Yukawa and/or gauge couplings and Λ is the new physics scale. This is a helpful but crude approximation, which is in fact not fulfilled by several mechanisms to be discussed in the following. However, the current limit $\langle m_{ee} \rangle = 0.5$ eV corresponds to $\Lambda \simeq \text{TeV}$, by all means an interesting energy scale. In fact, we will encounter in what follows some alternative mechanisms with LHC phenomenology. On the other hand, it means that if the new physics scale exceeds, say, 10 TeV, then it will not contribute significantly to $0\nu\beta\beta$. In what follows we will aim at a complete list of non-standard realizations of neutrino-less double beta decay, for earlier reviews see^{190,191}.

An ideal experimental signature for drawing the conclusion that a mechanism different from active neutrino exchange is present would be that KATRIN and cosmological observations do not see a signal, but $0\nu\beta\beta$ is observed with a half-life corresponding to, say, $\langle m_{ee} \rangle \simeq 0.5$ eV. To put in another way, in plots of neutrino mass observables, such as in Fig. 12, one ends at points outside the allowed areas. On the other hand, if one ends in those plots in the allowed areas, then it is not necessary to consider non-standard interpretations, except for setting limits on the associated parameters.

5.1. *Heavy neutrinos*

An interesting way of realizing $0\nu\beta\beta$ is through the exchange of heavy Majorana neutrinos^{192,193,194}. The Feynman diagram is the same as in Fig. 8, with the neutrinos not being the ones whose oscillations are observed, and with the PMNS matrix elements U_{ei} replaced by S_{ei} , where S is the matrix describing the mixing of the

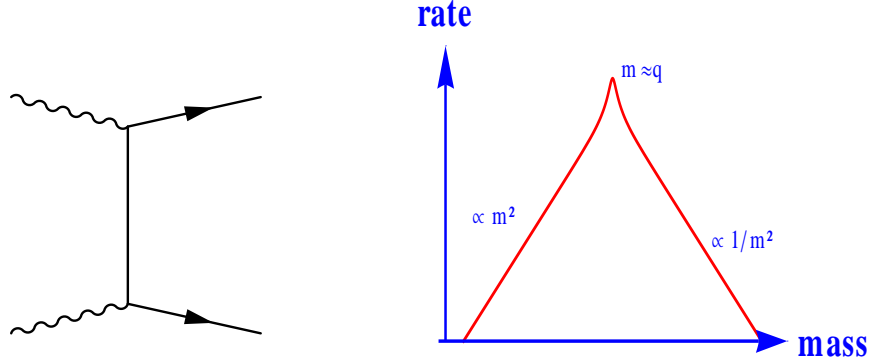


Fig. 23. Left: “lobster” diagram for lepton number violating processes with Majorana neutrino exchange. Right: typical behavior of $0\nu\beta\beta$ -like processes with free Majorana mass m : for small masses $m^2 \ll q^2$ the rate increases with m^2 , while for large masses $m^2 \gg q^2$ it decreases with m^{-2} . Here “small” and “large” are defined relative to the energy scale q^2 of the process, which could be the mass of a decaying particle/nucleus, or the center of mass energy of a collider process. The maximum rate can be expected when the mass corresponds to the available energy.

heavy neutrinos with the SM charged leptons in the charged current term. Recall the form of the $0\nu\beta\beta$ -amplitude on the particle physics level:

$$\mathcal{A} \propto \frac{m_i}{q^2 - m_i^2} \propto \begin{cases} m_i & \text{for } q^2 \gg m_i^2, \\ \frac{1}{m_i} & \text{for } q^2 \ll m_i^2. \end{cases} \quad (69)$$

As mentioned before, due to the typical structure of the diagram, symbolically displayed in Fig. 23, one sometimes calls it “lobster diagram”. With $0\nu\beta\beta$ being a t (and u -) channel process there is no resonance. In Fig. 23 we show the typical behavior of $0\nu\beta\beta$ -like processes as a function of the Majorana mass. Let us stress that the maximum rate can be expected when the mass corresponds to the available energy, i.e. about 100 MeV for $0\nu\beta\beta$. In analogous processes of neutrino-less double beta decay (see Section 7) the energy scale and therefore the range in which the strongest limits on the mass and mixing arise, may be different. In addition, there could be s -channel processes in which a resonance could be hit, leading to even stronger constraints. If $m_i \gtrsim 100$ MeV, the rate is proportional to

$$\sqrt{\Gamma^{0\nu}} \propto \left\langle \frac{1}{m} \right\rangle \equiv \sum_i \frac{S_{ei}^2}{m_i}. \quad (70)$$

We will focus on this case of heavy neutrinos.

Turning to nuclear physics, the neutrino potential in Eq. (13) is modified because the neutrino energy and momentum are dominated by its heavy mass. A dependence on the axial mass $M_A \simeq 0.9$ GeV, which appears in the nuclear form factors and which takes into account the finite size of the nucleons, is introduced

because of the short-range nature of the process. Without the form factor the process would be exponentially suppressed due to the repulsion of the two decaying nuclei. Note that this is the first diagram for $0\nu\beta\beta$ which is purely short-range or point-like. Details of the nuclear physics can be found in Refs.^{195,2,57,196,197}. Often one writes the contribution of heavy neutrinos as $\sqrt{\Gamma^{0\nu}} \propto \langle \frac{1}{m} \rangle M_A^2 F(A, m_i)$, where $F(A, m_i) = \mathcal{O}(0.1)$ is a mildly varying function. One can write the decay width as $\Gamma_h^{0\nu} = G_h(Q, Z) |\eta_h \mathcal{M}_h|^2$, where in the context of Eq. (66) one can write the LNV parameter for heavy neutrino exchange as $m_p \langle \frac{1}{m} \rangle$, with m_p the proton mass. The same phase space factors as in the standard case apply, and the matrix elements absorb now various factors such as the dependence on M_A or $F(A, m_i)$. The particle physics parameter $\langle \frac{1}{m} \rangle$ contains all singlet fermions coupling with SM charged leptons in the charged current terms, including heavy neutrinos from the type I and III seesaw mechanisms, as well as generalizations thereof, such as inverse seesaw¹⁹⁸.

Ref.⁹² has recently calculated within the QRPA approach the NMEs \mathcal{M}_h in the above convention and found a range of roughly a factor of two: 172 – 412 for ^{76}Ge , 165 – 408 for ^{82}Se , 185 – 404 for ^{100}Mo and 171 – 384 for ^{130}Te . The spread originates from variation of g_A , the nucleon-nucleon potential and the model space size. The NMEs seem to be much larger than the ones for the standard case, but as mentioned above they absorb several parameters. With the current limits on the half-lives from Table 2 and the phase space factors from Table 1, we find

$$\langle \frac{1}{m} \rangle \leq \begin{cases} (0.75 - 1.8) \times 10^{-8} \text{ GeV}^{-1} & \text{for } ^{76}\text{Ge}, \\ (2.8 - 6.9) \times 10^{-8} \text{ GeV}^{-1} & \text{for } ^{82}\text{Se}, \\ (1.3 - 2.8) \times 10^{-8} \text{ GeV}^{-1} & \text{for } ^{100}\text{Mo}, \\ (0.82 - 1.8) \times 10^{-8} \text{ GeV}^{-1} & \text{for } ^{130}\text{Te}, \end{cases} \quad (71)$$

The dimensionless LNV parameter for heavy neutrino exchange is

$$\eta_h = m_p \langle \frac{1}{m} \rangle \leq 1.7 \times 10^{-8}, \quad (72)$$

where m_p is the proton mass. Interestingly the best limit $\langle \frac{1}{m} \rangle \leq 1.8 \times 10^{-8} \text{ GeV}^{-1}$ stems jointly from ^{76}Ge and ^{130}Te . For heavy neutrinos the limit $\sum_i |S_{ei}|^2 \leq 0.0052$ from global fits applies, and this constraint on $|S_{ei}|^2$ is stronger for $m_i \gtrsim 2.9 \times 10^5 \text{ GeV}$. Naively, one can simply compare the particle physics amplitudes $G_F^2 \langle m_{ee} \rangle / q^2$ and $G_F^2 \langle \frac{1}{m} \rangle$. With $\langle m_{ee} \rangle \lesssim 0.5 \text{ eV}$ and $q \simeq 100 \text{ MeV}$ it follows that $\langle \frac{1}{m} \rangle \lesssim 5 \times 10^{-8} \text{ GeV}^{-1}$, which is basically the same number as Eq. (71), given the NME uncertainty. As we will see in the following, the comparison of an alternative mechanism of $0\nu\beta\beta$ to the standard mechanism *on the amplitude level* is remarkably successful, and gives constraints which are consistent with literature values taking the onerous nuclear physics aspects into account. Formulated provocatively, matrix elements are order one numbers with a corresponding uncertainty, and comparing the particle physics amplitudes introduces an order one factor uncertainty, which often is good enough to understand the particle physics implications of $0\nu\beta\beta$.

Fig. 24 shows the exclusion limits on mass and mixing of heavy sterile neutrinos from Ref.¹⁹⁶. The calculation covers all masses from keV to 10^{15} GeV . As

expected, the limits are strongest when the neutrino mass corresponds to the energy scale $q \simeq 100$ MeV.

There is an obvious source of heavy neutrinos, namely the ones from the type I seesaw mechanism, N_{Ri} , with masses M_i . Note that these particles provide two sources of $0\nu\beta\beta$: a *direct* one realized by exchange of N_{Ri} and an *indirect* one by light neutrino exchange. However, the N_{Ri} are typically very heavy and have suppressed mixing $S \simeq m_D/M_R \simeq m_\nu/m_D \simeq \sqrt{m_\nu/M_R}$, therefore they lead to basically vanishing $\langle \frac{1}{m} \rangle$. Without any strong, instable and fine-tuned cancellations¹⁹⁹, the direct contribution from $\langle m_{ee} \rangle$ is larger in seesaw scenarios^{200,156,197}. Within type I seesaw there is an exact relation

$$\sum_i N_{ei}^2 m_i + S_{ei}^2 M_i = 0, \quad (73)$$

where $|\sum N_{ei}^2 m_i|$ is the effective mass $\langle m_{ee} \rangle$ in type I seesaw scenarios in which the PMNS matrix is strictly speaking not unitary and thus denoted here by N . The zero on the rhs of the above equation is nothing but the upper left zero in the full seesaw mass matrix in Eq. (18). Therefore, with Eq. (73), the limit on $\langle m_{ee} \rangle \lesssim 0.5$ eV directly translates to $|\sum S_{ei}^2 M_i| \lesssim 0.5$ eV, which in the absence of cancellations is much more stringent than $|\sum S_{ei}^2/M_i| \lesssim 1.8 \times 10^{-8} \text{ GeV}^{-1}$. If a low scale seesaw mechanism is applied and both the m_i and the M_i are below 100 MeV, then there will be no neutrino-less double beta decay because²⁰¹ of the exact seesaw relation Eq. (73).

In type III seesaw scenarios the neutral component of the triplet plays the role

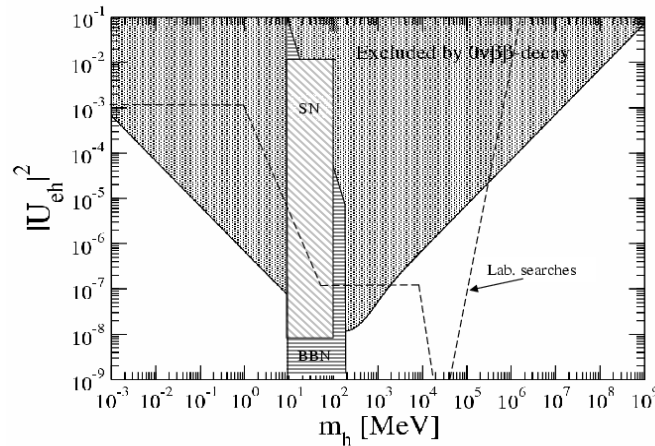


Fig. 24. Exclusion plot in the $|U_{eh}|^2$ - m_h plane, where m_h and $|U_{eh}|$ are heavy neutrino masses and their mixing with the SM electron doublet. The shaded regions are excluded by $0\nu\beta\beta$ -decay, by Big Bang nucleosynthesis and by SN1987A neutrino observations. Taken from¹⁹⁶.

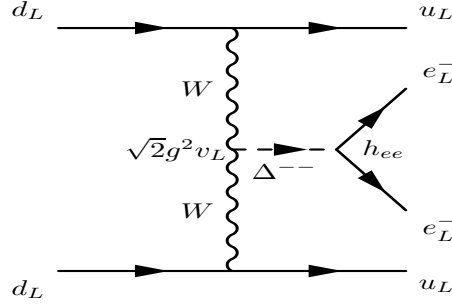


Fig. 25. Quark level Feynman diagram for the triplet realization of neutrino-less double beta decay.

of the heavy neutrino in the type I seesaw and the discussion is analogous.

5.2. Higgs triplets

Higgs triplets contain a doubly charged scalar and can directly couple to two electrons and to two W -bosons, giving rise to the quark level Feynman diagram shown in Fig. 25, first noted in²⁰². This is the first diagram for $0\nu\beta\beta$ which does not contain a neutrino line. We will show in this Section that in the simple version based solely on $SU(2)_L \times U(1)_Y$ the triplet does not play a significant role in $0\nu\beta\beta$. In left-right symmetric theories this changes, and we will deal with this class of theories in the next Section.

The $SU(2)_L$ triplet can be written as

$$\Delta = \begin{pmatrix} \Delta^-/\sqrt{2} & \Delta^{--} \\ \Delta^0 & -\Delta^-/\sqrt{2} \end{pmatrix}, \quad (74)$$

and the neutral component receives a vev $\langle \Delta^0 \rangle = v_L/2$, which induces from the Lagrangian $\mathcal{L}_\Delta = h_{\alpha\beta} \bar{L}_\alpha^c i\tau_2 \Delta L_\beta$, where L_α are Lepton doublets of flavor α , the neutrino mass matrix $m_\nu = h v_L$. The vev v_L is constrained from the electroweak ρ parameter to be less than about 8 GeV, and current limits on the triplet masses are around 100 GeV²⁰³. The particle physics amplitude for $0\nu\beta\beta$ can be read off from Fig. (25) as

$$\mathcal{A}_\Delta \simeq G_F^2 \frac{h_{ee} v_L}{m_\Delta^2} \lesssim G_F^2 \frac{(m_\nu)_{ee}}{m_\Delta^2} = G_F^2 \frac{\langle m_{ee} \rangle}{m_\Delta^2}. \quad (75)$$

If the triplet was responsible for neutrino mass (type II seesaw) then $h_{ee} v_L = (m_\nu)_{ee}$, which is the largest possible value of $h_{ee} v_L$, unless unnatural cancellations of different seesaw terms take place. Comparing with the standard amplitude in Eq. (40) we see that the rate for triplet exchange is suppressed with respect to the standard mechanism by at least a factor $(q/m_\Delta)^4 \lesssim 10^{-12}$ and hence not of relevance^{204,205}. Nuclear physics details add some additional suppression²⁰⁶.

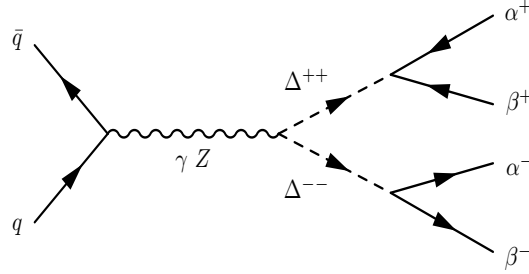


Fig. 26. Drell-Yan production of Higgs triplets at the LHC with subsequent decay into like-sign lepton pairs. In left-right symmetric theories this process is possible as well.

There are additional diagrams in which one or two of the W -bosons in Fig. 25 are replaced by singly charged scalars Δ^- (see e.g.²⁰⁷) but those amplitudes are suppressed by a factor v_L/v for each Δ^- -quark vertex and by $(m_W/m_{\Delta^-})^2$ for each Δ^- propagator. In principle one can evade these constraints by adding exotic scalars with specific hypercharge and isospin quantum numbers^{204,208}.

Finally, we should mention the possibility of Higgs triplet production at the LHC, which is possible up to masses of about 800 GeV²⁰⁹. The relevant diagram is shown in Fig. 26. If their branching ratio into leptons is larger than into a W boson pair, then their decay can give information on the neutrino mass matrix if in addition the pure type II seesaw is realized. In fact, $\text{BR}(\Delta^{--} \rightarrow \alpha^- \beta^-) \propto (m_\nu)_{\alpha\beta}$, and an alternative method to probe Majorana neutrino properties was possible, as studied e.g. in^{209,210,207}. Note in particular that the branching ratio for decays into two electrons is proportional to the effective mass. The other entries of the mass matrix could be directly studied as well, which is not possible with other processes, see Section 7. In case both the triplet and the type I seesaw are at work, the exact seesaw relation in Eq. (73) is modified to

$$\sum_i N_{ei}^2 m_i + S_{ei}^2 M_i = h_{ee} v_L, \quad (76)$$

which links in principle light and heavy neutrino parameters with triplet parameters.

5.3. Left-right symmetric theories

Left-right (LR) symmetric theories are a popular and appealing extension of the Standard Model, in which $SU(2)_L \times SU(2)_R \times U(1)_{B-L}$ is the extended gauge group. Such a gauge symmetry can be arranged in breaking patterns of larger groups such as $SO(10)$ or the Pati-Salam group. It is a natural framework to justify the type I + II seesaw terms in Eq. (20). The Higgs sector of the theory contains²¹¹ a “left-handed triplet” Δ_L with quantum numbers $(3, 1, 2)$, a “right-handed triplet”

Δ_R with quantum numbers $(1, 3, 2)$, and a bi-doublet Φ with $(2, 2, 0)$, which is not important for $0\nu\beta\beta$. At low energies the potential consequences of LR symmetry are mainly right-handed currents mediated by a W_R with coupling strength $g_L = g_R = g$, and the presence of Δ_L and Δ_R . Here Δ_L can be responsible for a contribution $M_L = h v_L$ to neutrino mass. It can give a direct contribution to $0\nu\beta\beta$, as discussed in Section 5.2, where we have learned that it is suppressed. The Δ_R gives mass to the right-handed neutrinos $M_R = f v_R$, where v_R is the vev of its neutral component and f a Yukawa coupling matrix. Often it is assumed that a discrete LR symmetry holds in addition, in which case $h = f^*$, or $M_L = M_R^*$. Consequently¹, with writing $m_D = y v$ it follows

$$m_\nu = M_L - m_D^T M_R^{-1} m_D = v_L \left(h - \frac{v^2}{v_R v_L} y^T f^{-1} y \right) = v_L \left(h - \frac{v^2}{v_R v_L} y^T h^{*-1} y \right). \quad (77)$$

From the analysis of the scalar potential it follows $v_L \propto v^2/v_R$ and therefore neutrino mass is zero in the limit $v_R \rightarrow \infty$, in which case there are no RH currents, because $M_{W_R} \simeq g_R v_R$. This connection of small neutrino mass and almost maximal parity violation makes LR symmetric theories very interesting.

In what regards $0\nu\beta\beta$, there are now several diagrams which allow for it. In certain variants of LR symmetric models one of the diagrams will dominate over the other, but we will not enter discussion of the details, and simply give the limits arising from each diagram individually.

First of all, the Δ_R can mediate the process in analogy to the diagram in Fig. 25. It couples to the W_R instead of the W , and the two emitted electrons (as well as the quarks) are right-handed instead of left-handed. The amplitude goes as

$$\mathcal{A}_{\Delta_R} \simeq G_F^2 \left(\frac{m_W}{M_{W_R}} \right)^4 \frac{f_{ee} v_R}{m_{\Delta_R}^2} = G_F^2 \left(\frac{m_W}{M_{W_R}} \right)^4 \frac{(M_R)_{ee}}{m_{\Delta_R}^2}, \quad (78)$$

where $(M_R)_{ee}$ can be written as $\sum V_{ei}^2 M_i$, with M_i the right-handed neutrino masses whose mass matrix M_R is diagonalized with V . Comparing with the naive amplitude in Eq. (68) gives $\Lambda^5 \simeq (m_{\Delta_R}^2 M_{W_R}^4)/|(M_R)_{ee}|$, and from the standard amplitude (40) it follows

$$\frac{|(M_R)_{ee}|}{m_{\Delta_R}^2 M_{W_R}^4} \lesssim 10^{-15} \text{ GeV}^{-5}. \quad (79)$$

Expressing it with a dimensionless quantity is possible by defining

$$\eta_{\Delta_R} = \frac{|(M_R)_{ee}|}{m_{\Delta_R}^2 M_{W_R}^4} \frac{m_p}{G_F^2} \lesssim 6.9 \times 10^{-6}. \quad (80)$$

¹Often one considers $h = f$, or $M_L = M_R$, which happens when the discrete LR symmetry is connected to charge conjugation instead of parity. The limits from LFV and CP violation in the quark sector case are stronger in this case²¹².

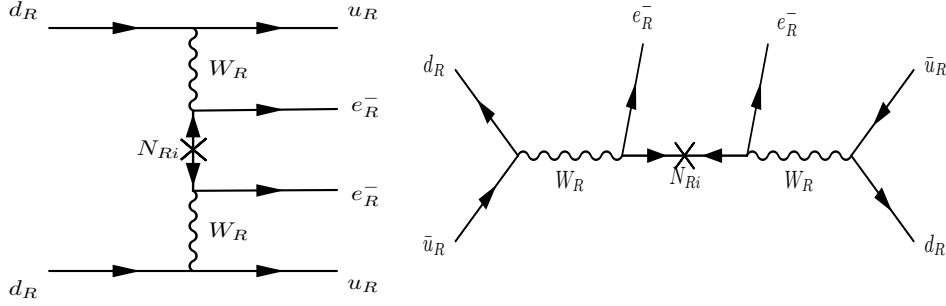


Fig. 27. Left: quark level Feynman diagrams for left-right symmetric realizations of neutrino-less double beta decay with heavy neutrino exchange. Right: the corresponding diagram at LHC.

The limit is compatible with TeV-scale left-right symmetry, one could for instance rewrite it as

$$M_{W_R} \gtrsim 1.9 \left(\frac{|(M_R)_{ee}|}{500 \text{ GeV}} \right)^{1/4} \left(\frac{200 \text{ GeV}}{m_{\Delta_R}} \right)^{1/2} \text{ TeV}. \quad (81)$$

In fact, limits from $0\nu\beta\beta$ are competitive to other means of probing the parameters associated to LR symmetry^{213,212}. Higgs triplets can be produced at the LHC, in the same way as shown in Fig. 26. Their decay into electrons or positrons probes $f_{ee} = (M_R)_{ee}/v_R$. An interesting possibility in these models is that M_L dominates the type I + II seesaw formula: $m_\nu = M_L$. In this case $M_R \propto m_\nu$, i.e. the heavy neutrinos get diagonalized by the PMNS matrix and $(M_R)_{ee}$ becomes less arbitrary. However, in those cases it turns out that constraints from LFV, in particular $\mu \rightarrow 3e$, which can be mediated by triplets at tree level, force $m_\Delta \ll M_i$. This in turn implies that heavy neutrino exchange in connection with RH currents gives a larger contribution to $0\nu\beta\beta$ ²¹⁴.

Recall that heavy neutrino coupling to the usual LH currents is suppressed by small mixing m_D/M_R . The diagram to study is therefore the standard one from Fig. (8) with W_R exchange²¹⁵, shown in Fig. 27. The amplitude goes as

$$\mathcal{A}_{N_R} \simeq G_F^2 \left(\frac{m_W}{M_{W_R}} \right)^4 \sum \frac{V_{ei}^2}{M_i}. \quad (82)$$

If $f = h$ (or $f = h^*$) and type II dominance holds, then $V = U$ ($V = U^*$) and the PMNS matrix appears in this expression. By noting that the NMEs are the same as for the heavy neutrino exchange discussed in Section 5.1, we can use the limit from Eq. (71) to find

$$\left| \sum \frac{V_{ei}^2}{M_{W_R}^4 M_i} \right| \leq \begin{cases} (1.8 - 4.3) \times 10^{-16} \text{ GeV}^{-5} & \text{for } ^{76}\text{Ge}, \\ (6.7 - 16.6) \times 10^{-16} \text{ GeV}^{-5} & \text{for } ^{82}\text{Se}, \\ (3.1 - 16.6) \times 10^{-16} \text{ GeV}^{-5} & \text{for } ^{100}\text{Mo}, \\ (2.0 - 4.3) \times 10^{-16} \text{ GeV}^{-5} & \text{for } ^{130}\text{Te}, \end{cases} \quad (83)$$

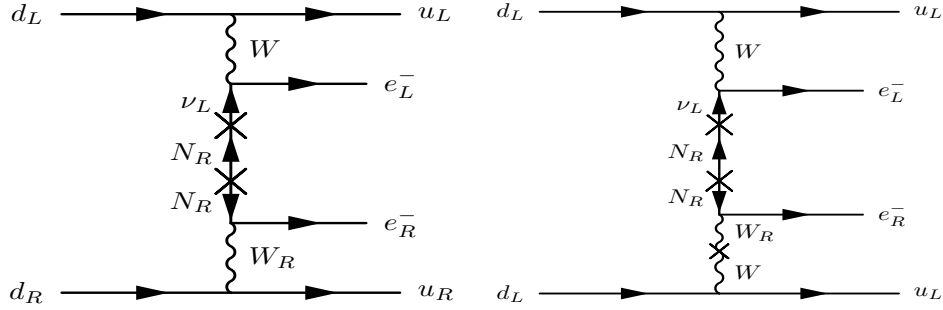


Fig. 28. Quark level Feynman diagrams for left-right symmetric realizations of neutrino-less double beta decay. Left is the λ -mechanism, right the η -mechanism.

and hence the dimensionless particle physics parameter has the same limit as η_h in Eq. (72):

$$\eta_{N_R} = m_p \left| \sum \frac{V_{ei}^2}{M_i} \right| \left(\frac{m_W}{M_{W_R}} \right)^4 \leq 1.7 \times 10^{-8}. \quad (84)$$

This limit again corresponds to TeV scale, which can be seen by rewriting it as

$$M_{W_R} \gtrsim 1.5 \left(\frac{500 \text{ GeV}}{V_{ei}^2/M_i} \right)^{1/4} \text{ TeV}. \quad (85)$$

A straightforward phenomenological LHC aspect of heavy neutrino exchange in left-right symmetric theories is seen in Fig. 27. Like-sign lepton production²¹⁶ is possible and allows to directly test this mechanism. The current limit on M_{W_R} set by LHC data is 1.4 TeV, both for very light right-handed neutrino mass²¹⁷, as well as for masses between²¹⁸ 100 GeV and M_{W_R} . In the future, LHC can detect masses up to a few TeV, and right-handed neutrinos up to TeV. This will test contributions of right-handed neutrino exchange to $0\nu\beta\beta$.

The remaining two diagrams for LR symmetry are stemming from mixing of the left- and right-handed sectors. First of all, one of the W bosons in the standard diagram could be right-handed, leading to the left diagram in Fig. 28. Its amplitude is

$$\mathcal{A}_\lambda \simeq G_F^2 \left(\frac{m_W}{M_{W_R}} \right)^2 \sum U_{ei} \tilde{S}_{ei} \frac{1}{q}, \quad (86)$$

where \tilde{S} is the matrix which quantifies the mixing of the SM leptons with RH currents. Note that one of the hadronic currents is right-handed. The dependence on $1/q$ can be understood from the RH nature of one of the vertices (see the comments after Eq. (36)). The dimensionless particle physics parameter is

$$\langle \lambda \rangle \equiv \eta_\lambda = \left(\frac{m_W}{M_{W_R}} \right)^2 \left| \sum U_{ei} \tilde{S}_{ei} \right|. \quad (87)$$

The other contribution takes W - W_R mixing, quantified by $\tan \zeta$, into account and has an amplitude given by

$$\mathcal{A}_\eta \simeq G_F^2 \tan \zeta \sum U_{ei} \tilde{S}_{ei} \frac{1}{q}. \quad (88)$$

Here both hadronic currents are left-handed. The dimensionless particle physics parameter is

$$\langle \eta \rangle \equiv \eta_\eta = \tan \zeta \left| \sum U_{ei} \tilde{S}_{ei} \right|. \quad (89)$$

Note that the usual way in which both diagrams in Fig. 28 are drawn may be confusing. They are actually long-range diagrams with light neutrino exchange, and the lower vertex receives due to mixing with the RH current a (small) factor $\tilde{S}_{ei} \simeq m_D/M_R$. This term requires non-zero m_D and M_R less than infinitely heavy. Without M_R and hence without lepton number violation it would obviously not be there. The implicit lepton number violation necessary for the existence of the diagram is illustrated by a Majorana mass term and a Dirac mass term, which gives a total contribution m_D/M_R .

In both the λ and the η diagrams one of the emitted electrons is right-handed. The nuclear physics becomes more complicated now, because the momentum dependence of the amplitudes, $\mathcal{A} \propto q^\mu = (\omega, \vec{q})$, which introduces matrix elements corresponding to the time and space components of q^μ . In fact, the space components can give rise to $0^+ \rightarrow 2^+$ transitions, whose observation would therefore be a clear signal⁸⁴ of the presence of right-handed currents in $0\nu\beta\beta$. The main point here is that the time component (ω) parts turn out to be suppressed by order $(E_1 - E_2)/\omega \sim 10^{-2}$ due to cancellation of the two diagrams with interchanged electron lines, whose energies are E_1 and E_2 . This suppression makes the time component parts of the same order as the space component (\vec{q}) parts. The latter contain for $\langle \eta \rangle$ (not for $\langle \lambda \rangle$) two extra matrix elements, one of which stems from the nuclear recoil $\vec{Q} \sim \vec{q}$ (with the electrons emitted as s -waves). This contribution dominates and compensates the $(E_1 - E_2)/\omega$ suppression. These features are explained in detail e.g. in Ref.³.

We are not aware of any recent comparative study of the relevant NMEs for these processes. Ref.⁹⁰ has recently summarized the calculation from²¹⁹. We add to these results the ones from²²⁰ (which do not contain ^{150}Nd) and take the two sets of calculations as a span of NMEs. The result is

$$\langle \eta \rangle = \eta_\eta \leq \begin{cases} (4.0 - 11) \times 10^{-9} & \text{from } ^{76}\text{Ge}, \\ (1.4 - 4.4) \times 10^{-8} & \text{from } ^{82}\text{Se}, \\ (5.4 - 100.6) \times 10^{-9} & \text{from } ^{100}\text{Mo}, \\ (4.0 - 6.2) \times 10^{-9} & \text{from } ^{130}\text{Te}, \\ (1.2 - 1.6) \times 10^{-8} & \text{from } ^{136}\text{Xe}, \\ 1.4 \times 10^{-8} & \text{from } ^{150}\text{Nd}. \end{cases} \quad (90)$$

The best limit from ^{130}Te of about 6×10^{-9} corresponds to the naive result obtained by comparing the standard amplitude (40) with \mathcal{A}_η , from which $\langle \eta \rangle \lesssim 5 \times 10^{-9}$

is found. Again, comparing on the particle physics amplitude works amazingly well. However, this is here somewhat accidental, because the usually dominating time component part is suppressed by a factor 10^{-2} . This suppression in turn is compensated by terms from the space components such as the nuclear recoil term.

However, for $\langle\lambda\rangle$ one would be two orders of magnitude off. While the naive estimate would give $\langle\lambda\rangle \lesssim 5 \times 10^{-9}$, the more correct procedure described above gives

$$\langle\lambda\rangle = \eta_\lambda \leq \begin{cases} (6.1 - 15) \times 10^{-7} & \text{from } ^{76}\text{Ge}, \\ (1.8 - 3.8) \times 10^{-6} & \text{from } ^{82}\text{Se}, \\ (9.8 - 54.5) \times 10^{-7} & \text{from } ^{100}\text{Mo}, \\ (5.8 - 8.9) \times 10^{-7} & \text{from } ^{130}\text{Te}, \\ (2.1 - 3.2) \times 10^{-6} & \text{from } ^{136}\text{Xe}, \\ 1.4 \times 10^{-6} & \text{from } ^{150}\text{Nd}. \end{cases} \quad (91)$$

Again ^{130}Te dominates the constraints and gives $\langle\lambda\rangle \lesssim 9 \times 10^{-7}$. The two orders of magnitude difference with respect to the naive limit originate from the suppression of the dominating time component part of the amplitude by a factor of electron energy $\sim \text{MeV}$ divided by neutrino momentum $\sim 100 \text{ MeV}$.

To sum up, the full glory of left-right symmetric theories provides several possible diagrams for $0\nu\beta\beta$: standard, heavy neutrino exchange, heavy neutrino exchange with RH currents, left-handed triplet, right-handed triplet, λ and η . In principle, all should be considered at the same time, yielding correlated constraints^{195,215,221,222} in a multi-dimensional parameter space spanned by parameters M_{WR} , $\tan\zeta$, m_{Δ_R} , $(M_R)_{ee}$, $\sum V_{ei}^2/M_i$ and $\sum U_{ei}\tilde{S}_{ei}$. One can expect that left-handed triplet and heavy neutrino exchange with LH currents can be neglected, but the remaining diagrams could give observable $0\nu\beta\beta$ if the relevant masses and scales do not exceed TeV too much. These scales correspond to values testable at the LHC, via lepton flavor violation or rare processes in the quark sector, and interesting works analyzing this interplay have recently been published^{212,214}.

5.4. *Supersymmetric theories*

In the context of supersymmetric theories R -parity often plays an important role. It is defined as $(-1)^{3B+L+2s}$, where B (L) is baryon (lepton) number and s spin. For particles $R = 1$ while for sparticles $R = -1$. The usual MSSM Lagrangian²²³ conserves R . If R is violated, the following renormalizable and gauge invariant Lagrangian is allowed:

$$\mathcal{L}_R = \lambda_{ijk} \hat{L}_i \hat{L}_j \hat{e}_k^c + \lambda'_{ijk} \hat{L}_i \hat{Q}_j \hat{d}_k^c + \lambda''_{ijk} \hat{u}_i^c \hat{d}_j^c \hat{d}_k^c + \epsilon_i \hat{L}_i \hat{H}_u. \quad (92)$$

Here the \hat{L}_i (\hat{Q}_i) are superfields which contain the SM lepton (quark) doublets as well as the corresponding slepton (squark) doublets, u_i^c, d_i^c, e_i^c are superfields containing the singlets of particles and sparticles, while \hat{H}_u contains the Higgs and

Higgsino doublets; $i = 1, 2, 3$ is the family index. The terms proportional to λ''_{ijk} violate baryon number, and have to be tiny to forbid too rapid proton decay. The remaining three terms in Eq. (92) violate lepton number by one unit. If R -parity is broken^m (see²²⁸ for a review), diagrams with two such vertices can therefore lead to neutrino-less double beta decay^{229,230,231}. Note that now there are two $\Delta L = 1$ vertices instead of one explicit $\Delta L = 2$ mass term.

There is again an interesting possible interplay here, namely that the R -parity violating (RPV) terms are responsible for the neutrino mass itself. It is well-known that loop-induced Majorana neutrino masses can be generated by the λ and λ' terms. This would be their indirect contribution to $0\nu\beta\beta$, to be compared with the direct contributions to be discussed in this Section. A systematic analysis of the interplay of direct and indirect contributions to $0\nu\beta\beta$ is still lacking, but most often the neutrino mass constraints are weaker than the ones from $0\nu\beta\beta$, or the parameter space is chosen such that the RPV contributions to $0\nu\beta\beta$ dominate.

The most simple possibility here is “bilinear R -parity violation”, in which only the term $\epsilon_i \tilde{L}_i \tilde{H}_u$ is present. This is a realization of the type I seesaw, with the Higgsino playing the role of a single (TeV scale) heavy neutrino, which means that only one light neutrino is massive. Radiative corrections can generate the necessary other neutrino masses²³². Bilinear R -parity violation leads to mixing of neutrinos with neutralinos and of charged leptons with charginos. Effective \tilde{d}_L-u-e^c , $\tilde{e}_L-e^c-\nu$, $\tilde{d}_R-d-\nu$ and $\tilde{u}_L-u^c-\nu$ vertices arise, and can lead to $0\nu\beta\beta$ in diagrams²²⁴ which are similar to the ones in Fig. 29. For instance, one could have the upper left diagram with W instead of \tilde{e}_L exchange, or the lower left one with neutrino and W exchange, instead of the \tilde{e}_L and χ , respectively. Those diagrams have been found to be suppressed with respect to the standard mass mechanism²³³. We will concentrate on the trilinear terms from now on.

The two RPV contributions to $0\nu\beta\beta$ are shown in Figs. 29 (neutralino/gluino exchange, or λ'_{111} mechanism) and 30 (squark exchange, or $\lambda'_{131} \lambda'_{113}$ mechanism). Here the pion exchange dominance^{87,88} mentioned in Section 3.2 is realized. Limits on RPV SUSY parameters from $0\nu\beta\beta$ have been derived in^{234,235}.

The short distance diagrams are shown in Fig. 30. The naive estimate for the amplitude is

$$\mathcal{A}_{\tilde{R}_1} \simeq \frac{\lambda_{111}^2}{\Lambda_{\text{SUSY}}^5}, \quad (93)$$

where we set all sparticle masses to the same SUSY scale Λ_{SUSY} and the only relevant coupling is λ'_{111} , because the other vertices are order one gauge couplings. Comparing with the standard amplitude (40) gives $\lambda_{111}^2/\Lambda_{\text{SUSY}}^5 \lesssim 7 \times 10^{-18} \text{ GeV}^{-5}$.

^mIn principle also the case of R -parity conservation can via box diagrams lead to $0\nu\beta\beta$, if L violating sneutrino mass terms are present²²⁴. These are connected to the amplitude of $0\nu\beta\beta$ and L violating Majorana neutrino mass terms in analogy to the black-box theorem: the presence of one of the three implies the presence of the other two^{225,226}. However, the constraints from the sneutrino contribution to neutrino mass are stronger than the ones from $0\nu\beta\beta$ ²²⁷.

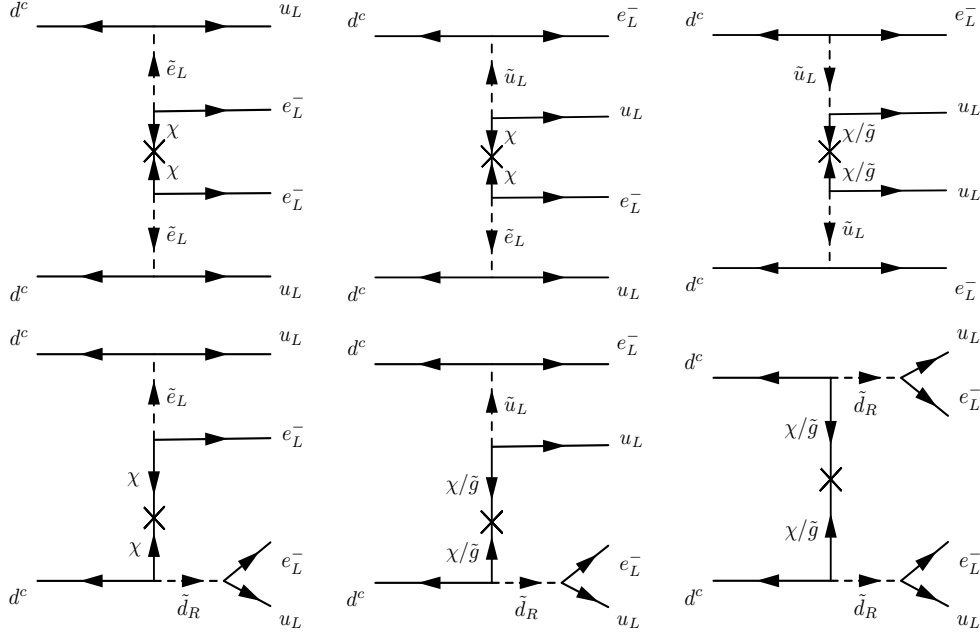


Fig. 29. Quark level Feynman diagrams for short-range R -parity violating SUSY contributions to $0\nu\beta\beta$, which are proportional to $\lambda_{111}^{\prime 2}$.

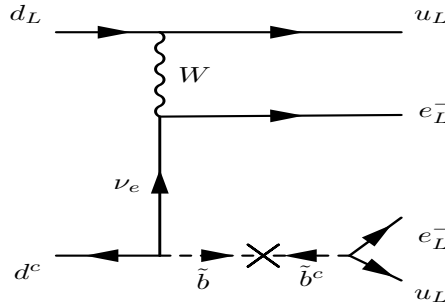


Fig. 30. Quark level Feynman diagram for long-range R -parity violating SUSY contribution to $0\nu\beta\beta$, which is proportional to $\lambda'_{131} \lambda'_{113}$.

The scale Λ_{SUSY}^5 differs for the six diagrams in Fig. 29, for instance it is related to $m_\chi m_{\tilde{e}_L}^4$ in the upper left and $m_{\tilde{g}} m_{\tilde{u}_L}^4$ in the upper right, etc.

Note that in the diagrams χ denotes all four neutralinos, which are linear combinations of neutral gauginos and Higgsinos. In case that gluinos and/or squarks are exchanged, Fierz transformations have to be performed to obtain colorless operators. As a result⁷, scalar, pseudoscalar and tensor matrix elements arise. At the

end of the day, one can express the matrix element as^{231,88,236}

$$\begin{aligned} \mathcal{M}_{\tilde{R}_1} = & \eta_{\tilde{g}} (\mathcal{M}_{\tilde{g}}^{2N} + \mathcal{M}^\pi) + \eta_\chi (\mathcal{M}_{\tilde{g}}^{2N} + \mathcal{M}^\pi) + \eta'_{\tilde{g}} \left(\mathcal{M}_{\tilde{f}}^{2N} + \frac{5}{8} \mathcal{M}^\pi \right) \\ & + \eta_{\chi\tilde{e}} \left(\mathcal{M}_{\tilde{f}}^{2N} + \frac{5}{8} \mathcal{M}^\pi \right) + \eta_{\chi\tilde{f}} \left(\mathcal{M}_{\tilde{f}}^{2N} + \frac{5}{8} \mathcal{M}^\pi \right), \end{aligned} \quad (94)$$

where $\mathcal{M}_{\tilde{g}}^{2N} = \mathcal{O}(100)$, $\mathcal{M}_{\tilde{f}}^{2N} = \mathcal{O}(10)$ are 2 nucleon NMEs and $\mathcal{M}^\pi = \mathcal{O}(100)$ pion exchange NMEs (their absolute magnitude exceeds the one of $\mathcal{M}_{\tilde{g}}^{2N}$). Whether neutralino or gluino exchange dominates depends on the SUSY parameters.

The particle physics parameters in Eq. (94) are^{231,88,236}

$$\begin{aligned} \eta_{\tilde{g}} &= \frac{\pi\alpha_3}{6} \frac{\lambda_{111}^{\prime 2}}{G_F^2} \frac{m_p}{m_{\tilde{g}}} \left(\frac{1}{m_{\tilde{u}_L}^4} + \frac{1}{m_{\tilde{d}_R}^4} - \frac{1}{2m_{\tilde{u}_L}^2 m_{\tilde{d}_R}^2} \right), \\ \eta_\chi &= \frac{\pi\alpha_2}{2} \frac{\lambda_{111}^{\prime 2}}{G_F^2} \sum_{i=1}^4 \frac{m_p}{m_{\chi_i}} \left(\frac{V_{L_i}^2(u)}{m_{\tilde{u}_L}^4} + \frac{V_{R_i}^2(d)}{m_{\tilde{d}_R}^4} - \frac{V_{L_i}(u)V_{R_i}(d)}{m_{\tilde{u}_L}^2 m_{\tilde{d}_R}^2} \right), \\ \eta'_{\tilde{g}} &= \frac{2\pi\alpha_3}{3} \frac{\lambda_{111}^{\prime 2}}{G_F^2} \frac{m_p}{m_{\tilde{g}}} \frac{1}{m_{\tilde{u}_L}^2 m_{\tilde{d}_R}^2}, \\ \eta_{\chi\tilde{e}} &= 2\pi\alpha_2 \frac{\lambda_{111}^{\prime 2}}{G_F^2} \sum_{i=1}^4 \frac{m_p}{m_{\chi_i}} \frac{V_{L_i}^2(e)}{m_{\tilde{e}_L}^4}, \\ \eta_{\chi\tilde{f}} &= \pi\alpha_2 \frac{\lambda_{111}^{\prime 2}}{G_F^2} \sum_{i=1}^4 \frac{m_p}{m_{\chi_i}} \left(\frac{V_{L_i}(u)V_{R_i}(d)}{m_{\tilde{u}_L}^2 m_{\tilde{d}_R}^2} - \frac{V_{L_i}(u)V_{L_i}(e)}{m_{\tilde{u}_L}^2 m_{\tilde{e}_L}^2} - \frac{V_{L_i}(e)V_{R_i}(d)}{m_{\tilde{e}_L}^2 m_{\tilde{d}_R}^2} \right), \end{aligned} \quad (95)$$

where α_3, α_2 are the $SU(3)_C$ and $SU(2)_L$ fine structure constants, respectively, and V are rotation matrices to go from the gaugino/Higgsino basis to the neutralino basis. As an example, consider gluino and pion exchange dominance, in which case the product of matrix elements and particle physics parameters in Eqs. (94,95) simplifies to

$$\eta_{\tilde{R}_1}^{\tilde{g}} \mathcal{M}_{\tilde{R}_1}^{\tilde{g}} \simeq \frac{\pi\alpha_3}{6} \frac{\lambda_{111}^{\prime 2}}{G_F^2} \frac{m_p}{m_{\tilde{g}}} \frac{1}{m_{\tilde{d}_R}^4} \left(1 + \left(\frac{m_{\tilde{d}_R}}{m_{\tilde{u}_L}} \right)^2 \right)^2 \mathcal{M}^\pi. \quad (96)$$

The relevant NMEs are⁹² between 387 – 569 for ^{76}Ge , 375 – 594 for ^{82}Se , 412 – 589 for ^{100}Mo and 385 – 540 for ^{130}Te . Hence, the current limits on $\eta_{\tilde{R}_1}^{\tilde{g}}$ are

$$\eta_{\tilde{R}_1}^{\tilde{g}} \leq \begin{cases} (4.9 - 7.5) \times 10^{-9} & \text{for } ^{76}\text{Ge}, \\ (0.9 - 1.8) \times 10^{-8} & \text{for } ^{82}\text{Se}, \\ (0.8 - 1.1) \times 10^{-8} & \text{for } ^{100}\text{Mo}, \\ (5.5 - 7.7) \times 10^{-9} & \text{for } ^{130}\text{Te}. \end{cases} \quad (97)$$

The value of $\eta_{\tilde{R}_1}^{\tilde{g}} \lesssim 7.5 \times 10^{-9}$ translates into $\lambda_{111}^{\prime 2}/(m_{\tilde{g}} m_{\tilde{d}_R}^4 (1 + m_{\tilde{d}_R}^2/m_{\tilde{u}_L}^2)^2) \lesssim 1.8 \times 10^{-17} \text{ GeV}^{-5}$, in very good agreement with the naive limit $\lambda_{111}^{\prime 2}/\Lambda_{\text{SUSY}}^5 \lesssim 7 \times 10^{-18} \text{ GeV}^{-5}$.

Of course, supersymmetric particles are expected to be produced at the LHC, and Refs.^{237,236} have recently analyzed the interplay of RPV contributions to

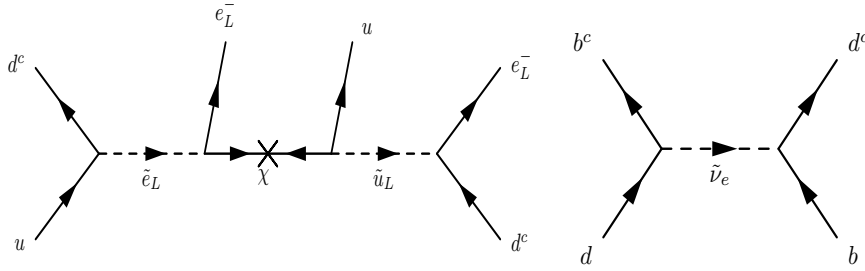


Fig. 31. Left: resonant selectron production at the LHC as test of the short-range λ'_{111} RPV diagrams in Fig. 29. Right: B^0 - \bar{B}^0 mixing as test of the long-range λ'_{131} λ'_{113} RPV diagram in Fig. 30.

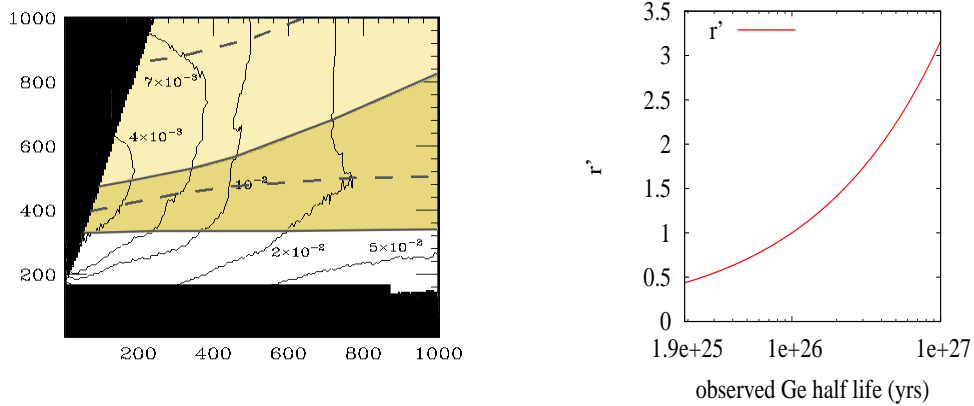


Fig. 32. Left: mSUGRA parameter space (m_0 vs. $m_{1/2}$) in which single slepton production may be observed at the LHC with $\sqrt{s} = 14$ TeV and 10 fb^{-1} of integrated luminosity. The labelled contours show the search reach given by the labelled value of λ'_{111} . The white, dark-shaded and light-shaded regions show for ^{76}Ge that observation of single slepton production at the 5σ level would imply $T_{1/2}^{0\nu} < 1.9 \times 10^{25} \text{ yrs}$, $10^{27} \text{ yrs} > T_{1/2}^{0\nu} > 1.9 \times 10^{25} \text{ yrs}$ and $T_{1/2}^{0\nu} > 10^{27} \text{ yrs}$, respectively. The upper and lower dashed curves show where the contour between the dark-shaded and light-shaded regions would move to if $\langle m_{ee} \rangle = 0.05 \text{ eV}$ were included with constructive or destructive interference, respectively. Right: ratio of the RPV amplitude (94) and the total amplitude of $0\nu\beta\beta$ vs. the half-life if $m_0 = 680 \text{ GeV}$ and $m_{1/2} = 440 \text{ GeV}$. Taken from²³⁶.

$0\nu\beta\beta$ and collider physics. In particular, resonant selectron production²³⁸, $u d^c \rightarrow \tilde{e}_L \rightarrow e \tilde{\chi} \rightarrow e u \tilde{u}_L \rightarrow e u e d^c$, was studied. The Feynman diagram is sketched in Fig. 31; note the typical like-sign dilepton structure. The first and last reactions in the chain involve λ'_{111} and the parton level cross section is proportional to λ'^2_{111}/\hat{s} . A numerical scan of a mSUGRA-like breaking scenario with m_0 and $m_{1/2}$ between

40 and 10^3 GeV, vanishing trilinear coupling A_0 and $\tan\beta = 10$ was performed, the result of which is given in Fig. 32. In the white region, resonant selectron production is forbidden by the current $0\nu\beta\beta$ -limits on ^{76}Ge . Observation in the darker shaded region implies that $0\nu\beta\beta$ should be observed in GERDA. Hence, if $0\nu\beta\beta$ is discovered, searching for resonant selectron production at LHC is a direct test of the λ'_{111} hypothesis. In light-shaded regions one does not expect observation of $0\nu\beta\beta$, and would hence rule out a possible contribution to the process.

There is the possibility that the R -parity violating diagram and the standard one contribute simultaneously (see Section 6). A possible effect of this is shown in Fig. 32: constructive interference of $\langle m_{ee} \rangle = 0.05$ eV would move the interesting dark-shaded region up, and render observation of resonant selectron production very difficult. Destructive interference would move it down and make it easier. The right plot in Fig. 32 shows the ratio of the R -parity violating amplitude Eq. (94) and the total amplitude of $0\nu\beta\beta$, for a particular point in parameter space. Extracting the value of λ'_{111} from LHC and measuring the half-life of $0\nu\beta\beta$ fixes this value.

The long-range diagram from Fig. 30, given first in²³⁹, involves no suppression by neutrino mass, and the amplitude can be estimated as

$$\mathcal{A}_{\mathcal{R}_2}^b \simeq G_F \frac{1}{q} U_{ei} \frac{m_b}{\Lambda_{\text{SUSY}}^3} \lambda'_{131} \lambda'_{113}. \quad (98)$$

Here we have set all SUSY masses to a common scale Λ_{SUSY} , and took into account that the $\tilde{b}\text{-}\tilde{b}^c$ mixing is proportional to $m_b/\Lambda_{\text{SUSY}}$ (see below). Comparing with the standard amplitude Eq. (40) gives the constraint $\lambda'_{131} \lambda'_{113}/\Lambda_{\text{SUSY}}^3 \lesssim 10^{-14} \text{ GeV}^{-3}$. A more precise calculation gives constraints on the following quantity

$$\eta_{\mathcal{R}_2}^b = \frac{\lambda'_{131} \lambda'_{113}}{2\sqrt{2} G_F} \sin 2\theta^b \left(\frac{1}{m_{b_1}^2} - \frac{1}{m_{b_2}^2} \right). \quad (99)$$

The angle θ^b and the masses $m_{b_{1,2}}^2$ in this expression arise from diagonalization of the symmetric matrix

$$\mathcal{M}_b^2 = \begin{pmatrix} m_{b_L}^2 + m_b^2 - 0.42 M_Z^2 \cos 2\beta & -m_b (A_b + \mu \tan \beta) \\ -m_b (A_b + \mu \tan \beta) & m_{b_R}^2 + m_b^2 - 0.08 M_Z^2 \cos 2\beta \end{pmatrix}, \quad (100)$$

where $\tan\beta$ is the ratio of up- and down-type Higgs vevs, μ is the μ -parameter, A_b the trilinear coupling of Higgs scalars and fermions, and $m_{b_L}^2$ ($m_{b_R}^2$) the soft masses of the SUSY partners of the left-handed (right-handed) b quark. Nuclear physics is again dominated by pion exchange²³⁵, with the relevant NMEs 2 to 3 orders of magnitude larger than the 2 nucleon NMEs. The spread of NMEs in⁹² is 396 – 728

for ^{76}Ge , 379 – 720 for ^{82}Se , 405 – 691 for ^{100}Mo and 382 – 641 for ^{130}Te . One finds

$$\eta_{R_2}^b \leq \begin{cases} (4.0 - 7.3) \times 10^{-9} & \text{for } ^{76}\text{Ge}, \\ (1.5 - 2.8) \times 10^{-8} & \text{for } ^{82}\text{Se}, \\ (0.7 - 1.2) \times 10^{-8} & \text{for } ^{100}\text{Mo}, \\ (4.6 - 7.7) \times 10^{-9} & \text{for } ^{130}\text{Te}. \end{cases} \quad (101)$$

The agreement with the naive limit is very good. We have only considered here the b squark diagram. There are identical diagrams with d and s squark mixing, proportional to $m_d \lambda'_{111} \lambda'_{111}$ and $m_s \lambda'_{121} \lambda'_{112}$, respectively. The first case depends therefore on the same parameters as the neutralino/gluino diagrams discussed above, but due to its dependence on m_d it is suppressed. The diagram with s squark mixing can be shown to be sub-leading due to strong limits from K^0 - \bar{K}^0 mixing²⁴⁰, in which at tree level sneutrino exchange takes place. Those limits are of order $\lambda'_{121} \lambda'_{112} \lesssim 10^{-9} (\Lambda_{\text{SUSY}}/100 \text{ GeV})^2$, whose dependence on the parameters is easy to understand. About the same order are the limits on $\lambda'_{131} \lambda'_{113}$ from B^0 - \bar{B}^0 mixing (Fig. 31 sketches the relevant Feynman diagram), which have to be compared with $\lambda'_{131} \lambda'_{113} \lesssim 10^{-8} (\Lambda_{\text{SUSY}}/100 \text{ GeV})^3$ from neutrino-less double beta decay. This implies an interesting interplay of B physics and $0\nu\beta\beta$: as long as the SUSY breaking scale does not exceed TeV, the limits are similar. However, as the B^0 - \bar{B}^0 mixing diagram proceeds with sneutrino exchange and the $0\nu\beta\beta$ -diagram with b squarks, a more detailed analysis is in order, which has been performed in Ref.²³⁶. As a result, the B^0 - \bar{B}^0 constraint is currently stronger than the one from $0\nu\beta\beta$, but can be responsible for observable half-lives of $10^{26} - 10^{27}$ yrs for ^{76}Ge , which was the isotope studied in²³⁶. In analogy to the right plot of Fig. 32 one could again define a ratio of matrix elements and study its range as a function of the half-life²³⁶.

5.5. Majorons

The term Majoron denotes very light or massless particles χ^0 which can couple to neutrinos. Originally Majorons were Goldstone bosons of spontaneously broken global lepton number. This Majoron could be part of a weak singlet²⁴¹, doublet or triplet²⁴², the latter two cases being ruled out by their unacceptable contribution to the Z width. Another set of important constraints stems from astrophysics^{243,244}. In the context of triplet Majorons it has been noted that the decay mode²⁴⁵

$$(A, Z) \rightarrow (A, Z + 2) + 2 e^- + \chi^0 \quad (102)$$

is induced, see Fig. 33. Several different approaches of (almost) massless scalar particles coupling to neutrinos and their impact on $0\nu\beta\beta$ have been made in the past^{246,247,248,249,250,251,252,253,254}. Those include scenarios in which Majorons are not Goldstone bosons, or carry lepton number, such that lepton number is actually conserved and $0\nu\beta\beta$ is forbidden. Other examples are when Majorons are vector particles²⁵¹, or doublet Majorons²⁴⁶ in which the Majoron is the SUSY partner of the neutrino. Extra-dimensional Majorons with a set of Kaluza-Klein modes was

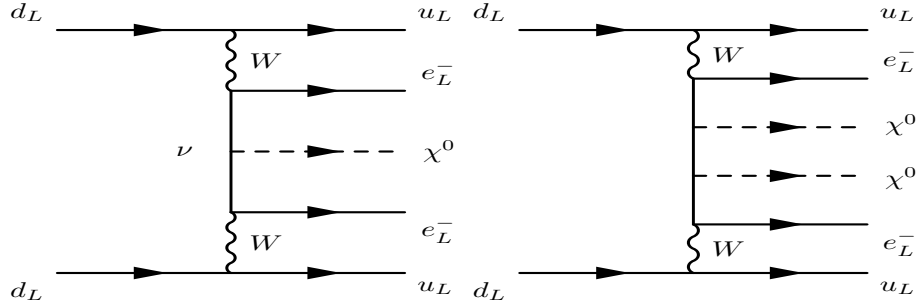


Fig. 33. Quark level Feynman diagram for a one and two Majoron realizations of neutrino-less double beta decay.

also proposed²⁵⁴. Simple singlet Majoron models allow coupling of χ^0 to right-handed neutrinos with strength m_ν/M , where M is the scale of spontaneous lepton number breaking, hence $M \simeq M_R$. Thus one does not expect sizable coupling and $0\nu\beta\beta$ -rates. This is different in more complicated models. It was also realized that decays with two Majorons in the final state are possible²⁴⁷:

$$(A, Z) \rightarrow (A, Z + 2) + 2 e^- + 2 \chi^0, \quad (103)$$

see Fig. 33. At the end of the day, one writes the decay rate as

$$\Gamma^{0\nu} = |\langle g_\chi \rangle|^{(2 \text{ or } 4)} |\mathcal{M}_\chi|^2 G_\chi(Q, Z), \quad (104)$$

where $|\langle g_\chi \rangle|$ is an averaged and model-dependent coupling constant, its power obviously depending on single or double emission. The phase space factor $G_\chi(Q, Z)$ depends also on the number of final state particles, but also on the model, in particular on the nature of the Majoron. The experimental quantity to distinguish Majoron modes from $0\nu\beta\beta$ is of course the energy spectrum of the two emitted electrons. In the original triplet model, with $g_\chi \bar{\nu} \chi \nu$ the coupling of the Majoron with two neutrinos, the amplitude can be written as $\mathcal{A} \simeq G_F^2 \langle g_\chi \rangle / q^2$, which has one dimension of energy less than the amplitudes considered before, because the phase space integration for one additional final state particle implies two powers of energy. Hence, the decay width goes as Q^7 ($n = 1$) instead of Q^5 for $0\nu\beta\beta$. Similar models with double Majoron emission have consequently a decay width proportional to Q^9 ($n = 3$). With the same logic it follows that single Majoron decays where the coupling goes with $\partial^\mu \chi$ have a width proportional to Q^9 ($n = 3$), while double Majoron decays go with Q^{13} ($n = 7$). The integer number n in the above considerations indicates the “spectral index” of the two electron spectrum²⁵²

$$\frac{d\Gamma^{0\nu}}{dE_1 dE_2} \propto (Q - E_1 - E_2)^n \sqrt{E_1^2 - m_e^2} \sqrt{E_2^2 - m_e^2} E_1 E_2, \quad (105)$$

neglecting Fermi functions and prefactors. Reasonable estimates could now be made, again by comparing the amplitudes, and taking into account the different

Table 13. Categories of Majoron models as first proposed in²⁵². Given are whether $0\nu\beta\beta$ can take place, if single or double Majoron emission is predicted, the spectral index and the lepton number of the Majoron, whether it is a Goldstone boson, and the limit on its coupling, taken from²⁵⁷. The limit for IF is estimated here.

category	$0\nu\beta\beta$	mode	n	L_χ	GB?	$\langle g_\chi \rangle$
IB	✓	χ^0	1	0	–	1.7×10^{-4}
IC	✓	χ^0	1	0	✓	1.7×10^{-4}
ID	✓	$\chi^0\chi^0$	3	0	–	1.5
IE	✓	$\chi^0\chi^0$	3	0	✓	1.5
IF (bulk)	✓	χ^0	2	0	✓	$\sim 10^{-4}$ *
IIB	–	χ^0	1	-2	–	1.7×10^{-4}
IIC	–	χ^0	3	-2	✓	0.024
IID	–	$\chi^0\chi^0$	3	-1	–	1.5
IIE	–	$\chi^0\chi^0$	7	-1	✓	1.3
IIF (vector)	–	χ^0	3	-2	–	0.024

Note: *this is a limit on $g^2/5/M$ in units of GeV^{-1} , where g is the $\chi^0\nu\nu$ coupling and M the low energy string scale in the extra-dimensional framework studied in²⁵⁴.

phase space dependence and a factor $2(2\pi)^3$ for each additional phase space integration. In this way one finds for instance that for single Majoron modes with $n = 1$ the standard contribution $(G_F^2 \langle m_{ee} \rangle / q^2)^2 Q^5$ has to be compared with $(G_F^2 \langle g_\chi \rangle / q^2)^2 Q^7 / (2(2\pi)^3)$, from which it follows $\langle g_\chi \rangle \lesssim 10^{-5}$, and for $n = 3$ that $\langle g_\chi \rangle \lesssim 1$. Nuclear physics aspects are dealt with in^{255,256}, and we will not go into detail here. For single Majoron and $n = 1$ cases the NMEs from the standard interpretation can be used, while for the other cases different NMEs need to be calculated, similar to the situation for the $\langle \lambda \rangle$ and $\langle \eta \rangle$ terms in the presence of right-handed currents, discussed in Section 5.3. We rather summarize the limits on the various model categories, which first have been described in²⁵². This is shown in Table 13.

5.6. Other mechanisms

We will discuss other proposed realizations of $0\nu\beta\beta$ in this Section.

Non-renormalizable effective operators \mathcal{O}^{4+d} in the Lagrangian $\mathcal{L}_{\text{eff}} = \mathcal{O}^{4+d}/\Lambda^d$ can generate neutrino Majorana masses and/or lepton number violation, the most simple example being the Weinberg operator of dimension $4 + d = 4 + 1 = 5$ in Eq. (17). Operators with $\Delta L = 2$ have been classified up to dimension 11 in^{258,259}. They can generate neutrino mass directly (the Weinberg operator) or via loops, by closing some of the external legs. It is also possible that those lepton number violating operators generate a direct contribution to $0\nu\beta\beta$ (note that $0\nu\beta\beta$ is effectively a $\bar{u}d\bar{u}d\bar{e}e$ operator, which has dimension 9). There are five dimension 9 and fifteen dimension 11 operators which have this property²⁵⁸. One example is $\mathcal{O}^9 = LLQQd^c d^c$. Closing the external Q and d^c lines with Higgs

loops gives a neutrino mass term of order $m_\nu \sim m_d^2/\Lambda/(16\pi^2)^2$. A limit on Λ is estimated from the direct contribution of \mathcal{O}^9 to $0\nu\beta\beta$, which has an amplitude of order Λ^{-5} . Hence one limits $\Lambda \gtrsim 3$ TeV, and therefore a tiny mass of $m_\nu \sim 10^{-4}$ eV is generated. All dimension 9 operators generate a limit of order 3 TeV on their associated suppression scale. Regarding dimension 11 operators, their $0\nu\beta\beta$ -amplitude can be estimated as v^2/Λ^7 , hence $\Lambda \gtrsim$ TeV. In²⁵⁹ all 129 operators up to dimension 11 have been studied and the scale Λ has been fixed by requiring the operator to generate $m_\nu \simeq 0.05$ eV. This fixes their contribution to $0\nu\beta\beta$. Some of the operators can now be disfavored, because their direct contribution to $0\nu\beta\beta$ can be too large²⁵⁹.

Leptoquarks can couple to quarks and leptons and the SM Higgs doublet, and have the potential to lead to lepton number violation and $0\nu\beta\beta$. Their properties are similar to R -parity violating mechanisms of $0\nu\beta\beta$. In Ref.²⁶⁰ the vertices for (S, V^μ) - d - ν , (S, V^μ) - d - e , (S, V^μ) - u - ν and (S, V^μ) - u - e interactions have been worked out, where S (V^μ) are scalar (vector) leptoquarks with electric charge $-\frac{1}{3}$ or $\frac{2}{3}$. Effective u - e - ν - d vertices arise and the coefficients depend on the original leptoquark couplings and masses, the latter obviously as $M_{S,V}^{-2}$. Writing the amplitude naively as $\mathcal{A}_{\text{LQ}} \sim G_F a/M_{S,V}^2/q$, where a the typical coefficient for the effective vertex, one finds limits of $a \lesssim 10^{-9}$ for 100 GeV leptoquarks, which is within one order of magnitude to the actual limits derived in²⁶⁰. In that paper the definition of the coefficients in terms of original parameters can be found.

In²⁶¹ **scalar bilinears** (coupling to two fermions) have been considered, and typically one dimensionful coupling μ and 3 propagators are present in the $0\nu\beta\beta$ -diagrams, leading to amplitudes of the form μ/M^6 , where M is the common mass of the bilinears (see also²⁶²).

Rather surprisingly, given the popularity of scenarios with **extra spatial dimensions**, there are only few papers discussing its consequences on $0\nu\beta\beta$. Ref.²⁶³ showed that within ADD scenarios small Majorana neutrino masses can result if lepton number is broken on distant branes, with the breaking being communicated to our brane by messenger particles. Ref.²⁶⁴ used this finding and translated limits on the Majorana mass $\langle m_{ee} \rangle$ in limits on the number of extra dimensions, compactification radius of the extra dimension and messenger mass. A generic feature of extra dimensional theories is the presence of Kaluza-Klein (KK) excitations of particles which feel the extra dimensions. If Majorana neutrinos do so, the associated tower contributes in principle to $0\nu\beta\beta$. The case of all excitations being Majorana neutrinos was discussed within a particular model in²⁶⁵. Excitations heavier than 100 MeV will have NMEs with the characteristic features of heavy neutrino exchange discussed in Section 5.1. In the model considered in²⁶⁵ two parameters had to be chosen, the radius R of the extra dimension and the brain shift parameter a , introduced to make the neutrinos with opposite CP parity couple to the W bosons with unequal strength. Constraints on those parameters are possible. Ref.²⁶⁶ studied an extra-dimensional scenario based on a warped Randall-Sundrum model

leading to low scale seesaw, in which also a tower of order GeV sterile neutrinos is present, which can be constrained by $0\nu\beta\beta$. Models in which only gauge bosons or Higgs scalars possess KK excitations, such as in²⁶⁷, are dominated by the usual light neutrino mass mechanism.

Scalar octet seesaw has been proposed in Ref.²⁶⁸ to have TeV scale neutrino mass generation with sizable LHC cross sections. In this mechanism a one-loop diagram including a weak scalar triplet S and weak fermion singlets or triplets ρ_i , all octets under $SU(3)_C$, produces a Majorana neutrino mass. The ρ and S particles could mediate double beta decay via the usual standard diagram with the W replaced by S and the neutrinos replaced by ρ_i . The amplitude is proportional to $c_{ud}^2/(m_S^4 m_{\rho_i})$, where c_{ud} is the coupling of S to u and d quarks, which is constrained from flavor violating transitions.

A **fourth generation** Majorana neutrino with mass M_4 behaves exactly as a heavy neutrino discussed in Section 5.1. Therefore²⁶⁹, it receives the constraint $|S_{e4}|^2/M_4 \leq 1.8 \times 10^{-8} \text{ GeV}^{-1}$, with S_{e4} being its mixing with the electron. Pushing its mass down to collider level would require cancellation with other contributions to $0\nu\beta\beta$.

Composite neutrinos²⁷⁰ lead to heavy neutrinos N^* which are excited states corresponding to a scale Λ_c of the SM neutrinos. Their coupling with gauge bosons goes with f/Λ_c , f being a coupling constant, and the amplitude for $0\nu\beta\beta$ goes with $f^2/\Lambda_c/M_{N^*}$ and is sensitive to TeV scale exciteness²⁷¹.

So-called **3-3-1 models** with an initial $SU(3)_L$ gauge symmetry contain new gauge bosons and scalars, which can contribute to $0\nu\beta\beta$. Those cases have been studied in Refs.^{272,253,273}, and constraints on the masses and mixings with the SM fermions have been obtained. Majoron emission is also possible in those models, because typically neutral scalars with lepton number exists, whose vevs induce spontaneous violation of lepton number, see Section 5.5.

We conclude this section with more exotic proposals. Effects of scalar unparticles in $0\nu\beta\beta$ have been discussed in²⁷⁴, and an unusual model with colored scalars coupling to leptons and quarks, which can mediate $0\nu\beta\beta$, in²⁷⁵. Recently it was proposed that a huge number of copies of SM particles exists²⁷⁶, which could solve the hierarchy problem and, if a permutation symmetry is added, explain also small neutrino masses. It was shown²⁷⁷ that this leads to basically vanishing amplitudes for $0\nu\beta\beta$.

6. Distinguishing mechanisms for neutrino-less double beta decay

We have seen in the last two Sections that there are several well motivated frameworks in which observable neutrino-less double beta decay can be expected. Obviously, means to distinguish the various possibilities are necessary. This is a common problem for all experiments looking for new physics, for instance lepton flavor violation, where observation of, say, $\mu \rightarrow e\gamma$ alone does not prove the presence of supersymmetry, but could mean a lot of different things (Higgs triplets, extra dimensions,

non-unitary PMNS matrix, etc.). In this Section we will classify three possible tests of the underlying mechanism of neutrino-less double beta decay. Mostly the dominance of one mechanism is assumed, but we will discuss the simultaneous presence of more than one mechanism as well.

6.1. *Distinguishing via effects in other observables*

This obvious possibility has been discussed at several occasions in the last Section. In particular within R -parity violating SUSY and left-right symmetric theories TeV scale particles can lead to observable $0\nu\beta\beta$. Production of such particles at the LHC is then a check of these mechanisms, in particular if the like-sign dilepton signature can be used, such as for heavy right-handed neutrino production²¹², Higgs triplet decays²⁰⁹, or resonant selectron production²³⁷. However, checks are also possible in processes in which lepton number is not violated, but instead quark or lepton flavor is not conserved²⁷⁸. To perform such studies, one can express the relevant processes in terms of effective operators suppressed by some high energy scale. The scales of flavor violation and lepton number violation could be different, but are related or even identical in some cases. The flavor parameters on which $0\nu\beta\beta$ and flavor violating processes depend can also be different.

Examples mentioned above are B^0 - \bar{B}^0 mixing induced by λ'_{131} λ'_{113} couplings²³⁶. Note that here the parameters corresponding to flavor (λ'_{131} λ'_{113}) are the same for $0\nu\beta\beta$ and B^0 - \bar{B}^0 mixing, but different particles are involved: squarks in $0\nu\beta\beta$ and sneutrinos in B^0 - \bar{B}^0 mixing. In left-right symmetric theories an important contribution to lepton flavor violation stems from Higgs triplet exchange, which can mediate $\mu \rightarrow 3e$ at tree level. Here the flavor physics parameters (also the ones for $\mu \rightarrow e\gamma$) are not directly related to the ones which govern $0\nu\beta\beta$. If TeV scale physics generates $0\nu\beta\beta$, and if no special flavor structures and not too different flavor and lepton number violating scales are present, one expects²⁷⁸ a ratio $R \gg 10^{-2}$ of the rates for μ - e conversion in nuclei and $\mu \rightarrow e\gamma$. Therefore, if $R \simeq 10^{-2}$ is observed, the standard interpretation of light neutrino exchange in $0\nu\beta\beta$ is favored^a.

6.2. *Distinguishing via decay products*

We have seen that the Lorentz structure of the different mechanisms of $0\nu\beta\beta$ can be different. This implies that energy and angular correlations of the two emitted electrons may be different^{3,79,80}. In particular the SuperNEMO experiment will be able to perform such measurements, because the set up of foils with $0\nu\beta\beta$ -isotopes in a magnetic field allows tracking of the individual electrons, instead of “only” measuring their total energy. The design of the detector allows direct detection of two electrons from double beta decay by a tracking chamber and a calorimeter measuring individual energies and times-of-flight. In Ref.²⁷⁹ the collaboration has

^aMassive neutrinos imply lepton flavor violation in decays like $\mu \rightarrow e\gamma$ at an unobservably small level.

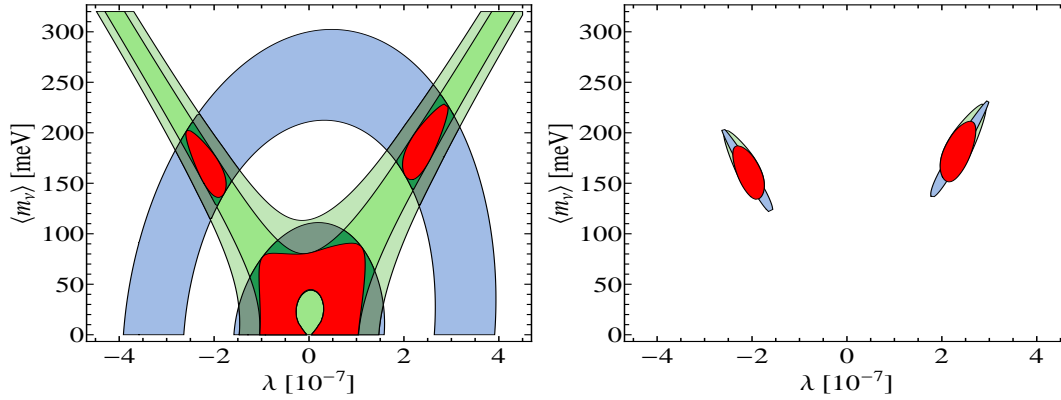


Fig. 34. Left: constraints at 1σ on the model parameters from an observation of $0\nu\beta\beta$ of ^{82}Se at half-life 10^{25} yrs (outer blue elliptical area) and 10^{26} yrs (inner blue elliptical area). Adding the reconstruction of the angular (outer, lighter green) and energy difference (inner, darker green) distribution drastically shrinks the allowed parameter space. Right: adding information from the decay of ^{150}Nd . In this example, 30% admixture of the λ -mechanism is assumed. Taken from²⁷⁹.

simulated the potential discrimination power between the standard mechanism and the λ -mechanism within left-right symmetry. The differential decay width can be written as^{3,79,80}

$$\frac{d\Gamma}{dE_1 dE_2 d\cos\theta} \propto \begin{cases} (1 - \beta_1 \beta_2 \cos\theta) & \text{standard mechanism} \\ (E_1 - E_2)^2 (1 + \beta_1 \beta_2 \cos\theta) & \lambda \text{ mechanism} \end{cases}, \quad (106)$$

where $E_{1,2}$ are the kinetic energies of the electrons, $\beta_{1,2}$ their velocities and θ the angle between them. One can define an asymmetry $A_\theta = (N_+ - N_-)/(N_+ + N_-)$, where N_+ (N_-) is the number of events with $\theta > \pi/2$ ($\theta < \pi/2$). Another asymmetry is $A_E = (N_> - N_<)/(N_> + N_<)$, where $N_>$ ($N_<$) is the number of events with $E_1 - E_2 < Q/2$ ($E_1 - E_2 > Q/2$), where Q is the energy release. Fig. 34 shows a result from²⁷⁹, where a 30% error on the NMEs and the simultaneous presence of the standard term and 30% admixture of the λ -mechanism has been assumed. The energy difference distribution turns out to have a stronger discrimination power.

Another aspect of identifying the $0\nu\beta\beta$ -mechanism with the decay product is when the Majorons as additional particles are emitted, in which case the energy spectrum of the electrons is different from the $0\nu\beta\beta$ - or the $2\nu\beta\beta$ -spectrum, as discussed in Section 5.5.

6.3. Distinguishing via nuclear physics

We have not spent much attention on the nuclear physics details of the $0\nu\beta\beta$ -mechanisms, and argued mainly on the particle physics amplitude level. However, there is nuclear physics involved, and if its uncertainties can be kept under control, it could in fact be helpful^{189,90,91} to disentangle the various mechanisms of

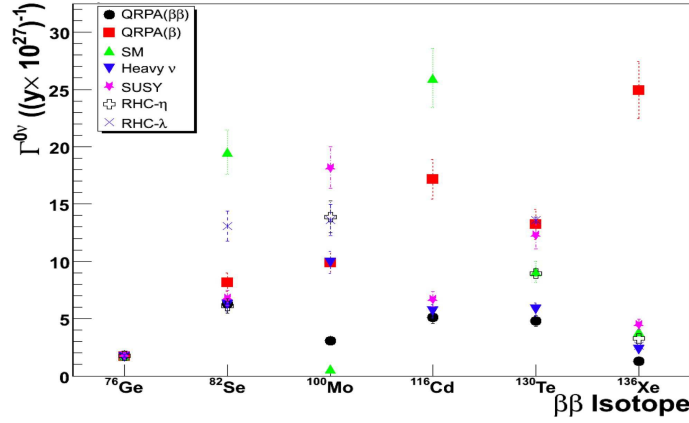


Fig. 35. Predictions for the inverse half-life for different NMEs, $0\nu\beta\beta$ -mechanisms and isotopes. Taken from⁹⁰.

$0\nu\beta\beta$. The use of multi-isotope determination of $0\nu\beta\beta$ to test NME models for the standard mechanism was discussed in^{63,62}. However, it should be clear that this is a quite challenging task, and in particular requires that the spread of the NME calculations is not much larger than the experimental error on the half-life. Nevertheless, the same strategy can be applied to disentangle different mechanisms of $0\nu\beta\beta$. Fig. 35 shows the result of Ref.⁹⁰, where different isotopes, NMEs and mechanisms of $0\nu\beta\beta$ were compared. Those were the λ and η diagrams within left-right symmetry, heavy neutrino exchange and R -parity violating SUSY. The NMEs were two sets of QRPA calculations (with their parameters fitted to reproduce single beta decay and $2\nu\beta\beta$, respectively) and a shell model evaluation. A 10% error on the calculations was assumed. The individual parameters of lepton number violation were chosen such that for ^{76}Ge the half-life is the same for all mechanisms. As can be seen from Fig. 35, for different isotopes there can be a significant spread of the half-lives. By simulating sets of $0\nu\beta\beta$ -rates it was estimated that 3 positive experimental results are required to pin down the mechanism of $0\nu\beta\beta$, if a total (theoretical, systematical and statistical) uncertainty of 20% or less can be achieved. For 40% uncertainty four results would be necessary. Analyses in similar spirit can be found in Refs.^{89,91}. Obviously, multi-isotope determination is here crucial.

Another possibility to distinguish the mechanisms is the rate of the ground-state-to-ground-state transitions to the rates of decays into excited states^{82,83,84,85}. The latter could be 0_1^+ or 2_1^+ . The decay into 0_1^+ is experimentally easier to identify because two photons associated with the transition first to 2_1^+ and then to the ground state are emitted. Transitions to 2_1^+ states have higher sensitivity to right-handed currents⁸⁴, and observation with large rates would signal the dominance of these mechanisms, in particular the λ -contribution. The experimental situation

is summarized in²⁸⁰, it is worth noting that $2\nu\beta\beta$ to 0_1^+ excited states has been observed. Observation of $0\nu\beta\beta$ into ground states and excited states in the same experiment could be used to rule out the possibility that an unidentified background peak mimics the $0\nu\beta\beta$ -signal²⁸¹. The development of high granularity detectors, large enough $0\nu\beta\beta$ -rates and precise nuclear physics is necessary to realize this consistency test. In the standard interpretation the decay to excited states occurs with a rate suppressed by a factor $R_{\text{ex}} \simeq 10^{2\cdots 3}$ with respect to the $0_{\text{g.s.}}^+ \rightarrow 0_{\text{g.s.}}^+$ transition. This factor is a combination of kinematics $((Q - E_{\text{ex}})/Q)^5$, $Q - E_{\text{ex}}$ being the energy release to the excited state, and nuclear physics $|\mathcal{M}_{\text{g.s.}}/\mathcal{M}_{\text{ex}}|^2$, and is sensitive to the mechanism of $0\nu\beta\beta$. For instance, Ref.⁸⁵ has found for ^{76}Ge suppression factors of $R_{\text{ex}} = 96, 48$ and 120 for the standard mechanism, heavy neutrino exchange and gluino exchange in R -parity violating SUSY, respectively. For ^{136}Xe the factors are $17, 38$ and 153 , while for ^{100}Mo the result was $17, 17$ and 59 . These differences may be used to distinguish the mechanism, if one assumes the nuclear physics uncertainties to be under control. In this respect we compare the NMEs for ^{76}Ge from Ref.⁸⁵ (QRPA) with the ones from⁵⁰ (IBM)^o. For ^{76}Ge the QRPA NMEs for ground state and 0_1^+ transitions are 2.80 and 0.994 , leading to a factor 7.93 in the relative half-lives. The IBM NMEs are 5.465 and 2.479 , hence a factor 4.84 . For ^{100}Mo the QRPA NMEs are 3.21 and 1.76 , thus a ratio 3.33 . IBM gives NME values of 3.732 and 0.419 , thus a ratio 21.26 . Therefore, the notorious NME uncertainty will again be a problem of the procedure described here. Nevertheless, important information to the field would be added by observation of $0\nu\beta\beta$ into excited states.

Another possibility^{81,195} to disentangle the mechanisms is the ratio of $0\nu\beta\beta$ to $0\nu\beta^+\beta^+$, $0\nu\beta^+\text{EC}$ or $0\nu\text{ECEC}$, see Eqs. (7,8,9). For instance⁸¹, the ratio of the rates of $0\nu\beta\beta$ of ^{76}Ge and $0\nu\beta^+\beta^+$ of ^{106}Cd are about $2087, 30435$ and 1826 for the standard, the λ - and the η -mechanism, respectively. For $0\nu\beta^+\text{EC}$ of ^{106}Cd the ratios are $148, 12$ and 217 . The same comments on nuclear physics uncertainties as for excited states apply here, in addition to the problem of even lower rates. Recall however the possibility of resonant enhancement⁴⁵ of $0\nu\text{ECEC}$. Double electron capture to excited states has recently been discussed as another way to distinguish mechanisms²⁸².

6.4. Simultaneous presence of several mechanisms

We will now discuss aspects of simultaneous presence of more than one $0\nu\beta\beta$ -mechanism. The different mechanisms can add coherently in the amplitude, see Eq. (66), and interference effects are possible. However, at leading order only terms in which the helicities of the emitted electrons are identical can interfere. The fact that helicity is not exactly equal to chirality for the emitted electrons with energy E_e

^oGiven the progress made in recent years it may not be fair to compare a 10 year old calculation with a very recent one. However, we are not aware of any recent QRPA re-evaluation and expect the ratios to be more stable than the NMEs themselves.

leads at the end to a phase space factor of the interference term suppressed^{92,93} by one order of magnitude (corresponding very roughly to $(E_e/Q)^2$), and interference is almost negligible. For instance, in the standard mechanism both electrons are left-handed, while in the λ -mechanism one is right-handed, thus these two diagrams do not interfere. The chirality of the emitted electrons is indicated in the respective quark level Feynman diagrams which are shown in this review. It is conceivable that destructive interference of several mechanisms leads to a vanishing rate of $0\nu\beta\beta$ in one or more isotopes. Nuclear physics differences of the relevant NMEs could, but do not have to, lead to a non-vanishing rate in other isotopes⁹².

The procedure to deal with the presence of several mechanisms has been outlined in^{283,93}. Consider first the presence of two essentially non-interfering mechanisms, e.g. light and heavy right-handed neutrino exchange. If two experiments using different isotopes have found evidence for $0\nu\beta\beta$, one has (see Eq. (4))

$$\begin{aligned} (T_{1/2}^a)^{-1} &= G^a (|\mathcal{M}_l^a|^2 |\eta|^2 + |\mathcal{M}_{N_R}^a|^2 |\eta_{N_R}|^2), \\ (T_{1/2}^b)^{-1} &= G^b (|\mathcal{M}_l^b|^2 |\eta|^2 + |\mathcal{M}_{N_R}^b|^2 |\eta_{N_R}|^2), \end{aligned} \quad (107)$$

where the superscript a, b denotes the two isotopes and the subscripts l and N_R denote standard light neutrino exchange and heavy right-handed neutrino exchange with W_R instead of W in left-right symmetric theories, see Eq. (82). Solving for the particle physics parameters gives

$$\begin{aligned} |\eta|^2 &= \frac{|\mathcal{M}_{N_R}^b|^2 / (T_{1/2}^a G^a) - |\mathcal{M}_{N_R}^a|^2 / (T_{1/2}^b G^b)}{|\mathcal{M}_l^a|^2 |\mathcal{M}_{N_R}^b|^2 - |\mathcal{M}_l^b|^2 |\mathcal{M}_{N_R}^a|^2}, \\ |\eta_{N_R}|^2 &= \frac{|\mathcal{M}_l^a|^2 / (T_{1/2}^b G^b) - |\mathcal{M}_l^b|^2 / (T_{1/2}^a G^a)}{|\mathcal{M}_l^a|^2 |\mathcal{M}_{N_R}^b|^2 - |\mathcal{M}_l^b|^2 |\mathcal{M}_{N_R}^a|^2}. \end{aligned} \quad (108)$$

Recall the present limits of $|\eta| \lesssim 9.8 \times 10^{-7}$ and $|\eta_{N_R}| \lesssim 1.7 \times 10^{-8}$ from Eqs. (67,84). Fig. 36, taken from⁹³ shows an example solution of Eq. (107). Knowing the half-life of one isotope constrains the half-lives of the other ones.

Consider now two interfering diagrams, for instance the standard mechanism and gluino exchange within R -parity violating SUSY, where the emitted electrons are both left-handed. There is an unknown phase between the two contributions, and the total half-life can be written as

$$(T_{1/2})^{-1} = G \left(|\mathcal{M}_l|^2 |\eta|^2 + |\mathcal{M}_{\tilde{R}_1}^{\tilde{g}}|^2 |\eta_{\tilde{R}_1}^{\tilde{g}}|^2 + 2 |\mathcal{M}_l| |\mathcal{M}_{\tilde{R}_1}^{\tilde{g}}| |\eta| |\eta_{\tilde{R}_1}^{\tilde{g}}| \cos \phi \right). \quad (109)$$

Obviously, three positive observations of $0\nu\beta\beta$ in three different isotopes are required in order to extract the three independent parameters $|\eta|$, $|\eta_{\tilde{R}_1}^{\tilde{g}}|$ and $\cos \phi$. An example from⁹³ is presented in Fig. 36. The current limit is $|\eta_{\tilde{R}_1}^{\tilde{g}}| \leq 7.5 \times 10^{-9}$, see Eq. (97).

7. Alternative Processes to Neutrino-less Double Beta Decay

The last section of this review deals shortly with alternative processes to $0\nu\beta\beta$, i.e. alternative probes of lepton number violation. The presence of $\Delta L = 2$ can

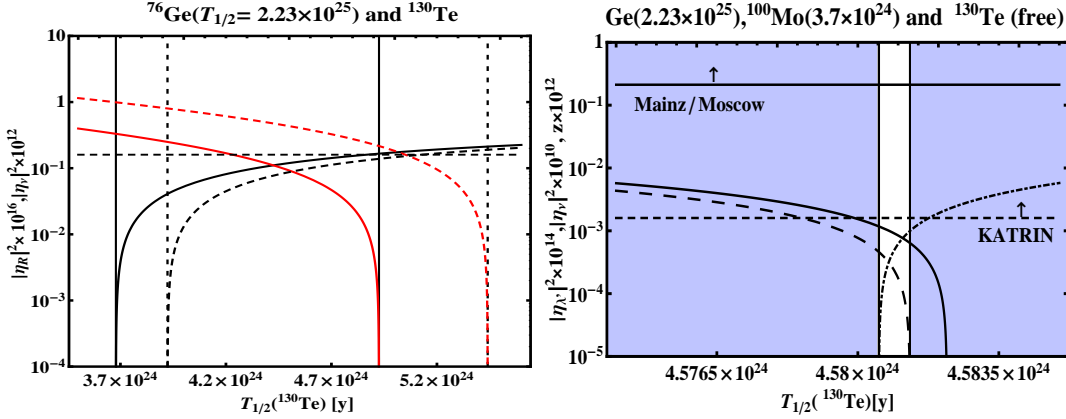


Fig. 36. Left: solving the case of non-interfering processes in Eq. (107) for the indicated hypothetical half-lives of ^{76}Ge and ^{130}Te . The black (red) lines are $|\eta|^2$ ($|\eta_{N_R}|^2$), the spread between the solid and dashed lines arises from varying the NMEs between 5.44 – 5.82 (4.18 – 4.70) and 411.5 – 264.9 (384.5 – 239.7) for ^{76}Ge (^{130}Te). The horizontal dashed line corresponds to $\langle m_{ee} \rangle \leq 0.2$ eV. The physical (positive) solutions for $|\eta|^2$ and $|\eta_{N_R}|^2$ are constrained within the solid (dashed) lines. Right: two interfering processes with constructive interference $\cos \phi = 1$ and fixed NMEs. The solid line is $|\eta|^2$, the dashed line is $|\eta_{N_R}^g|^2$, the dash-dotted line is $2|\eta||\eta_{N_R}^g|\cos \phi$. The blue areas are forbidden. Taken from⁹³.

manifest itself in going from lepton number $L = 0$ to $L = \pm 2$, typical for a decay process, or from $L = \pm 1$ to $L = \mp 1$, typical for conversion processes. It could also be that $|L| = 1$ goes to $|L| = 3$, e.g in lepton decays or collisions with initial leptons. Finally, in like-sign lepton collisions or $0\nu\text{ECEC}$ one could go from $L = -2$ to $L = 0$.

Neutrino oscillation probabilities are not sensitive to the Majorana nature of neutrinos. However, in principle $\nu_\alpha \rightarrow \bar{\nu}_\beta$ transitions are possible, whose probabilities are unfortunately suppressed by the factor $(m_i/E)^2$, in analogy to the standard mechanism of $0\nu\beta\beta$. There are in principle differences between Dirac and Majorana neutrinos, for instance it is easy to show that Majorana neutrinos do not have a vector current. Again, in amplitudes the difference of Dirac and Majorana neutrinos due to the absence of vector currents for the latter goes with m_i/E . This annoying property is known as the²⁸⁴ “practical Dirac-Majorana confusion theorem”.

A recent review on the electromagnetic properties of neutrinos can be found in²⁸⁵. In short, Majorana neutrinos cannot possess diagonal magnetic moments, i.e. $(\nu_e) \rightarrow \bar{\nu}_e$ transitions would only be possible for Dirac neutrinos. This can be seen by looking at the magnetic moment operators²⁸⁶ $\mu_{\alpha\beta} \bar{\nu}_{L\alpha} \sigma_{\mu\nu} (\nu_R)_\beta F^{\mu\nu}$ for Dirac and $\mu_{\alpha\beta} \bar{\nu}_{L\alpha} \sigma_{\mu\nu} (\nu_L^c)_\beta F^{\mu\nu}$ for Majorana neutrinos. In $\nu_e e$ scattering experiments the helicity and flavor of the final state neutrino cannot be measured and there is no way to distinguish Dirac from Majorana in this way. One possibility

would be via spin flavor transitions in supernovae, in which a magnetic field triggers $(\nu_e)_L \rightarrow (\bar{\nu}_\mu)_R$, with subsequent oscillation of the active $(\bar{\nu}_\mu)_R$ into $(\bar{\nu}_e)_R$. The usual ν_e neutronization burst can be heavily affected by this effect²⁸⁷. While the SM extended with massive neutrinos does generate too small magnetic moments, $\mu \propto m_\nu$, in some extensions of the SM it would be possible to generate the required large magnetic moments²⁸⁸.

We have mentioned already high energy tests of lepton number violation such as the like-sign dilepton signature of heavy Majorana neutrino production^{103,212}, Higgs triplet decays²⁰⁹, or resonant selectron production²³⁷. One may wonder whether there are *low energy processes*, in analogy to $0\nu\beta\beta$, which can probe the effective Majorana mass, maybe even without any nuclear physics complications. However, the $(m_i/E)^2$ suppression of the rate together with Avogadro's number N_A render $0\nu\beta\beta$ the only realistic probe. With order kg of a $0\nu\beta\beta$ -isotope one has order N_A atoms, which compensates the Dirac/Majorana factor $(m_i/q)^2$. In principle, there are decays like $K^+ \rightarrow \pi^- e^+ e^+$, which depend on the effective mass in the same way as $0\nu\beta\beta$ does, and do not suffer from NME uncertainties. However, calculating the branching ratio yields²⁸⁹

$$\text{BR}(K^+ \rightarrow \pi^- e^+ e^+) \sim 10^{-33} \left(\frac{\langle m_{ee} \rangle}{\text{eV}} \right)^2, \quad (110)$$

to be compared with the experimental upper limit^{290,203} of $\text{BR}(K^+ \rightarrow \pi^- e^+ e^+) \leq 6.4 \times 10^{-10}$. If it was possible to increase the number of charged kaons by 20 orders of magnitude, one could go for decays like²⁹¹ $K^+ \rightarrow \pi^- \mu^+ \mu^+$ (“neutrinoless double muon decay”) and test $\langle m_{\mu\mu} \rangle$, i.e. the other entries of the mass matrix^{292,293,294,295,289,296}. Other decays which have been studied in the past include lepton number violating decays of τ leptons^{296,297}, top quarks and W bosons²⁹⁸, D and B meson decays^{299,289,300,301}, or hyperons³⁰². Collider processes such as³⁰³ $\nu_\mu N \rightarrow X \mu^- \alpha^+ \beta^+$ or³⁰⁴ $e^- p \rightarrow X \nu_e \alpha^+ \beta^+$ have also been discussed. In addition, searches for conversion processes such as^{3,305,306} $\mu^- (A, Z) \rightarrow e^+ (A, Z-2)$ or³⁰⁷ $\mu^- (A, Z) \rightarrow \mu^+ (A, Z-2)$ have been proposed.

For very light and very heavy Majorana neutrinos the above processes are not very helpful. Recall however the general property of Majorana neutrino exchange as displayed in Fig. 23: for neutrinos whose masses correspond to the typical energy scale of the process the sensitivity is largest. Taking $K^+ \rightarrow \pi^- \mu^+ \mu^+$ as an example, Ref.²⁹⁵ has obtained very strong limits on masses between 245 MeV and 389 MeV, with $|U_{\mu i}|^2$ down to the 10^{-9} regime. The constraints are strong because there can be “ s -channel” diagrams. Other decays have been analyzed in^{300,308}.

Not many works exist which study the above processes in non-standard mechanisms. Examples include Ref.³⁰⁹, where meson decays such as $K^+ \rightarrow \pi^- \mu^+ \mu^+$ mediated by R -parity violating SUSY were found to provide no significant limits. The same was shown in³¹⁰ for (μ^-, μ^+) conversion, or for (μ^-, e^+) conversion in various mechanisms³¹¹. Doubly charged Higgs exchange in $K^+ \rightarrow \pi^- \mu^+ \mu^+$ was

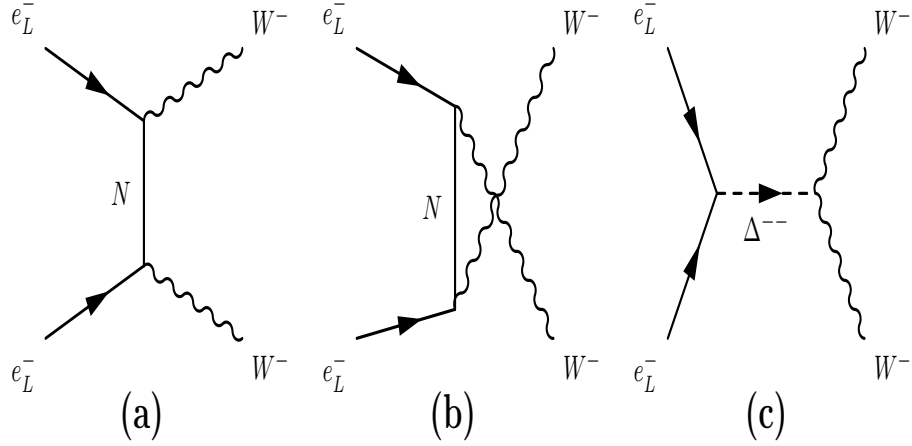


Fig. 37. Feynman diagram for inverse neutrino-less double beta decay. Diagrams (a) and (b) are Majorana neutrino N exchange, diagram (c) triplet exchange.

also found to generate negligible rates³¹².

A particularly clean probe of lepton number violation is “inverse neutrino-less double beta decay”. This is not $(A, Z + 2)^{++} + 2 e^- \rightarrow (A, Z)$, but

$$e^- e^- \rightarrow W^- W^- . \quad (111)$$

This reaction can be tested if a future linear collider is run in a basically background-free like-sign mode, and has frequently been proposed as a probe of LNV and new physics in general³¹³. The process does not involve any nuclear, hadronic or atomic uncertainties or difficulties and is presumably the cleanest probe of lepton number violation. If Majorana neutrinos are exchanged, see Fig. 37, and with neglecting the mass of the W , the cross section reads

$$\frac{d\sigma}{d\cos\theta} = \frac{G_F^2}{32\pi} \left\{ \sum (M_\nu)_i V_{ei}^2 \left(\frac{t}{t - (M_\nu)_i} + \frac{u}{u - (M_\nu)_i} \right) \right\}^2 , \quad (112)$$

where t and u are the usual Mandelstam variables, $(M_\nu)_i$ is the mass of the neutrinos (including light m_i and heavy M_i) and V_{ei} their mixing with electrons (N_{ei} and S_{ei}). There are interesting special cases for the cross section:

- if only light active Majorana neutrinos contribute to the process, then the cross section is

$$\begin{aligned} \sigma(e^- e^- \rightarrow W^- W^-) &= \frac{G_F^2}{4\pi} \langle m_{ee} \rangle^2 \\ &\leq 4.2 \times 10^{-18} \left(\frac{\langle m_{ee} \rangle}{1 \text{ eV}} \right)^2 \text{ fb} , \end{aligned} \quad (113)$$

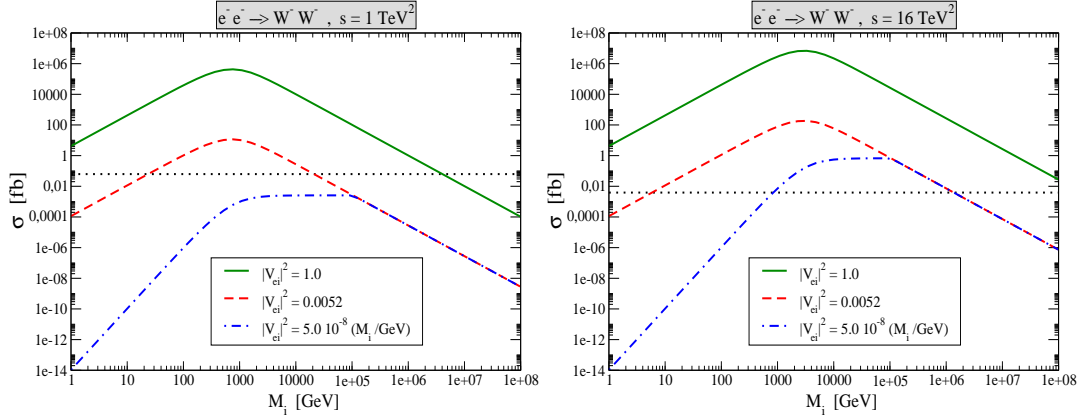


Fig. 38. Cross section for $e^-e^- \rightarrow W^-W^-$ with $\sqrt{s} = 1$ TeV (left) and $\sqrt{s} = 4$ TeV (right) and three limits for the mixing parameter $|V_{ei}|^2$. The dotted line corresponds to five events for an assumed luminosity of $80 (s/\text{TeV}^2) \text{ fb}^{-1}$.

hence far too small to be observable;

- if only heavy Majorana neutrinos contribute to the process, then we can bound the cross section using the $0\nu\beta\beta$ -limit from Eq. (71) as

$$\sigma(e^-e^- \rightarrow W^-W^-) = \frac{G_F^2}{16\pi} s^2 \left\langle \frac{1}{m} \right\rangle^2 \leq 2.6 \times 10^{-3} \left(\frac{\sqrt{s}}{\text{TeV}} \right)^4 \left(\frac{\langle \frac{1}{m} \rangle}{5 \times 10^{-8} \text{ GeV}^{-1}} \right)^2 \text{ fb} \quad (114)$$

again far too small to be observable;

- the high energy limit of $\sqrt{s} \rightarrow \infty$ is

$$\sigma(e^-e^- \rightarrow W^-W^-) = \frac{G_F^2}{4\pi} (V_{ei}^2 (M_\nu)_i)^2. \quad (115)$$

This seems to violate unitarity, because the cross section for an s -wave process should vanish in the high energy limit. However, recall the exact seesaw relation $\sum N_{ei}^2 m_i + S_{ei}^2 M_i = 0$, as discussed in in Eq. (73). This relation guarantees that the cross section vanishes in the high energy limit.

While small and large masses cannot give sizable cross sections, intermediate scale neutrino masses $(M_\nu)_i \sim \sqrt{s}$ can give appreciable event numbers, as expected from the general behavior of LNV processes with Majorana neutrinos involved. In Fig. 38 we show an example of the cross section as a function of neutrino mass. Different limits on the mixing V_{ei} are inserted: no limit, the global limit and the limit as implied from the limit on $\langle \frac{1}{m} \rangle = |V_{ei}|^2/M_i$. Note how the case of $|V_{ei}|^2 = 1$ follows the general trend of Fig. 23. The above processes can also be searched for at $e^- \mu^-$ or $\mu^- \mu^-$ machines.

The process $e^-e^- \rightarrow W^-W^-$ can also be mediated by a Higgs triplet, but due to small neutrino masses has a tiny cross sections unless a very narrow resonance

is met. One can show that if neutrino and triplet exchange occur simultaneously, the unitarity of the cross section is saved by the relation in Eq. (76). Right-handed Higgs triplets or W_R could be observed, however, if the electron beams are properly polarized.

Double chargino production $e^-e^- \rightarrow \chi^- \chi^-$ in supersymmetry has been studied in³¹⁴. The diagram is basically the same as (a) and (b) in Fig. 37, with the W replaced by χ and the neutrino by a sneutrino. Recall that lepton number violation in the sneutrino sector implies Majorana neutrinos²²⁵. It turns out that the limits from $0\nu\beta\beta$ render double chargino production cross sections too small. Other works on lepton number violating e^-e^- collisions within supersymmetry can be found in³¹⁵.

As mentioned before, lepton number violating sneutrino mass terms, the amplitude of $0\nu\beta\beta$ and Majorana neutrino mass terms imply each other: if one of the three is present, the other two are there as well^{225,226}. This leads to a splitting in the $\tilde{\nu}-\bar{\tilde{\nu}}$ system and therefore to lepton number violating sneutrino–anti-sneutrino mixing³¹⁶, whose parameters depend heavily on SUSY parameters, and whose observation is usually a very challenging task³¹⁷.

8. Summary

Neutrino-less double beta decay experiments are much more than neutrino mass experiments, their importance is much broader and deeper. The violation of lepton and baryon number is a rather generic feature of theories beyond the Standard Model, and searches for $0\nu\beta\beta$ or proton decay are probes of fundamental physics related to high energies, with a variety of important consequences in particle physics and cosmology. The significance of the decay is underlined by the excessive list of references provided in this review.

In the next 20-30 years $0\nu\beta\beta$ will be the only realistic probe to test the conservation of lepton number. The existing and upcoming results, when interpreted in terms of a specific particle physics scenario, allow to constrain a variety of important parameters, some of which can only be probed by $0\nu\beta\beta$, others can also be tested in different and complementary experiments. Best motivated is presumably the standard interpretation of light neutrino exchange, where the inverted mass ordering will begin to be tested within this decade. Quasi-degenerate neutrinos will generate a signal, and should in this case be detectable also in direct searches and cosmological observations. This would be the ideal case to identify the mechanism. There are however many non-standard interpretations of $0\nu\beta\beta$, the most frequently discussed mechanisms for the decay are summarized in Table 14. The unambiguous determination of the underlying mechanism is in general less straightforward than for quasi-degenerate neutrinos. However, naive estimates show that an effective mass of order 0.1 eV is associated with an amplitude that corresponds to the amplitude for exchange of TeV scale heavy particles. This energy scale has a variety of potential effects in currently running particle physics experiments, such as

Table 14. Most important mechanisms for neutrino-less double beta decay. Given are the absolute value of the amplitude ($q \simeq 0.1$ GeV is the momentum exchange for long-range processes) with the particle physics parameter written in bold face. The current limits on these quantities are provided, and tests to identify the mechanism by other means are indicated. RHC denotes right-handed currents, \cancel{R} stands for R -parity violation and there are several Majoron variants.

mechanism	amplitude and particle physics parameter	current limit	test
light neutrino exchange	$\frac{G_F^2}{q^2} U_{ei}^2 m_i $	0.5 eV	oscillations, cosmology, neutrino mass
heavy neutrino exchange	$G_F^2 \frac{S_{ei}^2}{M_i^2}$	$2 \times 10^{-8} \text{ GeV}^{-1}$	LFV, collider
heavy neutrino and RHC	$G_F^2 m_W^4 \frac{V_{ei}^2}{M_i^2 M_{WR}^4}$	$4 \times 10^{-16} \text{ GeV}^{-5}$	flavor, collider
Higgs triplet and RHC	$G_F^2 m_W^4 \left \frac{(M_R)_{ee}}{m_{\Delta_R}^2 M_{WR}^4} \right $	$10^{-15} \text{ GeV}^{-1}$	flavor, collider e^- distribution
λ -mechanism with RHC	$G_F^2 \frac{m_W^2}{q} \left \frac{U_{ei} \tilde{S}_{ei}}{M_{WR}^2} \right $	$1.4 \times 10^{-10} \text{ GeV}^{-2}$	flavor, collider, e^- distribution
η -mechanism with RHC	$G_F^2 \frac{1}{q} \tan \zeta \left U_{ei} \tilde{S}_{ei} \right $	6×10^{-9}	flavor, collider, e^- distribution
short-range \cancel{R}	$\frac{ \chi_{111}^2 }{\Lambda_{\text{SUSY}}^5}$ $\Lambda_{\text{SUSY}} = f(m_{\tilde{g}}, m_{\tilde{u}_L}, m_{\tilde{d}_R}, m_{\chi_i})$	$7 \times 10^{-18} \text{ GeV}^{-5}$	collider, flavor
long-range \cancel{R}	$\frac{G_F}{q} \left \sin 2\theta^b \lambda'_{131} \lambda'_{113} \left(\frac{1}{m_{b1}^2} - \frac{1}{m_{b2}^2} \right) \right $	$2 \times 10^{-13} \text{ GeV}^{-2}$	flavor, collider
	$\sim \frac{G_F}{q} m_b \frac{ \lambda'_{131} \lambda'_{113} }{\Lambda_{\text{SUSY}}^3}$	$1 \times 10^{-14} \text{ GeV}^{-3}$	
Majorons	$\propto \langle g_\chi \rangle \text{ or } \langle g_\chi \rangle ^2$	$10^{-4} \dots 1$	spectrum, cosmology

LHC, lepton flavor violation, FCNC, etc. It should be noted that, though some progress was made in recent years, high precision physics with $0\nu\beta\beta$ will presumably not be possible: nuclear matrix elements are unlikely to be known with more than 20% precision. Currently, one has to accept the (shrinking) $\mathcal{O}(1)$ ranges of NME calculations and perform analyses of $0\nu\beta\beta$ -results keeping them in mind.

An impressive number of upcoming experiments promises an exciting future for the field. Multi-isotope determination of $0\nu\beta\beta$ with different experimental approaches will be possible and is crucial in order to make an unambiguous claim of observation, help clarifying the nuclear matrix element calculations, and distinguish the different mechanisms. In order to identify the origin of neutrino-less double beta decay (the “inverse problem” of $0\nu\beta\beta$) three different possibilities exist: via effects in other observables, via exploring the decay products, and via nuclear physics effects. After the violation of lepton number is established, a highly interesting physics program of identifying the underlying mechanism and its origin will be possible.

Acknowledgements

I am very grateful for discussions with E. Akhmedov, M. Duerr, M. Lindner and K. Zuber, and thank J. Barry, A. Dueck and M. Duerr for help in producing figures and tables. This work was supported by the ERC under the Starting Grant MAN-ITOP and by the DFG in the project RO 2516/4-1 as well as in the Transregio 27 “Neutrinos and Beyond”.

References

1. W. H. Furry, Phys. Rev. **56** (1939) 1184.
2. W. C. Haxton and G. J. Stephenson, Prog. Part. Nucl. Phys. **12** (1984) 409.
3. M. Doi, T. Kotani and E. Takasugi, Prog. Theor. Phys. Suppl. **83** (1985) 1.
4. J. Engel, P. Vogel, M. R. Zirnbauer, Phys. Rev. C **37** (1988) 731-746.
5. T. Tomoda, Rept. Prog. Phys. **54** (1991) 53-126.
6. J. Suhonen and O. Civitarese, Phys. Rept. **300** (1998) 123.
7. J. D. Vergados, Phys. Rept. **361** (2002) 1 [arXiv:hep-ph/0209347].
8. C. Aalseth *et al.*, arXiv:hep-ph/0412300.
9. F. T. Avignone, S. R. Elliott and J. Engel, Rev. Mod. Phys. **80** (2008) 481 [arXiv:0708.1033 [nucl-ex]].
10. A. Faessler and F. Simkovic, J. Phys. G **24** (1998) 2139 [arXiv:hep-ph/9901215]; V. Rodin, arXiv:0910.5866 [nucl-th].
11. A. S. Barabash, Phys. Atom. Nucl. **73** (2010) 162 [arXiv:0807.2948 [hep-ex]]; arXiv:1101.4502 [nucl-ex].
12. A. Giuliani, Acta Phys. Polon. B **41** (2010) 1447.
13. E. Majorana, Nuovo Cimento **14** (1937) 171.
14. J. Schechter and J. W. F. Valle, Phys. Rev. D **25** (1982) 2951.
15. J. F. Nieves, Phys. Lett. B **147** (1984) 375; E. Takasugi, Phys. Lett. B **149** (1984) 372.
16. M. Duerr, M. Lindner, A. Merle, JHEP **1106** (2011) 091 [arXiv:1105.0901 [hep-ph]].
17. M. Goepfert-Mayer, Phys. Rev. **48** (1935) 512.
18. S. Umehara *et al.*, Phys. Rev. C **78** (2008) 058501 [arXiv:0810.4746 [nucl-ex]].
19. H. V. Klapdor-Kleingrothaus *et al.*, Eur. Phys. J. A **12** (2001) 147 [arXiv:hep-ph/0103062].
20. C. E. Aalseth *et al.* [IGEX Collaboration], Phys. Rev. D **65** (2002) 092007 [arXiv:hep-ex/0202026].
21. A. S. Barabash *et al.* [NEMO Collaboration], arXiv:1002.2862 [nucl-ex]; R. Arnold *et al.* [NEMO Collaboration], Phys. Rev. Lett. **95** (2005) 182302 [arXiv:hep-ex/0507083].
22. J. Argyriades *et al.* [NEMO-3 Collaboration], Nucl. Phys. A **847** (2010) 168 [arXiv:0906.2694 [nucl-ex]].
23. F. A. Danevich *et al.*, Phys. Rev. C **68** (2003) 035501.
24. C. Arnaboldi *et al.* [CUORICINO Collaboration], Phys. Rev. C **78** (2008) 035502 [arXiv:0802.3439 [hep-ex]].
25. R. Bernabei *et al.*, Phys. Lett. B **546** (2002) 23.
26. J. Argyriades *et al.* [NEMO Collaboration], Phys. Rev. C **80** (2009) 032501 [arXiv:0810.0248 [hep-ex]].
27. M. G. Inghram, J. H. Reynolds, Phys. Rev. **78** (1950) 822-823; T. Kirsten, W. Gentner, O. A. Schaeffer, Z. Phys. **202** (1967) 273.
28. F. T. Avignone, G. S. King, Y. G. Zdesenko, New J. Phys. **7** (2005) 6.

29. S. Umehara *et al.*, J. Phys. Conf. Ser. **39** (2006) 356.
30. K. Zuber, Phys. Lett. B **519** (2001) 1 [arXiv:nucl-ex/0105018].
31. C. Arnaboldi *et al.* [CUORE Collaboration], Astropart. Phys. **20** (2003) 91 [arXiv:hep-ex/0302021].
32. N. Ishihara *et al.*, Nucl. Instrum. Meth. A **443** (2000) 101.
33. M. Danilov *et al.*, Phys. Lett. B **480** (2000) 12 [arXiv:hep-ex/0002003].
34. I. Abt *et al.*, arXiv:hep-ex/0404039.
35. A. Terashima *et al.* [KamLAND Collaboration], J. Phys. Conf. Ser. **120** (2008) 052029.
36. See e.g., talks by A. Giuliani at BEYOND 2010 or by C. Nones at NOW 2010.
37. R. Gaitskell *et al.* [Majorana Collaboration], arXiv:nucl-ex/0311013.
38. H. Ejiri *et al.*, Phys. Rev. Lett. **85** (2000) 2917 [arXiv:nucl-ex/9911008].
39. F. Granena *et al.* [The NEXT Collaboration], arXiv:0907.4054 [hep-ex].
40. M. C. Chen [SNO+ Collaboration], arXiv:0810.3694 [hep-ex].
41. A. S. Barabash [NEMO Collaboration], Czech. J. Phys. **52** (2002) 575.
42. Y. Takeuchi, *Prepared for 32nd International Conference on High-Energy Physics (ICHEP 04), Beijing, China, 16-22 Aug 2004*
43. H. V. Klapdor-Kleingrothaus, A. Dietz, H. L. Harney and I. V. Krivosheina, Mod. Phys. Lett. A **16** (2001) 2409 [arXiv:hep-ph/0201231].
44. C. E. Aalseth *et al.*, Mod. Phys. Lett. A **17** (2002) 1475 [arXiv:hep-ex/0202018]; Yu. G. Zdesenko, F. A. Danevich and V. I. Tretyak, Phys. Lett. B **546** (2002) 206; A. Strumia and F. Vissani, Nucl. Phys. B **726** (2005) 294 [arXiv:hep-ph/0503246].
45. J. Bernabeu, A. De Rujula, C. Jarlskog, Nucl. Phys. B **223** (1983) 15; Z. Szejkowski and S. Wycech, Phys. Rev. C **70** (2004) 052501 [arXiv:hep-ph/0312040]; M. I. Krivoruchenko, F. Simkovic, D. Frekers and A. Faessler, arXiv:1012.1204 [hep-ph].
46. S. Eliseev *et al.*, Phys. Rev. Lett. **106** (2011) 052504.
47. F. Simkovic *et al.*, Phys. Rev. C **79** (2009) 055501 [arXiv:0902.0331 [nucl-th]]; D. L. Fang *et al.*, Phys. Rev. C **82** (2010) 051301 [arXiv:1009.5579 [nucl-th]].
48. M. Kortelainen, O. Civitarese, J. Suhonen and J. Toivanen, Phys. Lett. B **647** (2007) 128 [arXiv:nucl-th/0701052]; M. Kortelainen and J. Suhonen, Phys. Rev. C **75** (2007) 051303 [arXiv:0705.0469 [nucl-th]]; Phys. Rev. C **76**, 024315 (2007) [arXiv:0708.0115 [nucl-th]].
49. J. Menendez, A. Poves, E. Caurier and F. Nowacki, Nucl. Phys. A **818** (2009) 139 [arXiv:0801.3760 [nucl-th]].
50. J. Barea and F. Iachello, Phys. Rev. C **79** (2009) 044301; See also F. Iachello, talk at NOW 2010.
51. T. R. Rodriguez and G. Martinez-Pinedo, Phys. Rev. Lett. **105** (2010) 252503 [arXiv:1008.5260 [nucl-th]].
52. P. K. Rath *et al.*, Phys. Rev. C **82** (2010) 064310.
53. F. Simkovic *et al.*, Phys. Rev. C **77** (2008) 045503 [arXiv:0710.2055 [nucl-th]].
54. S. T. Cowell, Phys. Rev. C **73** (2006) 028501 [arXiv:nucl-th/0512012]; A. Smolnikov and P. Grabmayr, Phys. Rev. C **81** (2010) 028502.
55. A. Dueck, W. Rodejohann and K. Zuber, Phys. Rev. **D83** (2011) 113010 [arXiv:1103.4152 [hep-ph]].
56. A. Faessler *et al.*, Phys. Rev. D **79** (2009) 053001 [arXiv:0810.5733 [hep-ph]].
57. F. Simkovic *et al.*, Phys. Rev. C **60** (1999) 055502 [arXiv:hep-ph/9905509].
58. J. G. Hirsch, O. Castanos, P. O. Hess, Nucl. Phys. A **582** (1995) 124-140 [nucl-th/9407022].
59. J. J. Gomez-Cadenas *et al.*, JCAP **1106** (2011) 007 [arXiv:1010.5112 [hep-ex]].

60. A. Faessler, arXiv:1104.3700 [nucl-th].
61. S. M. Bilenky, A. Faessler, W. Potzel, F. Simkovic, arXiv:1104.1952 [hep-ph].
62. A. Faessler *et al.*, Phys. Rev. D **79** (2009) 053001 [arXiv:0810.5733 [hep-ph]].
63. S. M. Bilenky, J. A. Grifols, Phys. Lett. B **550** (2002) 154-159 [hep-ph/0211101]; S. M. Bilenky and S. T. Petcov, arXiv:hep-ph/0405237.
64. V. A. Rodin, A. Faessler, F. Simkovic and P. Vogel, Nucl. Phys. A **766** (2006) 107 [Erratum-ibid. A **793** (2007) 213] [arXiv:0706.4304 [nucl-th]].
65. J. Suhonen, Phys. Lett. B **607** (2005) 87 [arXiv:nucl-th/0412064].
66. A. Faessler *et al.*, J. Phys. G **35** (2008) 075104 [arXiv:0711.3996 [nucl-th]].
67. J. N. Bahcall, H. Murayama and C. Pena-Garay, Phys. Rev. D **70** (2004) 033012 [arXiv:hep-ph/0403167].
68. K. Zuber, arXiv:nucl-ex/0511009.
69. D. Frekers, Prog. Part. Nucl. Phys. **64** (2010) 281.
70. V. Rodin and A. Faessler, Phys. Rev. C **80** (2009) 041302 [arXiv:0906.1759 [nucl-th]].
71. J. P. Schiffer *et al.*, Phys. Rev. Lett. **100** (2008) 112501 [arXiv:0710.0719 [nucl-ex]]; B. P. Kay *et al.*, Phys. Rev. C **79** (2009) 021301 [arXiv:0810.4108 [nucl-ex]].
72. M. Kortelainen and J. Suhonen, Europhys. Lett. **58** (2002) 666 [arXiv:nucl-th/0201007].
73. M. Redshaw, E. Wingfield, J. McDaniel and E. G. Myers, Phys. Rev. Lett. **98** (2007) 053003; S. Rahaman *et al.*, Phys. Lett. B **662** (2008) 111 [arXiv:0712.3337 [nucl-ex]]; M. Redshaw, B. J. Mount, E. G. Myers and F. T. Avignone, Phys. Rev. Lett. **102** (2009) 212502.
74. K. Blaum, Phys. Rep. **425** (2006) 1.
75. D. Frekers, J. Dilling, and I. Tanihata, Can. J. Phys. **99** (2006) 1.
76. H. Pas, M. Hirsch, H. V. Klapdor-Kleingrothaus and S. G. Kovalenko, Phys. Lett. B **453** (1999) 194.
77. H. Pas, M. Hirsch, H. V. Klapdor-Kleingrothaus and S. G. Kovalenko, Phys. Lett. B **498** (2001) 35 [arXiv:hep-ph/0008182].
78. G. Prezeau, M. Ramsey-Musolf, P. Vogel, Phys. Rev. D **68** (2003) 034016 [hep-ph/0303205].
79. M. Doi, T. Kotani, H. Nishiura, E. Takasugi, Prog. Theor. Phys. **69** (1983) 602.
80. M. Doi, T. Kotani, H. Nishiura, E. Takasugi, Prog. Theor. Phys. **70** (1983) 1353; A. Ali, A. V. Borisov and D. V. Zhuridov, arXiv:hep-ph/0606072; Phys. Rev. D **76** (2007) 093009 [arXiv:0706.4165 [hep-ph]].
81. M. Hirsch, K. Muto, T. Oda and H. V. Klapdor-Kleingrothaus, Z. Phys. A **347** (1994) 151.
82. F. Simkovic *et al.*, Phys. Rev. C **64**, 035501 (2001) [arXiv:nucl-th/0107016].
83. M. Aunola, J. Suhonen, Nucl. Phys. A **602** (1996) 133-166; J. Suhonen, Phys. Lett. B **477** (2000) 99-106.
84. T. Tomoda, Phys. Lett. B **474** (2000) 245 [arXiv:hep-ph/9909330].
85. F. Simkovic, A. Faessler, Prog. Part. Nucl. Phys. **48** (2002) 201-209 [hep-ph/0112272].
86. J. D. Vergados, Phys. Rev. C **24** (1981) 640.
87. J. D. Vergados, Phys. Rev. D **25** (1982) 914.
88. A. Faessler, S. Kovalenko, F. Simkovic, J. Schwieger, Phys. Rev. Lett. **78** (1997) 183-186 [hep-ph/9612357]; A. Faessler, S. Kovalenko, F. Simkovic, Phys. Rev. D **58** (1998) 115004 [hep-ph/9803253].
89. F. Deppisch and H. Pas, Phys. Rev. Lett. **98**, 232501 (2007) [arXiv:hep-ph/0612165].
90. V. M. Gehman and S. R. Elliott, J. Phys. G **34**, 667 (2007) [Erratum-ibid. G **35**, 029701 (2008)] [arXiv:hep-ph/0701099].

91. G. L. Fogli, E. Lisi and A. M. Rotunno, Phys. Rev. D **80** (2009) 015024 [arXiv:0905.1832 [hep-ph]].
92. A. Faessler *et al.*, arXiv:1103.2504 [hep-ph].
93. A. Faessler *et al.*, Phys. Rev. **D83** (2011) 113003 [arXiv:1103.2434 [hep-ph]].
94. S. M. Bilenky, S. T. Petcov, Rev. Mod. Phys. **59** (1987) 671.
95. S. F. King, Rept. Prog. Phys. **67** (2004) 107 [arXiv:hep-ph/0310204].
96. R. N. Mohapatra *et al.*, Rept. Prog. Phys. **70** (2007) 1757-1867 [hep-ph/0510213].
97. R. N. Mohapatra, A. Y. Smirnov, Ann. Rev. Nucl. Part. Sci. **56** (2006) 569-628 [hep-ph/0603118].
98. S. Weinberg, Phys. Rev. Lett. **43** (1979) 1566-1570.
99. E. Ma, Phys. Rev. Lett. **81** (1998) 1171 [arXiv:hep-ph/9805219].
100. P. Minkowski, Phys. Lett. B **67** (1977) 421; T. Yanagida, in *Proceedings of the Workshop on the Unified Theory and the Baryon Number in the Universe* (O. Sawada and A. Sugamoto, eds.), KEK, Tsukuba, Japan, 1979, p. 95; M. Gell-Mann, P. Ramond, and R. Slansky, *Complex spinors and unified theories*, in *Supergravity* (P. van Nieuwenhuizen and D. Z. Freedman, eds.), North Holland, Amsterdam, 1979, p. 315; S. L. Glashow, *The future of elementary particle physics*, in *Proceedings of the 1979 Cargèse Summer Institute on Quarks and Leptons* (M. Lévy, J.-L. Basdevant, D. Speiser, J. Weyers, R. Gastmans, and M. Jacob, eds.), Plenum Press, New York, 1980, pp. 687-713. R. N. Mohapatra and G. Senjanovic, Phys. Rev. Lett. **44** (1980) 912.
101. M. Magg and C. Wetterich, Phys. Lett. B **94** (1980) 61; G. Lazarides, Q. Shafi and C. Wetterich, Nucl. Phys. B **181** (1981) 287; R. N. Mohapatra and G. Senjanovic, Phys. Rev. D **23** (1981) 165.
102. R. Foot, H. Lew, X. G. He and G. C. Joshi, Z. Phys. C **44** (1989) 441.
103. F. del Aguila, J. de Blas, A. Carmona and J. Santiago, Fortsch. Phys. **58** (2010) 675 [arXiv:1003.5799 [hep-ph]].
104. M. -C. Chen, J. Huang, Mod. Phys. Lett. **A21** (2011) 1147-1167 [arXiv:1105.3188 [hep-ph]].
105. S. Antusch *et al.*, JHEP **0610** (2006) 084 [hep-ph/0607020].
106. A. Y. Smirnov, arXiv:hep-ph/0411194.
107. For a recent review see S. Davidson, E. Nardi, Y. Nir, Phys. Rept. **466** (2008) 105-177 [arXiv:0802.2962 [hep-ph]].
108. M. C. Gonzalez-Garcia, M. Maltoni, Phys. Rept. **460** (2008) 1-129 [arXiv:0704.1800 [hep-ph]].
109. A. Strumia and F. Vissani, arXiv:hep-ph/0606054.
110. S. M. Bilenky, J. Hosek and S. T. Petcov, Phys. Lett. B **94** (1980) 495; J. Schechter, J. W. F. Valle, Phys. Rev. D **22** (1980) 2227; M. Doi, T. Kotani, H. Nishiura, K. Okuda and E. Takasugi, Phys. Lett. B **102** (1981) 323.
111. J. F. Nieves and P. B. Pal, Phys. Rev. D **36** (1987) 315; J. A. Aguilar-Saavedra and G. C. Branco, Phys. Rev. D **62** (2000) 096009 [arXiv:hep-ph/0007025].
112. L. Wolfenstein, Phys. Lett. B **107** (1981) 77; B. Kayser, Phys. Rev. D **30** (1984) 1023; S. M. Bilenky, N. P. Nedelcheva and S. T. Petcov, Nucl. Phys. B **247** (1984) 61.
113. T. Schwetz, M. Tortola and J. W. F. Valle, New J. Phys. **13** (2011) 063004 [arXiv:1103.0734 [hep-ph]].
114. G. L. Fogli, E. Lisi, A. Marrone, A. Palazzo and A. M. Rotunno, Phys. Rev. Lett. **101** (2008) 141801 [arXiv:0806.2649 [hep-ph]].
115. G. L. Fogli, E. Lisi, A. Marrone, A. Palazzo and A. M. Rotunno, arXiv:1106.6028 [hep-ph]; T. Schwetz, M. Tortola, J. W. F. Valle, arXiv:1108.1376 [hep-ph].

116. K. Abe *et al.* [T2K Collaboration], Phys. Rev. Lett. **107** (2011) 041801 [arXiv:1106.2822 [hep-ex]].
117. P. F. Harrison and W. G. Scott, Phys. Lett. B **535** (2002) 163 [arXiv:hep-ph/0203209]; Z. Z. Xing, Phys. Lett. B **533** (2002) 85 [arXiv:hep-ph/0204049]; X. G. He and A. Zee, Phys. Lett. B **560** (2003) 87 [arXiv:hep-ph/0301092].
118. G. Altarelli and F. Feruglio, Rev. Mod. Phys. **82**, 2701 (2010) [arXiv:1002.0211 [hep-ph]]; H. Ishimori *et al.*, Prog. Theor. Phys. Suppl. **183** (2010) 1 [arXiv:1003.3552 [hep-th]].
119. C. Athanassopoulos *et al.* [LSND Collaboration], Phys. Rev. Lett. **77** (1996) 3082 [arXiv:nucl-ex/9605003]; Phys. Rev. Lett. **81** (1998) 1774 [arXiv:nucl-ex/9709006]; Phys. Rev. C **58** (1998) 2489 [arXiv:nucl-ex/9706006].
120. E. D. Church, K. Eitel, G. B. Mills and M. Steidl, Phys. Rev. D **66** (2002) 013001 [arXiv:hep-ex/0203023].
121. M. Maltoni and T. Schwetz, Phys. Rev. D **76** (2007) 093005 [arXiv:0705.0107 [hep-ph]].
122. C. Giunti and M. Laveder, Phys. Rev. D **82** (2010) 093016 [arXiv:1010.1395 [hep-ph]].
123. B. Armbruster *et al.* [KARMEN Collaboration], Phys. Rev. D **65** (2002) 112001 [arXiv:hep-ex/0203021].
124. A. A. Aguilar-Arevalo *et al.* [The MiniBooNE Collaboration], Phys. Rev. Lett. **98** (2007) 231801 [arXiv:0704.1500 [hep-ex]]; Phys. Rev. Lett. **105** (2010) 181801 [arXiv:1007.1150 [hep-ex]].
125. M. Sorel, J. M. Conrad and M. Shaevitz, Phys. Rev. D **70** (2004) 073004 [arXiv:hep-ph/0305255]; M. Maltoni, T. Schwetz, Phys. Rev. D **76** (2007) 093005 [arXiv:0705.0107 [hep-ph]]; G. Karagiorgi, Z. Djurcic, J. M. Conrad, M. H. Shaevitz and M. Sorel, Phys. Rev. D **80** (2009) 073001 [Erratum-ibid. D **81** (2010) 039902] [arXiv:0906.1997 [hep-ph]].
126. S. Goswami and W. Rodejohann, JHEP **0710** (2007) 073 [arXiv:0706.1462 [hep-ph]].
127. G. Mention *et al.*, Phys. Rev. D **83** (2011) 073006 [arXiv:1101.2755 [hep-ex]]; see also P. Huber, arXiv:1106.0687 [hep-ph].
128. J. Kopp, M. Maltoni and T. Schwetz, arXiv:1103.4570 [hep-ph].
129. J. Kopp, A. Merle, Phys. Rev. C **81** (2010) 045501 [arXiv:0911.3329 [hep-ph]]; M. Lindroos, B. McElrath, C. Orme, T. Schwetz, Eur. Phys. J. C **64** (2009) 549-560 [arXiv:0904.1089 [hep-ph]].
130. C. Kraus *et al.*, Eur. Phys. J. C **40** (2005) 447 [arXiv:hep-ex/0412056].
131. V. M. Lobashev, Nucl. Phys. A **719** (2003) 153.
132. A. Osipowicz *et al.* [KATRIN Collaboration], arXiv:hep-ex/0109033.
133. O. Host, O. Lahav, F. B. Abdalla and K. Eitel, Phys. Rev. D **76** (2007) 113005 [arXiv:0709.1317 [hep-ph]].
134. A. Monfardini *et al.*, Nucl. Instrum. Meth. A **559** (2006) 346 [arXiv:hep-ex/0509038].
135. E. W. Otten, C. Weinheimer, Rept. Prog. Phys. **71** (2008) 086201 [arXiv:0909.2104 [hep-ex]].
136. B. Monreal and J. A. Formaggio, Phys. Rev. D **80** (2009) 051301 [arXiv:0904.2860 [nucl-ex]].
137. J. Bonn *et al.*, arXiv:0704.3930 [hep-ph]; A. S. Riis, S. Hannestad and C. Weinheimer, arXiv:1105.6005 [nucl-ex].
138. S. Hannestad, Prog. Part. Nucl. Phys. **65** (2010) 185-208 [arXiv:1007.0658 [hep-ph]].
139. T. M. Nieuwenhuizen, Europhys. Lett. **86** (2009) 59001 [arXiv:0812.4552 [astro-ph]].
140. S. Hannestad, Phys. Rev. Lett. **95** (2005) 221301 [arXiv:astro-ph/0505551].
141. M. C. Gonzalez-Garcia, M. Maltoni and J. Salvado, JHEP **1008** (2010) 117

- [arXiv:1006.3795 [hep-ph]].
142. E. Komatsu *et al.* [WMAP Collaboration], *Astrophys. J. Suppl.* **192** (2011) 18 [arXiv:1001.4538 [astro-ph.CO]].
 143. J. Hamann *et al.*, *JCAP* **1007** (2010) 022 [arXiv:1003.3999 [astro-ph.CO]]; B. A. Reid, L. Verde, R. Jimenez and O. Mena, *JCAP* **1001** (2010) 003 [arXiv:0910.0008 [astro-ph.CO]].
 144. Y. I. Izotov and T. X. Thuan, *Astrophys. J.* **710** (2010) L67 [arXiv:1001.4440 [astro-ph.CO]]; E. Aver, K. A. Olive and E. D. Skillman, *JCAP* **1005** (2010) 003 [arXiv:1001.5218 [astro-ph.CO]].
 145. J. Hamann *et al.*, *Phys. Rev. Lett.* **105** (2010) 181301 [arXiv:1006.5276 [hep-ph]].
 146. K. N. Abazajian *et al.*, arXiv:1103.5083 [astro-ph.CO].
 147. S. T. Petcov and A. Y. Smirnov, *Phys. Lett. B* **322** (1994) 109 [arXiv:hep-ph/9311204]; S. M. Bilenky, A. Bottino, C. Giunti and C. W. Kim, *Phys. Rev. D* **54** (1996) 1881 [arXiv:hep-ph/9602216]; S. M. Bilenky, C. Giunti, C. W. Kim and S. T. Petcov, *Phys. Rev. D* **54** (1996) 4432 [arXiv:hep-ph/9604364]; S. M. Bilenky, C. Giunti and W. Grimus, *Eur. Phys. J. C* **1**, 247 (1998) [arXiv:hep-ph/9607372]; H. Minakata and O. Yasuda, *Phys. Rev. D* **56** (1997) 1692 [arXiv:hep-ph/9609276]; T. Fukuyama, K. Matsuda and H. Nishiura, *Phys. Rev. D* **57** (1998) 5844 [arXiv:hep-ph/9711415]; *Mod. Phys. Lett. A* **13** (1998) 2279 [arXiv:hep-ph/9804262]; F. Vissani, *JHEP* **9906** (1999) 022 [arXiv:hep-ph/9906525]; C. Giunti, *Phys. Rev. D* **61** (2000) 036002 [hep-ph/9906275]; S. M. Bilenky *et al.*, *Phys. Lett. B* **465** (1999) 193 [arXiv:hep-ph/9907234]; W. Rodejohann, *Nucl. Phys. B* **597** (2001) 110 [arXiv:hep-ph/0008044]; S. M. Bilenky, S. Pascoli and S. T. Petcov, *Phys. Rev. D* **64** (2001) 053010 [arXiv:hep-ph/0102265]; M. Czakon, J. Gluza, J. Studnik and M. Zralek, *Phys. Rev. D* **65** (2002) 053008 [arXiv:hep-ph/0110166]; V. Barger, S. L. Glashow, D. Marfatia, K. Whisnant, *Phys. Lett. B* **532** (2002) 15-18 [hep-ph/0201262]; F. Feruglio, A. Strumia and F. Vissani, *Nucl. Phys. B* **637** (2002) 345 [Addendum-ibid. **B 659** (2003) 359] [arXiv:hep-ph/0201291]; F. R. Joaquim, *Phys. Rev. D* **68** (2003) 033019 [arXiv:hep-ph/0304276]; H. Minakata and H. Sugiyama, *Phys. Lett. B* **567** (2003) 305 [arXiv:hep-ph/0212240]; H. Murayama, C. Pena-Garay, *Phys. Rev. D* **69** (2004) 031301 [hep-ph/0309114]; A. de Gouvea and J. Jenkins, arXiv:hep-ph/0507021; G. L. Fogli *et al.*, *Phys. Rev. D* **75** (2007) 053001 [arXiv:hep-ph/0608060]; S. Pascoli and S. T. Petcov, *Phys. Rev. D* **77** (2008) 113003 [arXiv:0711.4993 [hep-ph]]; G. L. Fogli *et al.*, *Phys. Rev. D* **78** (2008) 033010 [arXiv:0805.2517 [hep-ph]].
 148. H. V. Klapdor-Kleingrothaus, H. Pas and A. Y. Smirnov, *Phys. Rev. D* **63** (2001) 073005 [arXiv:hep-ph/0003219].
 149. Y. Farzan, O. L. G. Peres and A. Y. Smirnov, *Nucl. Phys. B* **612** (2001) 59 [arXiv:hep-ph/0105105].
 150. S. Pascoli and S. T. Petcov, *Phys. Lett. B* **544** (2002) 239 [arXiv:hep-ph/0205022]; *Phys. Lett. B* **580** (2004) 280 [arXiv:hep-ph/0310003].
 151. S. Pascoli, S. T. Petcov and T. Schwetz, *Nucl. Phys. B* **734** (2006) 24 [arXiv:hep-ph/0505226].
 152. S. Choubey and W. Rodejohann, *Phys. Rev. D* **72** (2005) 033016 [arXiv:hep-ph/0506102].
 153. M. Lindner, A. Merle and W. Rodejohann, *Phys. Rev. D* **73** (2006) 053005 [arXiv:hep-ph/0512143].
 154. S. T. Petcov, *Phys. Scripta* **T121** (2005) 94-101 [hep-ph/0504166].
 155. N. F. de Barros and K. Zuber, arXiv:1103.5757 [hep-ph].
 156. W. Rodejohann, *Phys. Lett. B* **684** (2010) 40 [arXiv:0912.3388 [hep-ph]].

157. W. Maneschg, A. Merle and W. Rodejohann, *Europhys. Lett.* **85** (2009) 51002 [arXiv:0812.0479 [hep-ph]].
158. S. Hannestad, arXiv:0710.1952 [hep-ph].
159. J. Bergstrom, A. Merle and T. Ohlsson, *JHEP* **1105** (2011) 122 [arXiv:1103.3015 [hep-ph]].
160. S. Pascoli, S. T. Petcov and W. Rodejohann, *Phys. Lett. B* **558** (2003) 141 [arXiv:hep-ph/0212113].
161. H. Minakata and H. Sugiyama, *Phys. Lett. B* **526** (2002) 335 [arXiv:hep-ph/0111269]; A. Merle and W. Rodejohann, *Adv. High Energy Phys.* **2007** (2007) 82674 [arXiv:hep-ph/0703135].
162. A. de Gouvea, B. Kayser and R. N. Mohapatra, *Phys. Rev. D* **67** (2003) 053004 [arXiv:hep-ph/0211394].
163. S. Pascoli, S. T. Petcov and L. Wolfenstein, *Phys. Lett. B* **524** (2002) 319 [arXiv:hep-ph/0110287]; W. Rodejohann, *Nucl. Phys. B* **597** (2001) 110 [arXiv:hep-ph/0008044]; arXiv:hep-ph/0203214; K. Matsuda, N. Takeda, T. Fukuyama and H. Nishiura, *Phys. Rev. D* **63** (2001) 077301 [arXiv:hep-ph/0007237]; *Phys. Rev. D* **64** (2001) 013001 [arXiv:hep-ph/0012357]; F. Deppisch, H. Pas and J. Suhonen, *Phys. Rev. D* **72** (2005) 033012 [arXiv:hep-ph/0409306]; A. Joniec and M. Zralek, *Phys. Rev. D* **73** (2006) 033001 [arXiv:hep-ph/0411070].
164. V. Barger, S. L. Glashow, P. Langacker and D. Marfatia, *Phys. Lett. B* **540** (2002) 247 [arXiv:hep-ph/0205290].
165. S. Pascoli, S. T. Petcov and W. Rodejohann, *Phys. Lett. B* **549** (2002) 177 [arXiv:hep-ph/0209059].
166. Z. Z. Xing, *Phys. Rev. D* **68** (2003) 053002 [arXiv:hep-ph/0305195].
167. S. Dev and S. L. Kumar, *Mod. Phys. Lett. A* **22** (2007) 1401 [arXiv:hep-ph/0607048].
168. A. Merle and W. Rodejohann, *Phys. Rev. D* **73**, 073012 (2006) [arXiv:hep-ph/0603111].
169. P. H. Frampton, S. L. Glashow, D. Marfatia, *Phys. Lett. B* **536** (2002) 79-82 [hep-ph/0201008].
170. W. Grimus, A. S. Joshipura, L. Lavoura and M. Tanimoto, *Eur. Phys. J. C* **36**, 227 (2004) [arXiv:hep-ph/0405016].
171. J. Jenkins, *Phys. Rev. D* **79** (2009) 113003 [arXiv:0808.1702 [hep-ph]].
172. H. Hettmansperger, M. Lindner, W. Rodejohann, *JHEP* **1104** (2011) 123 [arXiv:1102.3432 [hep-ph]].
173. S. Ray, *Int. J. Mod. Phys. A* **25** (2010) 4339 [arXiv:1005.1938 [hep-ph]].
174. S. Antusch, J. Kersten, M. Lindner and M. Ratz, *Nucl. Phys. B* **674** (2003) 401 [arXiv:hep-ph/0305273].
175. M. Hirsch, A. S. Joshipura, S. Kaneko and J. W. F. Valle, *Phys. Rev. Lett.* **99** (2007) 151802 [arXiv:hep-ph/0703046].
176. J. Barry and W. Rodejohann, *Nucl. Phys. B* **842** (2011) 33 [arXiv:1007.5217 [hep-ph]].
177. G. Altarelli, F. Feruglio, *Nucl. Phys. B* **741** (2006) 215-235 [hep-ph/0512103].
178. M. Hirsch, S. Morisi and J. W. F. Valle, *Phys. Rev. D* **78**, 093007 (2008) [arXiv:0804.1521 [hep-ph]]; F. Bazzocchi, L. Merlo and S. Morisi, *Nucl. Phys. B* **816** (2009) 204 [arXiv:0901.2086 [hep-ph]]; G. J. Ding and D. M. Pan, arXiv:1011.5306 [hep-ph]; T. Fukuyama, H. Sugiyama and K. Tsumura, *Phys. Rev. D* **83** (2011) 056016 [arXiv:1012.4886 [hep-ph]]; H. -J. He, F. -R. Yin, arXiv:1104.2654 [hep-ph].
179. C. Giunti, *Phys. Rev. D* **61** (2000) 036002 [arXiv:hep-ph/9906275]; S. M. Bilenky, C. Giunti, W. Grimus, B. Kayser and S. T. Petcov, *Phys. Lett. B* **465** (1999) 193 [arXiv:hep-ph/9907234]; A. Kalliomaki and J. Maalampi, *Phys. Lett. B* **484** (2000)

- 64 [arXiv:hep-ph/0003281]; Y. Farzan, O. L. G. Peres and A. Y. Smirnov, Nucl. Phys. B **612** (2001) 59 [arXiv:hep-ph/0105105]; S. Pakvasa and P. Roy, Phys. Lett. B **535** (2002) 181 [arXiv:hep-ph/0203188]; S. M. Bilenky, S. Pascoli and S. T. Petcov, Phys. Rev. D **64** (2001) 113003 [arXiv:hep-ph/0104218]; S. Goswami and W. Rodejohann, Phys. Rev. D **73** (2006) 113003 [arXiv:hep-ph/0512234]; C. Giunti and M. Laveder, Phys. Rev. D **82** (2010) 053005 [arXiv:1005.4599 [hep-ph]].
180. J. Barry, W. Rodejohann and H. Zhang, JHEP **1107** (2011) 091 [arXiv:1105.3911 [hep-ph]].
181. A. S. Riis and S. Hannestad, JCAP **1102** (2011) 011 [arXiv:1008.1495 [astro-ph.CO]]; J. A. Formaggio, J. Barrett, arXiv:1105.1326 [nucl-ex].
182. A. de Gouvea, W. C. Huang and J. Jenkins, Phys. Rev. D **80** (2009) 073007 [arXiv:0906.1611 [hep-ph]].
183. J. Maalampi, J. Riittinen, Phys. Rev. D **81** (2010) 037301 [arXiv:0912.4628 [hep-ph]].
184. R. Allahverdi, B. Dutta and R. N. Mohapatra, Phys. Lett. B **695** (2011) 181 [arXiv:1008.1232 [hep-ph]].
185. J. Barry, R. N. Mohapatra and W. Rodejohann, Phys. Rev. D **83** (2011) 113012 [arXiv:1012.1761 [hep-ph]].
186. G. Barenboim, J. F. Beacom, L. Borissov, B. Kayser, Phys. Lett. B **537** (2002) 227-232 [hep-ph/0203261].
187. H. V. Klapdor-Kleingrothaus, H. Pas, U. Sarkar, Eur. Phys. J. A **5** (1999) 3-6 [hep-ph/9809396].
188. G. L. Fogli, E. Lisi, A. Marrone, G. Scioscia, Phys. Rev. D **60** (1999) 053006 [hep-ph/9904248].
189. A. D. Dolgov, A. Y. Smirnov, Phys. Lett. B **621** (2005) 1-10 [hep-ph/0501066]; A. S. Barabash *et al.*, Nucl. Phys. B **783** (2007) 90-111 [arXiv:0704.2944 [hep-ph]].
190. H. V. Klapdor-Kleingrothaus, hep-ex/9802007.
191. R. N. Mohapatra, Nucl. Phys. Proc. Suppl. **77** (1999) 376-385 [hep-ph/9808284].
192. P. Bamert, C. P. Burgess and R. N. Mohapatra, Nucl. Phys. B **438** (1995) 3 [arXiv:hep-ph/9408367].
193. A. Halprin, P. Minkowski, H. Primakoff, S. P. Rosen, Phys. Rev. D **13** (1976) 2567.
194. A. Halprin, S. T. Petcov, S. P. Rosen, Phys. Lett. B **125** (1983) 335.
195. J. D. Vergados, Nucl. Phys. B **218** (1983) 109.
196. P. Benes, A. Faessler, F. Simkovic, S. Kovalenko, Phys. Rev. D **71** (2005) 077901 [hep-ph/0501295].
197. M. Blennow, E. Fernandez-Martinez, J. Lopez-Pavon, J. Menendez, JHEP **1007** (2010) 096 [arXiv:1005.3240 [hep-ph]].
198. A. Ibarra, E. Molinaro, S. T. Petcov, JHEP **1009** (2010) 108 [arXiv:1007.2378 [hep-ph]].
199. A. Ibarra, E. Molinaro, S. T. Petcov, arXiv:1103.6217 [hep-ph].
200. Z. Z. Xing, Phys. Lett. B **679** (2009) 255-259 [arXiv:0907.3014 [hep-ph]].
201. A. de Gouvea, J. Jenkins, N. Vasudevan, Phys. Rev. D **75** (2007) 013003 [hep-ph/0608147].
202. R. N. Mohapatra and J. D. Vergados, Phys. Rev. Lett. **47** (1981) 1713.
203. K. Nakamura *et al.* [Particle Data Group], J. Phys. G **37** (2010) 075021.
204. J. Schechter and J. W. F. Valle, Phys. Rev. D **25** (1982) 774.
205. L. Wolfenstein, Phys. Rev. D **26**, 2507 (1982).
206. W. C. Haxton, S. P. Rosen and G. J. Stephenson, Phys. Rev. D **26** (1982) 1805.
207. S. T. Petcov, H. Sugiyama, Y. Takanishi, Phys. Rev. D **80** (2009) 015005 [arXiv:0904.0759 [hep-ph]].
208. C. -S. Chen, C. Q. Geng, J. N. Ng, Phys. Rev. D **75** (2007) 053004 [hep-ph/0610118];

- C. -S. Chen, C. -Q. Geng, J. N. Ng, J. M. S. Wu, JHEP **0708** (2007) 022 [arXiv:0706.1964 [hep-ph]].
209. T. Han, B. Mukhopadhyaya, Z. Si, K. Wang, Phys. Rev. D **76** (2007) 075013 [arXiv:0706.0441 [hep-ph]].
210. J. Garayoa, T. Schwetz, JHEP **0803** (2008) 009 [arXiv:0712.1453 [hep-ph]]; M. Kadastik, M. Raidal, L. Rebane, Phys. Rev. D **77** (2008) 115023 [arXiv:0712.3912 [hep-ph]]; A. G. Akeroyd, M. Aoki, H. Sugiyama, Phys. Rev. D **77** (2008) 075010 [arXiv:0712.4019 [hep-ph]]; P. Fileviez Perez, T. Han, G. -y. Huang, T. Li, K. Wang, Phys. Rev. D **78** (2008) 015018 [arXiv:0805.3536 [hep-ph]].
211. R. N. Mohapatra, G. Senjanovic, Phys. Rev. D **23** (1981) 165.
212. A. Maiezza, M. Nemevsek, F. Nesti, G. Senjanovic, Phys. Rev. D **82** (2010) 055022 [arXiv:1005.5160 [hep-ph]].
213. D. Guadagnoli, R. N. Mohapatra, Phys. Lett. B **694** (2011) 386-392 [arXiv:1008.1074 [hep-ph]].
214. V. Tello, M. Nemevsek, F. Nesti, G. Senjanovic, F. Vissani, Phys. Rev. Lett. **106** (2011) 151801 [arXiv:1011.3522 [hep-ph]].
215. R. N. Mohapatra, Phys. Rev. D **34** (1986) 909.
216. W. -Y. Keung, G. Senjanovic, Phys. Rev. Lett. **50** (1983) 1427.
217. S. Chatrchyan *et al.* [CMS Collaboration], arXiv:1103.0030 [hep-ex].
218. M. Nemevsek, F. Nesti, G. Senjanovic, Y. Zhang, Phys. Rev. **D83** (2011) 115014 [arXiv:1103.1627 [hep-ph]].
219. K. Muto, E. Bender, H. V. Klapdor, Z. Phys. A **334** (1989) 187-194.
220. G. Pantis, F. Simkovic, J. D. Vergados, A. Faessler, Phys. Rev. C **53** (1996) 695-707 [nucl-th/9612036].
221. J. Suhonen and O. Civitarese, Phys. Lett. B **312** (1993) 367.
222. M. Hirsch, H. V. Klapdor-Kleingrothaus and O. Panella, Phys. Lett. B **374** (1996) 7 [arXiv:hep-ph/9602306].
223. H. P. Nilles, Phys. Rept. **110** (1984) 1-162; H. E. Haber, G. L. Kane, Phys. Rept. **117** (1985) 75-263.
224. A. Faessler, S. Kovalenko, F. Simkovic, Phys. Rev. D **58** (1998) 055004 [hep-ph/9712535].
225. M. Hirsch, H. V. Klapdor-Kleingrothaus, S. G. Kovalenko, Phys. Lett. B **398** (1997) 311-314 [hep-ph/9701253].
226. M. Hirsch, H. V. Klapdor-Kleingrothaus, S. G. Kovalenko, Phys. Lett. **B403** (1997) 291-296.
227. M. Hirsch, H. V. Klapdor-Kleingrothaus, S. G. Kovalenko, Phys. Rev. D **57** (1998) 1947-1961 [hep-ph/9707207].
228. R. Barbier *et al.*, Phys. Rept. **420** (2005) 1 [arXiv:hep-ph/0406039].
229. R. N. Mohapatra, Phys. Rev. D **34** (1986) 3457.
230. J. D. Vergados, Phys. Lett. B **184** (1987) 55.
231. M. Hirsch, H. V. Klapdor-Kleingrothaus and S. G. Kovalenko, Phys. Rev. D **53** 1329 (1996) 1329 [arXiv:hep-ph/9502385].
232. M. Hirsch, M. A. Diaz, W. Porod, J. C. Romao, J. W. F. Valle, Phys. Rev. D **62** (2000) 113008 [hep-ph/0004115].
233. M. Hirsch, J. W. F. Valle, Nucl. Phys. B **557** (1999) 60-78 [hep-ph/9812463].
234. M. Hirsch, H. V. Klapdor-Kleingrothaus and S. G. Kovalenko, Phys. Rev. Lett. **75** (1995) 17; H. Pas, M. Hirsch and H. V. Klapdor-Kleingrothaus, Phys. Lett. B **459** (1999) 450 [arXiv:hep-ph/9810382]; A. Wodecki, W. A. Kaminski, F. Simkovic, Phys. Rev. D **60** (1999) 115007 [hep-ph/9902453].
235. A. Faessler, T. Gutsche, S. Kovalenko, F. Simkovic, Phys. Rev. D **77** (2008) 113012

- [arXiv:0710.3199 [hep-ph]].
236. B. C. Allanach, C. H. Kom, H. Pas, JHEP **0910** (2009) 026 [arXiv:0903.0347 [hep-ph]].
 237. B. C. Allanach, C. H. Kom, H. Pas, Phys. Rev. Lett. **103** (2009) 091801 [arXiv:0902.4697 [hep-ph]].
 238. H. K. Dreiner, S. Grab, M. Kramer and M. K. Trenkel, Phys. Rev. D **75** (2007) 035003 [arXiv:hep-ph/0611195].
 239. K. S. Babu, R. N. Mohapatra, Phys. Rev. Lett. **75** (1995) 2276-2279 [hep-ph/9506354].
 240. D. Choudhury, P. Roy, Phys. Lett. B **378** (1996) 153-158 [hep-ph/9603363].
 241. Y. Chikashige, R. N. Mohapatra, R. D. Peccei, Phys. Lett. B **98** (1981) 265; Phys. Rev. Lett. **45** (1980) 1926.
 242. G. B. Gelmini and M. Roncadelli, Phys. Lett. B **99** (1981) 411.
 243. G. G. Raffelt, Phys. Rept. **198** (1990) 1-113.
 244. R. Tomas, H. Pas, J. W. F. Valle, Phys. Rev. D **64** (2001) 095005 [hep-ph/0103017].
 245. H. M. Georgi, S. L. Glashow, S. Nussinov, Nucl. Phys. B **193** (1981) 297.
 246. C. S. Aulakh, R. N. Mohapatra, Phys. Lett. B **119** (1982) 136.
 247. R. N. Mohapatra, E. Takasugi, Phys. Lett. B **211** (1988) 192.
 248. A. Masiero, J. W. F. Valle, Phys. Lett. B **251** (1990) 273-278.
 249. Z. G. Berezhiani, A. Y. Smirnov, J. W. F. Valle, Phys. Lett. B **291** (1992) 99-105 [hep-ph/9207209].
 250. C. P. Burgess, J. M. Cline, Phys. Lett. B **298** (1993) 141-148 [hep-ph/9209299]; Phys. Rev. D **49** (1994) 5925-5944 [hep-ph/9307316].
 251. C. D. Carone, Phys. Lett. B **308** (1993) 85-88 [hep-ph/9302290].
 252. P. Bamert, C. P. Burgess, R. N. Mohapatra, Nucl. Phys. B **449** (1995) 25-48 [hep-ph/9412365].
 253. J. C. Montero, C. A. de Sousa Pires, V. Pleitez, Phys. Rev. D **64** (2001) 096001 [hep-ph/0003284].
 254. R. N. Mohapatra, A. Perez-Lorenzana, C. A. de S Pires, Phys. Lett. B **491** (2000) 143-147 [hep-ph/0008158].
 255. M. Doi, T. Kotani, E. Takasugi, Phys. Rev. D **37** (1988) 2575.
 256. M. Hirsch, H. V. Klapdor-Kleingrothaus, S. G. Kovalenko, H. Pas, Phys. Lett. B **372** (1996) 8-14 [hep-ph/9511227].
 257. R. Arnold *et al.* [NEMO Collaboration], Nucl. Phys. A **765** (2006) 483-494 [hep-ex/0601021].
 258. K. S. Babu, C. N. Leung, Nucl. Phys. B **619** (2001) 667-689 [hep-ph/0106054].
 259. A. de Gouvea, J. Jenkins, Phys. Rev. D **77** (2008) 013008 [arXiv:0708.1344 [hep-ph]].
 260. M. Hirsch, H. V. Klapdor-Kleingrothaus and S. G. Kovalenko, Phys. Rev. D **54** (1996) 4207 [arXiv:hep-ph/9603213].
 261. H. V. Klapdor-Kleingrothaus, U. Sarkar, Phys. Lett. B **554** (2003) 45-50 [hep-ph/0211274].
 262. B. Brahmachari, E. Ma, Phys. Lett. B **536** (2002) 259-262 [hep-ph/0202262].
 263. N. Arkani-Hamed, S. Dimopoulos, G. R. Dvali, J. March-Russell, Phys. Rev. D **65** (2002) 024032 [hep-ph/9811448].
 264. M. Gozdz, W. A. Kaminski, Phys. Rev. D **68** (2003) 057901 [hep-ph/0305041]; M. Gozdz, W. A. Kaminski, A. Faessler, Phys. Rev. D **71** (2005) 096005.
 265. G. Bhattacharyya, H. V. Klapdor-Kleingrothaus, H. Pas, A. Pilaftsis, Phys. Rev. D **67** (2003) 113001 [hep-ph/0212169].
 266. M. Duerr, D. P. George and K. L. McDonald, arXiv:1105.0593 [hep-ph].
 267. C. H. Chang, W. F. Chang and J. N. Ng, Phys. Lett. B **558** (2003) 92 [arXiv:hep-

- ph/0301271].
268. P. Fileviez Perez, M. B. Wise, Phys. Rev. D **80** (2009) 053006 [arXiv:0906.2950 [hep-ph]].
 269. A. Lenz, H. Pas and D. Schalla, arXiv:1104.2465 [hep-ph]; D. Atwood, S. K. Gupta and A. Soni, arXiv:1104.3874 [hep-ph].
 270. O. Panella, Y. N. Srivastava, Phys. Rev. D **52** (1995) 5308-5313 [hep-ph/9411224]; E. Takasugi, Prog. Theor. Phys. **94** (1995) 1097-1104 [hep-ph/9506379]; Prog. Theor. Phys. **98** (1997) 977-985 [hep-ph/9706240].
 271. O. Panella, C. Carimalo, Y. N. Srivastava and A. Widom, Phys. Rev. D **56** (1997) 5766 [arXiv:hep-ph/9701251].
 272. V. Pleitez and M. D. Tonasse, Phys. Rev. D **48** (1993) 5274 [arXiv:hep-ph/9302201].
 273. A. G. Dias *et al.*, Phys. Rev. D **72** (2005) 035006 [hep-ph/0503014]; D. Van Soa *et al.*, J. Exp. Theor. Phys. **108** (2009) 757-763 [arXiv:0805.4456 [hep-ph]].
 274. C. X. Zhang, M. Q. Huang and M. Zhong, Phys. Rev. D **78** (2008) 096006.
 275. P. -H. Gu, arXiv:1101.5106 [hep-ph].
 276. G. Dvali, Fortsch. Phys. **58** (2010) 528 [arXiv:0706.2050 [hep-th]]; G. Dvali and M. Redi, Phys. Rev. D **80** (2009) 055001 [arXiv:0905.1709 [hep-ph]].
 277. S. Kovalenko, H. Pas and I. Schmidt, Phys. Rev. D **83** (2011) 051901 [arXiv:1011.4915 [hep-ph]].
 278. V. Cirigliano, A. Kurylov, M. J. Ramsey-Musolf, P. Vogel, Phys. Rev. Lett. **93** (2004) 231802 [hep-ph/0406199].
 279. R. Arnold *et al.* [SuperNEMO Collaboration], Eur. Phys. J. C **70** (2010) 927-943 [arXiv:1005.1241 [hep-ex]].
 280. A. S. Barabash, AIP Conf. Proc. **942** (2007) 8-12 [arXiv:0710.2194 [nucl-ex]].
 281. M. Duerr, M. Lindner, K. Zuber, arXiv:1103.4735 [hep-ph].
 282. J. D. Vergados, arXiv:1107.3296 [hep-ph].
 283. F. Simkovic, J. Vergados, A. Faessler, Phys. Rev. D **82** (2010) 113015 [arXiv:1006.0571 [hep-ph]].
 284. B. Kayser, Phys. Rev. D **26** (1982) 1662.
 285. C. Giunti, A. Studenikin, Phys. Atom. Nucl. **72** (2009) 2089-2125 [arXiv:0812.3646 [hep-ph]].
 286. J. E. Kim, Phys. Rev. D **14** (1976) 3000; K. Fujikawa, R. Shrock, Phys. Rev. Lett. **45** (1980) 963; J. Schechter, J. W. F. Valle, Phys. Rev. D **24** (1981) 1883-1889; P. B. Pal, L. Wolfenstein, Phys. Rev. D **25** (1982) 766; R. E. Shrock, Nucl. Phys. B **206** (1982) 359; J. F. Nieves, Phys. Rev. D **26** (1982) 3152.
 287. C. S. Lim, W. J. Marciano, Phys. Rev. D **37** (1988) 1368-1373; E. K. Akhmedov, Z. G. Berezhiani, Nucl. Phys. B **373** (1992) 479-497.
 288. See e.g. L. B. Okun, M. B. Voloshin, M. I. Vysotsky, Sov. Phys. JETP **64** (1986) 446-452; M. Fukugita, T. Yanagida, Phys. Rev. Lett. **58** (1987) 1807; N. F. Bell *et al.*, Phys. Lett. B **642** (2006) 377-383 [hep-ph/0606248].
 289. A. Ali, A. V. Borisov, N. B. Zamorin, Eur. Phys. J. C **21** (2001) 123-132 [hep-ph/0104123].
 290. L. S. Littenberg, R. E. Shrock, Phys. Rev. Lett. **68** (1992) 443-446.
 291. J. Abad, J. G. Esteve, A. F. Pacheco, Phys. Rev. D **30** (1984) 1488.
 292. H. Nishiura, K. Matsuda, T. Fukuyama, Mod. Phys. Lett. A **14** (1999) 433-446 [hep-ph/9809556]; K. Matsuda, N. Takeda, T. Fukuyama, H. Nishiura, Phys. Rev. D **62** (2000) 093001 [hep-ph/0003055].
 293. W. Rodejohann, Phys. Rev. D **62** (2000) 013011 [hep-ph/0003149]; J. Phys. G **28** (2002) 1477-1498.
 294. K. Zuber, Phys. Lett. B **479** (2000) 33-36 [hep-ph/0003160].

295. C. Dib, V. Gribov, S. Kovalenko, I. Schmidt, Phys. Lett. B **493** (2000) 82-87 [hep-ph/0006277].
296. A. Atre, V. Barger, T. Han, Phys. Rev. D **71** (2005) 113014 [hep-ph/0502163].
297. V. Gribov, S. Kovalenko, I. Schmidt, Nucl. Phys. B **607** (2001) 355-368 [hep-ph/0102155].
298. S. Bar-Shalom, N. G. Deshpande, G. Eilam, J. Jiang, A. Soni, Phys. Lett. B **643** (2006) 342-347 [hep-ph/0608309].
299. J. N. Ng, A. N. Kamal, Phys. Rev. D **18** (1978) 3412.
300. A. Atre, T. Han, S. Pascoli, B. Zhang, JHEP **0905** (2009) 030 [arXiv:0901.3589 [hep-ph]].
301. G. Cvetič, C. Dib, S. K. Kang, C. S. Kim, Phys. Rev. D **82** (2010) 053010 [arXiv:1005.4282 [hep-ph]].
302. C. Barbero, G. Lopez Castro, A. Mariano, Phys. Lett. B **566** (2003) 98-107 [nucl-th/0212083]; C. Barbero, L. -F. Li, G. Lopez Castro, A. Mariano, Phys. Rev. D **76** (2007) 116008 [arXiv:0709.2431 [hep-ph]].
303. M. Flanz, W. Rodejohann, K. Zuber, Eur. Phys. J. C **16** (2000) 453-460 [hep-ph/9907203]; W. Rodejohann, K. Zuber, Phys. Rev. D **63** (2001) 054031 [hep-ph/0011050].
304. M. Flanz, W. Rodejohann, K. Zuber, Phys. Lett. B **473** (2000) 324-329 [hep-ph/9911298]; W. Rodejohann, K. Zuber, Phys. Rev. D **62** (2000) 094017 [hep-ph/0005270].
305. A. N. Kamal, J. N. Ng, Phys. Rev. D **20** (1979) 2269.
306. P. Domin, S. Kovalenko, A. Faessler, F. Simkovic, Phys. Rev. C **70** (2004) 065501 [nucl-th/0409033].
307. J. H. Missimer, R. N. Mohapatra, N. C. Mukhopadhyay, Phys. Rev. D **50** (1994) 2067-2070.
308. J. C. Helo, S. Kovalenko, I. Schmidt, arXiv:1105.3019 [hep-ph].
309. L. S. Littenberg, R. Shrock, Phys. Lett. B **491** (2000) 285-290 [hep-ph/0005285]; A. Belyaev *et al.*, Eur. Phys. J. C **22** (2002) 715-726 [hep-ph/0008276].
310. F. Simkovic, A. Faessler, S. Kovalenko, I. Schmidt, Phys. Rev. D **66** (2002) 033005 [hep-ph/0112271].
311. G. K. Leontaris, J. D. Vergados, Nucl. Phys. B **224** (1983) 137.
312. C. Picciotto, Phys. Rev. D **56** (1997) 1612-1614 [hep-ph/9702313].
313. T. G. Rizzo, Phys. Lett. B **116** (1982) 23; Phys. Rev. D **25** (1982) 1355; D. London, G. Belanger and J. N. Ng, Phys. Lett. B **188** (1987) 155; P. H. Frampton and D. Ng, Phys. Rev. D **45** (1992) 4240; V. D. Barger, J. F. Beacom, K. m. Cheung and T. Han, Phys. Rev. D **50** (1994) 6704 [arXiv:hep-ph/9404335]; J. Gluza and M. Zralek, Phys. Rev. D **52** (1995) 6238 [arXiv:hep-ph/9502284]; G. Belanger, F. Boudjema, D. London and H. Nadeau, Phys. Rev. D **53** (1996) 6292 [arXiv:hep-ph/9508317]; Phys. Lett. B **372** (1996) 259 [arXiv:hep-ph/9510407]; C. A. Heusch and P. Minkowski, arXiv:hep-ph/9611353; J. Gluza, Phys. Lett. B **403** (1997) 304 [arXiv:hep-ph/9704202]; F. Cuyper and M. Raidal, Nucl. Phys. B **501** (1997) 3 [arXiv:hep-ph/9704224]; J. F. Gunion, Int. J. Mod. Phys. A **11** (1996) 1551 [arXiv:hep-ph/9510350]; M. Raidal, Phys. Rev. D **57** (1998) 2013 (1998) [arXiv:hep-ph/9706279]; P. Duka, J. Gluza and M. Zralek, Phys. Rev. D **58** (1998) 053009 (1998) [arXiv:hep-ph/9804372]; B. Mukhopadhyaya and S. K. Rai, Phys. Lett. B **633** (2006) 519 [arXiv:hep-ph/0508290]; W. Rodejohann, Phys. Rev. D **81** (2010) 114001 [arXiv:1005.2854 [hep-ph]]; W. Rodejohann, H. Zhang, Phys. Rev. D **83** (2011) 073005 [arXiv:1011.3606 [hep-ph]].
314. M. Hirsch, H. V. Klapdor-Kleingrothaus, S. Kolb, S. G. Kovalenko, Phys. Rev. D

- 57** (1998) 2020-2023.
315. F. Cuypers, G. J. van Oldenborgh and R. Ruckl, Nucl. Phys. B **409** (1993) 128 [arXiv:hep-ph/9305287]; K. Huitu, J. Maalampi and M. Raidal, Nucl. Phys. B **420** (1994) 449 [arXiv:hep-ph/9312235]; C. Blochinger, H. Fraas, G. A. Moortgat-Pick and W. Porod, Eur. Phys. J. C **24** (2002) 297 [arXiv:hep-ph/0201282]; J. L. Feng and M. E. Peskin, Phys. Rev. D **64** (2001) 115002 [arXiv:hep-ph/0105100].
316. Y. Grossman, H. E. Haber, Phys. Rev. Lett. **78** (1997) 3438-3441 [hep-ph/9702421].
317. K. Choi, K. Hwang, W. Y. Song, Phys. Rev. Lett. **88** (2002) 141801 [hep-ph/0108028]; A. Dedes, H. E. Haber, J. Rosiek, JHEP **0711** (2007) 059 [arXiv:0707.3718 [hep-ph]]; D. K. Ghosh, T. Honkavaara, K. Huitu, S. Roy, arXiv:1106.0601 [hep-ph].